NTNU
Norwegian University of
Science and Technology

Modelling a Membrane Contactor for CO2 Capture

Solomon Kahsay Gebremariam

Chemical Engineering
Submission date: July 2017
Supervisor: Diego Pinto, IKP
Co-supervisor: Øystein Jonassen, IKP

Norwegian University of Science and Technology
Department of Chemical Engineering

Abstract

Chemical absorption of CO_2 in conventional absorbers is the most mature and preferred technology today for post-combustion CO_2 capture. However, two major bottlenecks of this technology are the large solvent regeneration energy requirement and the large equipment size. Due to their much higher surface area to volume ratio, membrane contactors have been suggested as a promising alternative for absorber size reduction. Furthermore, some novel solvents with low regeneration energy requirement compared to the benchmark solvent (30wt% MEA) have been identified recently. However, at the price of high volatility, which could lead to solvent losses/emissions when applied in the conventional absorbers. The use of membrane contactors has also been suggested to overcome this problem.

Several studies have been performed on CO_2 absorption using membrane contactors, but most of them were conducted at laboratory-scale. Due to the large volume of flue gases coming from power plants, studies focusing on the modelling and design of large-scale membrane contactors are required. The objective of this thesis has been to develop a comprehensive two-dimensional mathematical model for CO_2 absorption in aqueous MEA solution in a hollow fiber membrane contactor (HFMC). The developed HFMC model has been applied for simulation of CO_2 absorption from a flue gas of an 800 MWe coal-fired power plant. This was intended to study the opportunities and challenges of the modelling, and design of CO_2 absorption in large-scale HFMC modules.

The HFMC model is based on mass and heat balance equations for the shell, membrane, and tube sides of the HFMC module. Reversible chemical reactions between CO_2 and MEA and the heat of CO_2 absorption are considered in the model. The radial variations of the diffusion coefficients of the species in the liquid-phase due to the radial viscosity gradient are also implemented in the model. A rigorous equilibrium model is employed to estimate the equilibrium partial pressure of CO_2 and the initial chemical speciation in the CO_2-MEA-H_2O system. The set of partial differential equations in the HFMC model is developed in the programming language MATLAB and solved using the method of lines/finite difference method.

The influence of changing the gas-phase velocity, liquid-phase velocity, solvent lean loading, membrane fiber length, and membrane mass transfer coefficient on the CO_2 capture performance of HFMC modules were studied. Results reveal that increasing the gas-phase velocity and membrane mass transfer coefficient, and decreasing the membrane fiber length enhance CO_2 absorption flux. In addition, increasing the membrane fiber length and membrane mass transfer coefficient, and decreasing the gas-phase velocity enhance CO_2 removal efficiency. Solvent lean loading and liquid-phase velocity have a negligible effect on the performance of the HFMC modules. It was concluded that the main mass transfer resistance is in the membrane.

Based on the sensitivity analysis, the membrane fiber length was optimized to capture 90% CO_2 from the flue gas of the 800 MWe power plant. The volume of the HFMC modules required for 90% CO_2 capture was compared with that of a structured packed column applied for the same case study from the literature. Results show that the HFMC modules provide a reduced absorber volume (by 86%) and flexibility. However, the study suggested that several challenges, limitations, and factors should be considered in the design of industrial-scale HFMC modules. These are a precise estimation of the membrane mass transfer coefficient, gas-phase and liquid-phase pressure drops, limitations in the size of commercial HFMC modules, lifetime of membranes, and choice of shell-side vs tube-side liquid-phase flow. The developed HFMC model predicts an axial and radial concentration and temperature profiles in the liquid-phase. Results show, during 90% CO_2 capture, an excellent radial heat transfer and an axial temperature rise by 20 K in the liquid phase.

The HFMC model results were finally compared with pilot-scale experimental data from the literature. Based on the comparison, the challenges of predicting the performance of large-scale HFMC modules are discussed. The limitations of the developed HFMC model when applied to the simulation of large-scale HFMC modules are also critically discussed.

Preface

This thesis was done during the spring of 2017 in the partial fulfillment of the requirement for the degree of Master of Science in Chemical Engineering with specialization in Environmental Engineering and Reactor Technology. It has been carried out in collaboration with the 3rd Generation Membrane Contactor (3GMC) project at the Department of Chemical Engineering at the Norwegian University of Science and Technology (NTNU).

I am always fascinated by mathematical modelling. Mathematical modelling of chemical reactors is a valuable tool for understanding, improving, and design of reactor systems. At the same time, I am curious on the growing global concerns over climate change effects. I always want to take part in research activities aiming at providing sustainable and far-reaching solutions to the concerns. As a result, most of my projects that I have done throughout my studies are related to these two research areas. When I encountered the opportunity of working on modelling of membrane contactors for CO_2 capture, it was like a dream come true. It gave me the opportunity of working on mathematical modelling together with areas related to global warming. As a result, I carried out my thesis work with a great passion and energy.

I would like to thank my supervisor, Associate Professor Diego Pinto, for giving me the opportunity to work on the thesis, and for his continuous guidance, professional discussion, advice, and help from the beginning to the end of the thesis. I am also thankful to my co-supervisor, Dr. Oystein Jonassen, for his support, discussion and advice on my thesis work. Thanks to Associate Professor Hanna Knuutila for her valuable contribution during the start-up of the work. Thanks to Professor Hallvard Svendsen for providing MATLAB codes and related helps. Thanks to Dr. Luca Ansaloni for his valuable discussion whenever asked. Thanks to the Norwegian Government for the financial support provided under the quota scheme scholarship. Last but not least, thanks to my beloved friends for these two memorable years during my stay in Trondheim, Norway.

"I declare that this is an independent work according to the exam regulations of the Norwegian University of Science and Technology (NTNU) "

Trondheim, 14^{th} of July 2017

Solomon Kahsay Gebremariam

Table of Contents

List of Tables

List of Figures

Nomenclature

Uppercase Latin Symbols

Symbol	Description	Unit
A	Flow cross sectional area	[m^2]
AARD	Average absolute relative deviation,	[–]
C_i	Liquid-phase concentration of comp i	[mol m^{-3}]
C_p	Molar heat capacity	[J mol^{-1} K^{-1}]
C_P	Specific heat capacity	[J $Kg^{-1}K^{-1}$]
D_h	Hydraulic diameter	[m]
D_i	Diffusivity of species i	[m^2s^{-1}]
ΔH_r	Heat of CO_2 absorption per moles of CO_2	[J mol^{-1}]
L	Fiber length	[m]
M	Molecular weight	[g mol^{-1}]
N_i	Molar flux	[mol $m^{-2}s^{-1}$]
P	Total pressure	[kPa]
Q	Heat flux	[Wm^{-2}]
R	Fiber inner radius	[m]
Re	Reynolds number	[–]
R_g	Gas constant	[J $K^{-1}mol^{-1}$]
R_y	Fiber outer radius	[m]
Sc	Schmith number	[–]
Sh	Sherwood number	[–]
T	Temperature	[K]
U	Overall heat transfer coefficient	[Wm^{-2} K^{-1}]

Lowercase Latin Symbols

Symbol	Description	Unit
a	Surface area to volume ratio	[m^2 m^{-3}]
h_g	Heat-transfer coefficients of the gas-phase	[Wm^{-2} K^{-1}]
K_{eq}	Equilibrium constant	[–]
k_g	Gas film mass transfer coefficient	[m s^{-1}]
k_{H_2O}	Kinetic rate constant of H_2O	[m^6 $kmol^{-2}$ s^{-2}]
k_{MEA}	Kinetic rate constant of MEA	[m^6 $kmol^{-2}$ s^{-2}]
n_{tubes}	Number of fiber/tubes per module	[–]
p	Partial pressure	[kPa]
r	Variable radius	[m]
r_{CO_2}	Reaction rate based on CO_2	[kmol m^{-3} s^{-1}]
r_{MEA}	Reaction rate based on MEA	[kmol m^{-3} s^{-1}]
r_{MEACOO^-}	Reaction rate based on $MEACOO^-$	[kmol m^{-3} s^{-1}]
$v_{z,av}$	Volumetric average velocity of the liquid-phase	[m s^{-1}]
x	Mole fraction in gas-phase	[–]
y	Mole fraction in liquid-phase	[–]
z	Variable length	[m]

Greek Symbols

Symbol	Description	Unit
α_{CO_2}	CO_2 loading	[mol CO_2 (mol MEA)$^{-1}$]
β	Dimensionless diffusion coeff.	[–]
χ	Dimensionless concentration.	[–]
Δ_i	Dimensionless pressure of comp i	[–]
ϵ_g	Volume fraction occupied by the gas-phase	[–]
η	Viscosity	[Pa s]
γ	Dimensionless radial distance	[–]
λ	Thermal conductivity	[$Wm^{-1}K^{-1}$]
μ	Dimensionless velocity	[–]
ρ	Density	[kg m^{-3}]
θ	Dimensionless temperature	[–]
ε	Dimensionless axial distance	[–]

Subscripts and Superscripts

Symbol	Description
0	Initial
i	Component i
L	Liquid-phase
g	Gas-phase
*	In equilibrium with bulk opposite phase
loaded	CO_2 loaded solution
unloaded	CO_2 free solution
m	Membrane
T	Temperature dependence

Abbreviations

Abbrev.	Description
1D	One dimensional
1D-2D	One dimensional-two dimensional
2D	Two dimensional
30% MEA	5 Molar MEA aqueous solution
3GMC	3rd generation membrane contactor
AMP	2-amino-2- methyl-1-propanol
CCS	CO_2 capture and storage
CFCs	Chloro-fluorocarbons
CFD	Computational fluid dynamics
CH_4	Methane
CO_2	Carbon dioxide
DEA	Diethanolamine
DEEA	N,N-Diethylethanolamine
DW	Distilled water
e-NRTL	Non-random two liquid for electrolytes activity model
FD	Finite difference
GHG	Greenhouse gas
H_2	Hydrogen
HCO_3	Bicarbonate
HFMC	Hollow fiber membrane contactor
LPG	Liquified petroleum gas
MAPA	3-(Methyl-amino) propylamine
MDEA	Methyl diethanolamine
MEA	Monoethanolamine
$MEACOO^-$	Carbamate ion of ethanolamine
$MEAH^+$	Protonated ethanolamine
MOL	Method of lines
MWe	Megawatt electrical
N_2O	Nitrous oxide
NaOH	Soduim hydroxide
NTNU	Norwegian university of science and technology
ODE	Ordinary differential equation.
OH^-	Hydroxide ion
PC	Propylene carbonate
PCC	Post-combustion CO_2 capture
PDE	Partial differential equation.
PDMS	Poly(dimethylsiloxane)
PG	Propylene glycol
PHPC	Promoted hot potassium carbonate
PMP	Polymethylpentene
PP	Polypropylene
ppm	Parts per million
PTFE	Polytetrafluoroethylene
PTMSP	Poly(1-trimethylsilyl-1-propyne)
PVDF	Polyvinylidene fluoride
TEA	Triethanolamine
t	Tonne
wt	Weight

Chapter 1

Introduction

1.1 Background and Motivation

1.1.1 Status of CO_2 capture and storage

CO_2 is the main greenhouse gas causing global warming. Before the start of industrial revolution (before 1750), the atmospheric CO_2 concentrations were around 280 ppm (Neftel et al., 1985; Change, 2001). These concentrations have significantly increased to 384 ppm in 2007 (Yu et al., 2008) and to 400 ppm in 2015 (Tans, 2017). Therefore, effective measures for controlling CO_2 emission are required. During the 21st century, CO_2 emission from fossil fuel-fired power plants is the main contributor to the global CO_2 concentration rise (Change, 2001; Freund, 2003). CO_2 capture and storage (CCS) is considered a key technology for mitigating CO_2 emission from these large emission sources. CCS involves CO_2 capture and compression from emission sources, which is then transported for storage or re-use.

There are three main pathways to capture CO_2: pre-combustion, oxy-combustion and post-combustion. Among these pathways, post-combustion CO_2 capture is the most promising method because it can be easily added to an existing power plants and combined with new ones without fundamental changes on them (Luis et al., 2012b; Zaidiza et al., 2016). Several processes have been suggested for post-combustion CO_2 capture, including absorption, membrane separation, adsorption and cryogenic distillation (Aaron and Tsouris, 2005; Luis et al., 2012b). Among these, amine-based absorption is the leading process because it has higher CO_2 capture efficiency (up to 90%) (Gabelman and Hwang, 1999; Feron, 2010) and it has been commercialized on large-scale (but not on industrial-scale) (Feron, 2010). However, there are several challenges associated with chemical absorption of CO_2 in the traditional absorbers. These include high solvent regeneration energy requirement, large footprint and thus high investment cost, vulnerability to corrosion, and several operational problems such as flooding, channeling, foaming and entrainment (Falk-Pedersen and Dannström, 1997; deMontigny et al., 2005; Rode et al., 2012; Zaidiza

et al., 2015).

To overcome the drawbacks of chemical absorption in the traditional absorbers, membrane gas absorption (also known as membrane contactor technology) is considered a promising alternative (Gabelman and Hwang, 1999; Klaassen et al., 2005; Cui and de-Montigny, 2013). Membrane contactor technology involves the transfer of CO_2 from a bulk gas-phase through a porous membrane to an absorbent solution. This technology combines the principles of membrane separation and absorption processes. Therefore, it is benefited from the selectivity nature of gas absorption, and the modular and compact nature of membrane separation (Franco et al., 2008). Compared with the traditional absorbers, membrane contactors offer several advantages such as a higher surface area to volume ratio, compact size, operational flexibility, modularity, and easy scale-up (Gabelman and Hwang, 1999; Li and Chen, 2005; Franco et al., 2008; Cui and deMontigny, 2013; Leung et al., 2014). Furthermore, the use of membrane contactors allows independent control of the liquid-phase and gas-phase and avoids the frequent operational problems of the traditional absorbers such as flooding, foaming, entrainment, and channeling . Unfortunately, membrane contactor technology has also drawbacks (Gabelman and Hwang, 1999; Li and Chen, 2005; Franco et al., 2008; Cui and deMontigny, 2013; Leung et al., 2014). First, the introduction of the membrane provides additional mass transfer resistance, which reduces the overall CO_2 absorption rate. However, the high surface area to volume ratio offered by the membrane can compensate this impact. Membrane wetting by the liquid-phase is another drawback of membrane contactors. Several studies (Rangwala, 1996; Mavroudi et al., 2006) have indicated that membrane wetting could significantly reduce the CO_2 capture performance of membrane contactors.

1.1.2 The 3rd generation membrane contactor project at NTNU

The solvent regeneration energy requirement of CO_2 capture using amines is associated with the solvent used. Thus, one of the approaches to reduce the energy penalty of amine-based CO_2 capture is the development of novel solvents having low regeneration energy requirement together with low volatility, fast reaction, high loading capacity, and good CO_2 selectivity (Bounaceur et al., 2012; Rode et al., 2012). In recent years, a new class of solvents called *"phase change solvents"* have shown the potential to have lower energy penalty compared to the benchmark solvent (30wt% MEA) (Pinto et al., 2014a; Monteiro et al., 2015). Blends of 3-(Methyl-amino) propylamine (MAPA)- N,N-Diethylethanolamine (DEEA) is the typical example of the *"phase change solvents"* identified currently (Arshad et al., 2013; Pinto et al., 2014a; Monteiro et al., 2015). DEEA-MAPA blends have higher CO_2 absorption capacity at 313 K and lower solvent regeneration energy requirement at 393 K compared to 30 wt% MEA (Ansaloni et al., 2016). The reboiler duty of CO_2 capture using DEEA- MAPA blends was found to be 2.4 GJ/t_{CO_2}, which is lower than that of MEA (3.5 GJ/t_{CO_2}) (Liebenthal et al., 2013). As a result, these solvents are considered a promising candidate for reducing the energy penalty of amine-based CO_2 capture. However, these solvents have high volatility, which could lead to large amine losses and emissions when applied in traditional absorbers at industrial operating conditions (Pinto et al., 2014a; Ansaloni et al., 2016, 2017). It was suggested that replacing the traditional absorbers with membrane contactors could provide a solution.

Currently, there is an ongoing project called the 3rd generation membrane contactor (3GMC) in the department of chemical engineering at NTNU. The objective of the 3GMC project is to combine the positive features of the chemical absorption process with membrane contactor technology allowing the *"phase change solvents"* to be used avoiding its primary problem: volatility. This leads to prevention of solvent losses and emissions while reducing the regeneration energy requirement of CO_2 capture. The project will also benefit from the several advantages of membrane contactors mentioned earlier. This thesis is done in collaboration with the 3GMC project where a model for a membrane contactor is developed.

1.2 Objective and Methodology

To evaluate the performances and limitations of CO_2 capture using membrane contactors, several theoretical and experimental studies have been performed. As discussed in Chapter 3, most of the modelling studies of post-combustion CO_2 absorption in membrane contactors were conducted at laboratory-scale considering fresh solvents, low absorbent conversion, and isothermal behavior. Few studies have considered initially loaded solvent, high absorbent conversion, and adiabatic conditions, which can represent industrial operating conditions. Furthermore, despite the promising features of membrane contactors, there is still a lack of theoretical and experimental investigations of CO_2 capture in membrane contactors at large-scale except, to the best of my knowledge, the modelling studies conducted by Hoff and Svendsen (2013) and Kimball et al. (2014). Due to the large volume of flue gases coming from power plants, studies focusing on the modelling and design of industrial-scale membrane contactors are required.

The main objective of the present work is to develop a comprehensive two-dimensional mathematical model for CO_2 absorption using 30 wt% MEA in hollow fiber membrane contactor (HFMC) made of polytetrafluoroethylene (PTFE). The model is applied for simulation of CO_2 capture from a flue gas of an 800 MWe coal-fired power plant. This was intended to study the opportunities and challenges of the modelling, and design of CO_2 capture using large-scale HFMC modules. First, the effect of important parameters such as liquid-phase velocity, gas-phase velocity, solvent lean loading, membrane fiber length, and membrane mass transfer coefficient on the performance of industrial-scale HFMC modules are investigated. Then the specifications of the HFMC modules such as length, total volume, and total surface area required for 90% CO_2 capture from the flue gas of the coal-fired power plant are estimated. The results are compared with specifications of a packed column applied for the same case study from the literature. Finally, the model results are compared with pilot-scale experimental data from the literature.

The HFMC model equations are implemented in MATLAB. And the method of lines (MOL)[1] procedure is followed to solve the set of partial differential equations in the HFMC model.

[1]The MOL is based on converting a set of partial differential equations to a set of ordinary differential equations, which are then integrated using appropriate ODE solver.

1.3 Thesis Outline

The thesis is structured as follows:

Chapter 1 presents a background information of the present work pointing out the importance of membrane contactors for post-combustion CO_2 capture. In addition, the 3rd generation membrane contactor project at NTNU, and the objectives and methodology of the thesis are given in the same chapter.

Chapter 2 presents different approaches for CCS. The principles of membrane gas separation are briefly discussed. Furthermore, the principles of post-combustion CO_2 capture using chemical absorption is presented. Finally, discussions on the principles, and advantages and disadvantages of membrane contactors for gas absorption are presented.

Chapter 3 presents a literature review on modelling studies of post-combustion CO_2 capture using membrane contactors. A summary of the operating conditions and membrane specifications used in the studies cited is also presented.

Chapter 4 describes the modelling approaches used in the present work. This includes the mass and heat balance equations, reaction mechanism and kinetics, equilibrium model, and correlations used for estimating transport properties.

Chapter 5 presents the simulation results together with their corresponding discussions.

Chapter 6 presents a summary of conclusions drawn based on the discussions in chapter 5. Finally, recommendations for future work are presented in the same chapter.

MATLAB files of the thesis are available by request to diego.d.pinto@ntnu.no or hanna.knuutila@ntnu.no.

Chapter 2

CO_2 Capture and Storage

2.1 Introduction

Currently, global warming is one of the critical environmental issues all over the world. Research indicates that *" most of the observed increase in global average temperatures since the mid-20th century is very likely [> 90% chance] due to the observed increase in anthropogenic greenhouse gas concentrations "* (Parry, 2007). CO_2, chloro-fluorocarbons (CFCs), methane (CH_4), and nitrous oxide (N_2O) are the main greenhouse gases (GHGs) causing global warming (Caillol et al., 2011). CO_2 is the most important GHG, which contributes around 60% of the global temperature rise (Bruder et al., 2011). Figure 2.1 shows the evolution of atmospheric CO_2 concentration over the years measured at Mauna Loa Observatory, Hawaii (Tans, 2017). The red line indicates the atmospheric CO_2 measured for all seasons of the year while the black line represents average values over the year. The figure indicates that the atmospheric CO_2 concentrations have increased from about 280 ppm before the industrial revolution (around 1960) to about 400 ppm in 2015. If no control mechanism is implemented, the global concentration of CO_2 is projected to rise above 750 ppm by the end of the century (Wang et al., 2011). Power plants are the main source CO_2 emission, which contribute around 40% of the total CO_2 emission (Change, 2001; Freund, 2003). Thus, control of CO_2 emission from these main emission sources would be an important strategy to mitigate the carbon emissions. To reduce CO_2 emission, different measures have been proposed and followed by several countries (Leung et al., 2014):

- Increasing utilization of renewable energy sources in the power sector.
- Applying climate engineering schemes such as biochar production, and afforestation and reforestation.
- Energy conservation and efficient utilization of energy.
- Increasing utilization of fuels with low carbon content such as liquified petroleum gas (LPG).

- CCS.

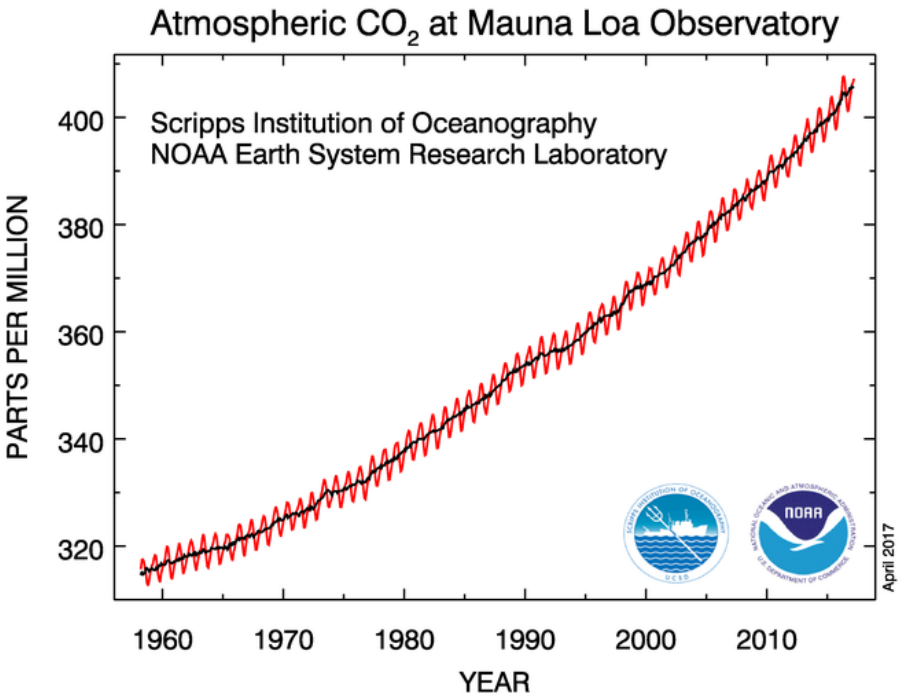

Figure 2.1: The evolution of atmospheric CO_2 concentration over the years measured at Mauna Loa Observatory, Hawaii. Reprinted from Tans (2017).

Amongst these measures to reduce CO_2 emission, CCS has been considered a vital approach to reduce CO_2 emission in the short term. Because it can be applied to fossil fuel based power plants and can achieve a higher CO_2 removal percentage (85-90%) (Leung et al., 2014). CCS involves separation and compression of CO_2 from flue gases, which is then transported for permanent storage or re-use. The cost of CO_2 capture process shares the major fraction of the overall cost of CCS (60-80%) (Metz et al., 2005; Blomen et al., 2009). Thus, the cost of CO_2 capture system needs to be reduced to make CCS more attractive. As a result, CO_2 capture is the most extensively studied stage of CCS.

2.1.1 Pathways of CO_2 capture

Generally, there are three ways to capture CO_2. These are pre-combustion, oxy-combustion, and post-combustion (see Figure 2.2) (Songolzadeh et al., 2014). Choice of these technologies is determined by the total pressure of an exhaust gas, partial pressure of CO_2 and the type of fuel utilized (gas, liquid or solid) (Leung et al., 2014).

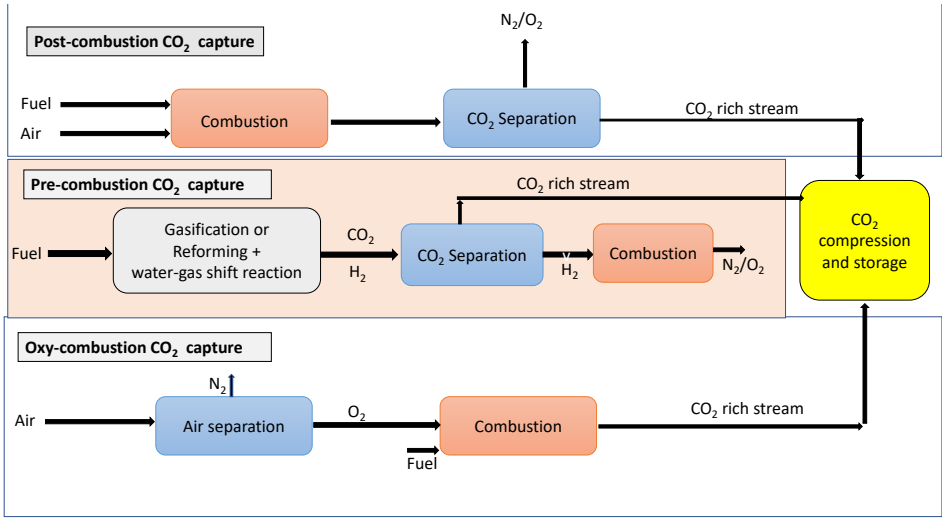

Figure 2.2: Types of CO_2 capture system from stationary sources. Adapted from Songolzadeh et al. (2014).

Pre-combustion CO_2 capture is based on a conversion of a fuel to synthesis gas (CO/H_2 mixture). CO in the product gas mixture reacts with steam to produce CO_2 and more H_2 . This reaction is called water gas shift reaction. The CO_2 is separated and the H_2 rich gas stream can be supplied to combustion turbine for electricity generation (Blomen et al., 2009; Songolzadeh et al., 2014). The main advantage of pre-combustion CO_2 capture is the higher partial pressure of CO_2 that can be achieved. This results in higher driving force for CO_2 separation. The main disadvantage of this pathway is the need of fuel processing and an extended unit operations ahead of the turbine (Blomen et al., 2009; Olajire, 2010).

Oxy-combustion CO_2 capture is based on the use of high purity oxygen for combustion of a fuel, which results in a flue gas consisting of largely water vapor and CO_2. CO_2 can be then separated by condensing the water vapor. This technology offers several advantages such as (i) high flame temperature, (ii) reduction of NOx emission, (iii) high CO_2 concentration (above 80% v/v) thus providing the potential of 100% CO_2 removal, and (iv) physical unit operations are used for CO_2 capture and O_2 production thus avoiding the use of chemicals (Blomen et al., 2009; Olajire, 2010; Songolzadeh et al., 2014). However, production of pure oxygen has a higher capital cost, and energy penalty (Blomen et al., 2009; Olajire, 2010; Songolzadeh et al., 2014).

Post-combustion CO_2 capture (PCC) involves separation of dilute CO_2 from flue gas after combustion of a fuel. This technology also removes NOx and SOx in addition to CO_2. Air is used for combustion, which results in a flue gas with a low concentration of CO_2. Table 2.1 shows typical compositions and conditions of flue gases of coal-fired and

natural gas-fired power plants. PCC is the most promising technology among the three strategies of CO_2 capture, since it can be integrated to new power plants and applied to an existing power plants (Songolzadeh et al., 2014; Zhao et al., 2016). Besides, it has a relatively lower cost and provides flexibility to the power plant (Leung et al., 2014).

Several techniques can be employed for PCC. Some of these include absorption, membrane, adsorption and cryogenic separation as shown in Figure 2.3. Among these unit operations, absorption is the most mature and preferred technology (Rao and Rubin, 2002). Membranes, on the other hand, have modular nature and low footprint (Franco et al., 2008).

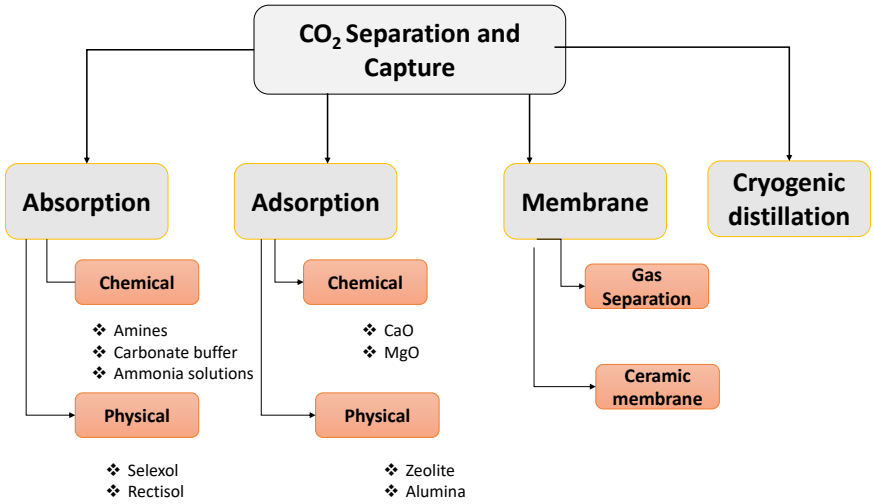

Figure 2.3: CO_2 separation and capture technologies. Adapted from Thiruvenkatachari et al. (2009)

Table 2.1: CO_2 concentration, temperature, and pressure of flue gases of coal-fired and natural gas-fired power plants. Data taken from Al-Fattah et al. (2011).

Source	Concentration of CO_2 (vol %)	Temperature (K)	Pressure (kPa)
Conventional coal-fired power plant	12-15	358-393	101.325
Natural gas fired conventional power plant (gas boiler)	7-10	358-393	101.325
Natural gas combined cycle power plant	3-4	368-378	101.325

2.2 Membrane Separation

In this process, a semi-permeable membrane is used for CO_2 separation. Separation is based on the permeability of the membrane for CO_2 (Feron et al., 1992). A pressurized CO_2 bearing flue gas is introduced to the membrane system. Then CO_2 is transferred through the membrane towards the low-pressure side of the membrane as shown in Figure 2.4. The driving force for separation is a pressure gradient over the membrane. This technology is easy to scale up, do not require any chemicals for separation, and requires small volume (Songolzadeh et al., 2014). However, since the partial pressure of CO_2 in flue gases is low, the driving force for post-combustion CO_2 separation using conventional membranes is low. Thus, a vast amount of energy is required for pressurizing the flue gas when membrane technology is applied for PCC. A study conducted by Brunetti et al. (2010) compared CO_2 separation performance of membranes with adsorption and cryogenic distillation separations. They indicated that the low partial pressure and concentration of CO_2 in flue gases significantly influenced the separation performance of membrane technology. Feron et al. (1992), in their study, indicated that the cost of membrane separation for PCC was two times higher than that of conventional amine absorption. The cost of flue-gas compression was the major contributor to the overall cost. Furthermore, they indicated that a two-stage system was required to get higher CO_2 capture rate.

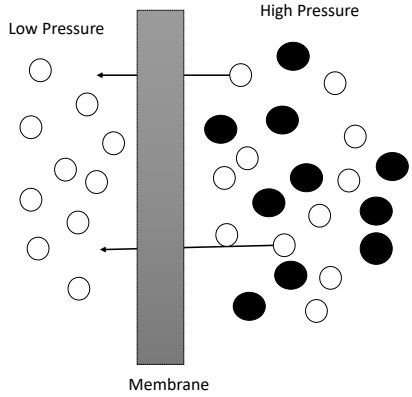

Figure 2.4: Principles of conventional membrane separation. Adapted from Feron et al. (1992)

An ideal membrane for PCC should have higher CO_2 selectivity and permeability, thermal and chemical stability, resistant to aging and plasticization, and relatively low cost (Brunetti et al., 2010). Several polymeric and inorganic membranes were studied for CO_2 separation. Generally, inorganic membranes had limited permeability and selectivity even though they had good thermal stability(Rui et al., 2009, 2011). Polymeric materials

such as polyaniline, polysulfones, and polyimides were also investigated for CO_2 capture application. These polymeric materials had higher CO_2 permeability and selectivity but limited thermal stability (Songolzadeh et al., 2014). To conclude, due to the high energy and large surface area requirement of membrane separation, extensive studies focusing on the preparation of materials for improved performance are still ongoing.

2.3 Chemical Absorption

CO_2 capture by absorption involves the transfer of CO_2 from the flue gas to a solution of absorbent in which it is soluble. Depending on the type of solvent used, absorption can be classified into two: physical and chemical absorption.

In **physical absorption**, CO_2 is transferred from the gas-phase to liquid-phase without chemically reacting with the absorbent (Dindore et al., 2005). The loaded solvent is then regenerated, for instance, by reducing the operating pressure. Physical absorption is suitable for bulk removal of CO_2 from gas streams having a high partial pressure of CO_2. This method has a simple design, low toxicity, and low solvent loss. However, it has limited CO_2 selectivity and is not suitable for removal of dilute CO_2 from exhaust gases. Thus, it is not suitable for treatment of power plant flue gases, which have a low partial pressure of CO_2 (Olajire, 2010).

Chemical absorption involves a reversible reaction between the solvent and CO_2, which produces a loosely bound intermediate product. The loaded solvent is then regenerated by reversing the equilibrium of the chemical reaction by increasing temperature of the system. Chemical absorption of CO_2 from flue gases have been in practice since the 1970s. Thus, this technology is a commercially recognized process. Figure 2.5 shows a typical flow sheet of PCC by chemical absorption. Sulfur free flue gas is cooled to absorption temperature (318-323 K) to increase the rate of CO_2 absorption and to prevent solvent loss. Then, the cooled flue gas enters the absorption column in a counter-current mode with the solvent. In the absorber, the CO_2 chemically reacts with the solvent. The treated gas is then emitted after being water washed to prevent solvent loss. The CO_2 loaded solvent passes through a cross heat exchanger where it takes heat from the lean solvent. It is then pumped to the top of a desorber, where CO_2 is released by applying steam at a higher temperature (373-393 K) and pressure (152-202.6 kPa) (Metz et al., 2005). Heat is required in the desorber for heating up the solvent, for steam production and for reversing the chemical reaction. The heat requirement of the desorber is provided by the reboiler. The regeneration step is energy intensive and it is responsible for most of the process energy penalty (Davidson, 2007). The lean solvent leaving the stripper is cooled to 313-338 K in the cross heat exchanger and additional cooler before it is pumped back to the absorber. The stream leaving the top of the stripper is partially condensed, leaving a CO_2 rich stream which is compressed for storage or utilization (Rao and Rubin, 2002; Zhao et al., 2016).

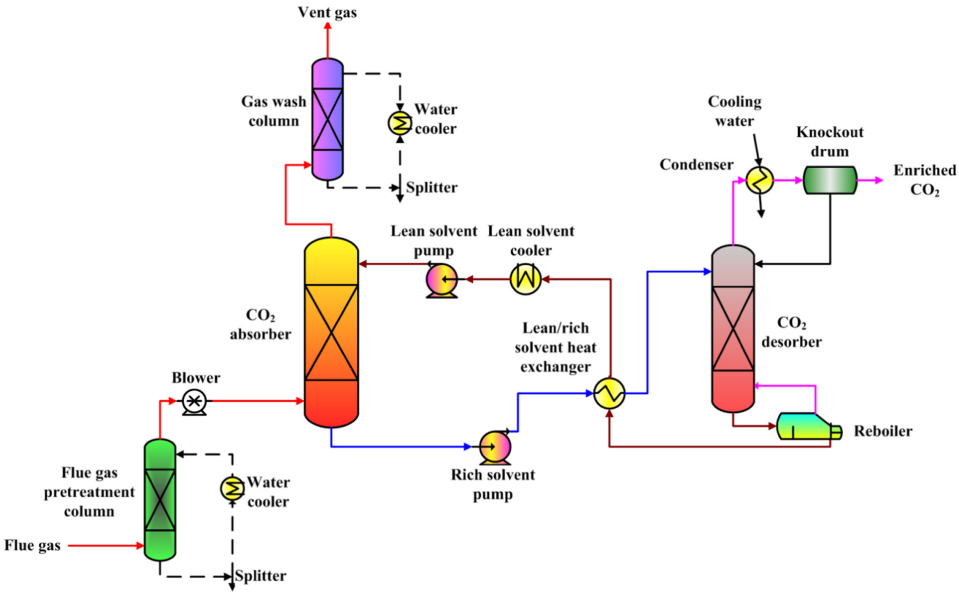

Figure 2.5: Typical flowsheet of post-combustion CO_2 capture by chemical absorption. Reprinted from Zhao et al. (2016).

2.3.1 Solvents for chemical absorption

An ideal solvent for application in PCC should have (Davidson, 2007):

- High rate of reaction with CO_2 - which would result in the reduction of the height of the absorption column and/or rate of solvent re-circulation.
- Low heat of reaction- which would reduce the energy requirement for solvent regeneration.
- High loading capacity for CO_2-which would reduce solvent re-circulation rate.
- Low volatility to prevent solvent loss.
- Nontoxic to the environment and biological system.
- Low cost.
- Thermal and chemical stability- which would reduce solvent replacement cost.

Alkanolamines are the commonly used absorbents for CO_2 capture due to their relatively higher cyclic capacity, higher CO_2 selectivity, suitability for flue gases with low -to moderate partial pressure of CO_2, lower cost and solvent recirculation rate, and fast reaction rate (Olajire, 2010; Wang et al., 2011; Luis et al., 2012a). There are three classes of alkanolamines depending on their structure. These are a) primary amines like MEA, b) secondary amines like diethanolamine (DEA), and c) tertiary amines like triethanolamine

(TEA).

CO_2 absorption using MEA is the most commercialized, proven, and reference technology. MEA has a high rate of CO_2 absorption, high cyclic capacity on a mass basis, realistic chemical and thermal stability, and relatively lower cost (Rao and Rubin, 2002; Davidson, 2007; Olajire, 2010). Thus, streams with almost pure CO_2 can be obtained when using MEA as absorbent. However, MEA has some disadvantages such as (i) high heat of reaction, which leads to large energy requirement for regeneration, (ii) corrosive nature, and (iii) low CO_2 loading on mole basis (Wang et al., 2011). Several absorbents such as Methyl diethanolamine (MDEA), TEA, blends of amines, and carbonate buffers are being studied. The purpose is to get solvents, which are better than MEA and have good balance between cyclic capacity, absorption rate and heat of absorption.

2.3.2 Advantages and disadvantages of chemical absorption

Packed column is the traditional gas-liquid contacting device in the chemical absorption of CO_2 from flue gases (deMontigny et al., 2005). The advantages of PCC using chemical absorption in packed column can be summarized below:

- It can be applied to new plants and retrofitted to existing ones.
- Solvent regeneration in the desorber means the solvent is recycled. This decreases the cost of solvent replacement.
- Product gas stream with high purity of CO_2 (above 95%) can be achieved.
- The technology is well known and proven, and new solvent systems are under study.

Unfortunately, PCC using chemical absorption in packed column has several disadvantages as discussed below:

- The regeneration system requires a large amount of energy, which results in high operating cost. The cost of power consumption in combustion plants is estimated to increase by 50-90% if amine-based absorption is utilized for 90% CO_2 capture from flue gases of the plant (Luis et al., 2012a). The solvent regeneration energy requirement can be minimized by identifying novel solvents with low heat of reaction together with high CO_2 loading capacity, fast reaction kinetics and higher CO_2 selectivity compared to 30% MEA. As discussed in section 1.1.2, *"phase change solvents"* are one of the novel solvents that have shown the potential to minimize the energy requirement of amine-based CO_2 capture. The major problem of these novel solvents is their high volatility, which can lead to solvent losses and emissions. Heat-integration can also decrease the energy penalty of the process.
- A large volume of flue gas needs to be treated due to the low pressure of flue gas (around 101.3 kPa) and dilute CO_2 in the flue gas (less than 16%)(see Table 2.1). This results in a huge size of CO_2 capture units and high associated investment cost (Olajire, 2010; Leung et al., 2014; Zhao et al., 2016).

- The technology faces several operational problems such as flooding, channeling, and foaming due to the interdependence of the gas and liquid-phases.
- Corrosion of equipment.
- Solvent losses due to degradation, evaporation or entertainment.

PCC using membrane contactors have been suggested as a promising substitutes to the CO_2 capture in the traditional absorbers (Gabelman and Hwang, 1999; Klaassen et al., 2005; Cui and deMontigny, 2013).

2.4 Membrane Contactors

2.4.1 Principles of membrane contactor

Membrane contactor technology combines the principles of membrane separation and absorption technology (Cui and deMontigny, 2013). Membrane contactors have been in use for gas and water treatments in different sectors such as chemical, pharmaceutical and petrochemical industries (Klaassen et al., 2008). Among these applications, PCC has, currently, got a great attention by researchers (Favre and Svendsen, 2012). A membrane is an essential element of this technology. The flue gas flows on one side of the membrane while the liquid-phase flows on the other side. Unlike the traditional membrane separation processes, which provide selectivity, the membrane in membrane contactors does not provide any selectivity for a component. It acts as a barrier between the fluids and provides a higher interfacial area for mass transfer (Klaassen et al., 2005; Cui and deMontigny, 2013). The selectivity is offered by the absorbent since an absorbent with a higher affinity towards the target component (CO_2 in this case) is used in this technology (Klaassen et al., 2005).

Transport of CO_2 from the gas-phase to the liquid-phase occurs by diffusion. The mass transfer can be divided into three steps (Klaassen et al., 2005) :

- Diffusion of CO_2 from the bulk gas-phase towards the membrane,
- Transport of CO_2 through the membrane pores towards the membrane-liquid interface, and
- CO_2 transfer from the membrane-liquid interface towards the bulk liquid-phase, where absorption takes place.

Thus, three resistances are involved in the transport of CO_2 from the gas-phase to the liquid-phase (see Figure 2.6). These are a) the gas-side mass transfer resistance, b) the membrane mass transfer resistance, and c) the liquid-side mass transfer resistance. The transport of CO_2 in membrane contactor can be modeled as a series of resistances. The same principle applies if other species such as water transfers between the two phases.

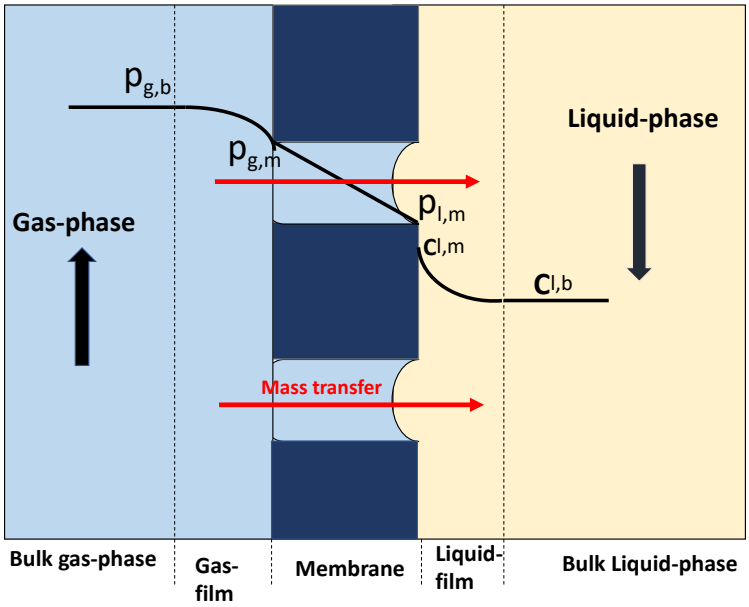

Figure 2.6: Concentration profiles of a species transferring from a gas-phase through a membrane pores to a liquid-phase. The membrane is filled by gas-phase. Adapted from Zhao et al. (2016).

The flux of a transfer component i in the three regions shown in Figure 2.6 can be expressed using the following expressions:

$$N_{g,i} = k_g(p_{g,b} - p_{g,m}) \tag{2.1}$$
$$N_{m,i} = k_m(p_{g,m} - p_{l,m}) \tag{2.2}$$
$$N_{l,i} = k_l(C_{l,m} - C_{l,b}) \tag{2.3}$$
$$\tag{2.4}$$

where $N_{g,i}$, $N_{m,i}$, and $N_{l,i}$ are the flux of species i in the gas film, membrane pores, and liquid film, respectively; k_g, k_m, and k_l are the gas, membrane, and liquid mass transfer coefficients, respectively; $p_{g,b}$, $p_{g,m}$, and $p_{l,m}$ are the partial pressure of transfer component at the bulk gas-phase, gas-membrane interface, and membrane-liquid interface, respectively; $C_{l,m}$, and $C_{l,b}$ are concentrations of the transfer component at the liquid-membrane interface, and bulk liquid-phase, respectively.

At steady state, the flux terms are equal (Zhao et al., 2016):

$$N = k_g(p_{g,b} - p_{g,m}) = k_m(p_{g,m} - p_{l,m}) = k_l(C_{l,m} - C_{l,b}) \tag{2.5}$$

The partial pressure and concentration terms of a species at the gas-liquid interface can be related to each other using an equilibrium expression. When a liquid and gas-phases are contacted, a species in the gas-phase dissolves in to the liquid-phase until an equilibrium

state is attained. At equilibrium, the partial pressure of the species in the gas-phase and its concentration in the liquid-phase can be related using Henry's law (Wiesler, 1996), which is given below:

$$p_i = HC_i \tag{2.6}$$

where p_i and C_i are the partial pressure and concentration of species i, respectively; H is Henry's constant, which is a function of the temperature of the liquid-phase.

Equation 2.6 can be used to determine the partial pressure term if the concentration term is known and vice-versa. The application of equation 2.6 in membrane contactors mass transfer modelling is to relate the gas-liquid interface partial pressure and concentration terms in equation 2.5. This is given below:

$$P_{l,m} = HC_{l,m} \tag{2.7}$$

Applying Henry's law, equation 2.5 can be expressed in terms of overall mass transfer coefficients, and the bulk partial pressure and concentration terms as follows:

$$N = K_g(P_{g,b} - HC_{l,b}) = K_L(\frac{P_{g,b}}{H} - C_{l,b}) \tag{2.8}$$

where K_g and K_L are the overall mass transfer coefficients based on the gas-phase and liquid-phase, respectively.

Combining equations 2.5, 2.7 and 2.8, the following expressions for the overall mass transfer coefficients is obtained:

$$\frac{1}{K_g} = \frac{1}{k_g} + \frac{1}{k_m} + \frac{H}{k_l} \tag{2.9}$$

$$\frac{1}{K_L} = \frac{1}{k_g H} + \frac{1}{k_m H} + \frac{1}{k_l} \tag{2.10}$$

The above expressions show that the total mass transfer resistance is the sum of the gas-phase, membrane, and liquid-phase resistances.

When a hollow fiber membrane contactor is used and the effect of a curvature in the tube is significant, it should be considered in the mass transfer coefficient expressions. The following expressions are proposed when the liquid-phase flows on the tube side and the gas-phase flows on the shell side (Zhao et al., 2016):

$$\frac{1}{K_g} = \frac{1}{k_g} + \frac{d_o}{k_m d_{ln}} + \frac{H d_o}{k_l d_i} \tag{2.11}$$

$$\frac{1}{K_L} = \frac{d_i}{d_o k_g H} + \frac{d_i}{k_m H d_{ln}} + \frac{1}{k_l} \tag{2.12}$$

where d_i, d_o and d_{lm} are the inner, outer and log mean diameters of the tube, respectively.

If there is a chemical reaction during mass transfer, an enhancement factor should be considered in the above expressions. The following expressions are proposed for a liquid-phase flowing on the tube-side (Zhao et al., 2016):

$$\frac{1}{K_g} = \frac{1}{k_g} + \frac{d_o}{k_m d_{ln}} + \frac{H d_o}{k_l E d_i} \tag{2.13}$$

$$\frac{1}{K_L} = \frac{d_i}{d_o k_g H} + \frac{d_i}{k_m H d_{ln}} + \frac{1}{E k_l} \tag{2.14}$$

where E is the enhancement factor, which considers the effect of chemical reaction on the rate of mass transfer.

2.4.2 Types of membrane module

In membrane contactors, the membranes can be organized as either a flat sheet or tubular. Flat sheet membrane arrangement can be easily fabricated and assembled. However, its application for CO_2 capture is not widely studied due to its much lower surface area to volume ratio (Zhang et al., 2008). In tubular membrane arrangement, the membranes are applied as a package of hollow fibers as shown in Figure 2.7. These HFMCs have been extensively studied for PCC because of their higher surface area to volume ratio. The configuration of the fibers in HFMC is like a shell and tube heat exchanger. The gas-phase flows either on the shell or tube-side and the liquid-phase flows on the opposite side of the membrane. Two type of membrane modules can be identified depending on the flow direction of the fluids relative to each other (Li and Chen, 2005). These are cross-flow and parallel-flow modules .

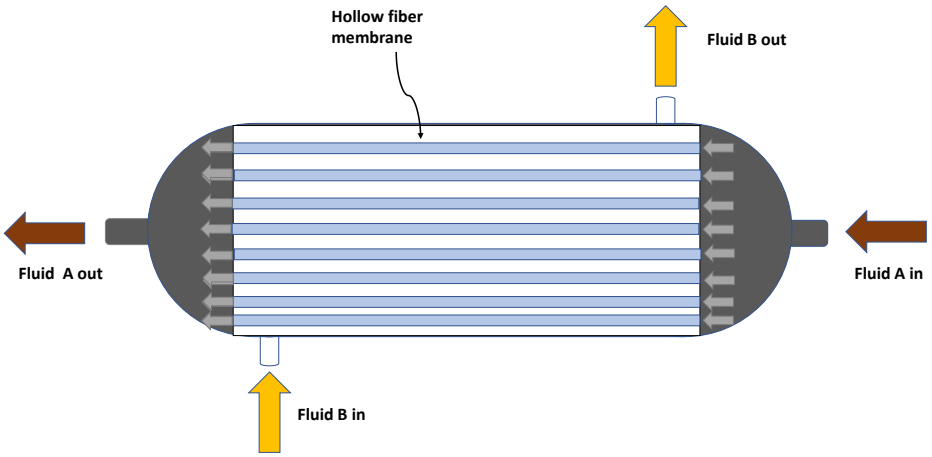

Figure 2.7: Hollow fiber membrane contactor in parallel-flow module (counter-current flow configuration). Adapted from Valdés et al. (2009).

Parallel-flow module

Parallel-flow module is also known as longitudinal flow module. In this configuration, the two fluids flow on the opposite side of the membrane in parallel to each other. The fluids can flow co-currently or counter-currently relative to each other. This module is the simplest and can be easily fabricated compared to the cross-flow configuration. As a result, this is the most researched module (Li and Chen, 2005; Zhao et al., 2016). However, this membrane module has lower CO_2 capture efficiency relative to the cross-flow module (Li and Chen, 2005; Cui and deMontigny, 2013). In addition, the performance of industrial application of this type of module can be affected by fluid-channeling and bypass on the shell side (Wickramasinghe et al., 1992). Improvements of this type of module have been developed and applied commercially. A typical example of the improvement of parallel-flow module is the *"Liqui-Cell Extra-Flow"* membrane contactor as shown in Figure 2.8. In this module, the important features of cross-flow module are combined by introducing a baffle into the center of the shell. The baffle minimizes shell side fluid bypass and allows fluid to flow perpendicularly to the membrane surface. This membrane module allows both counter-current flow configuration and cross-flow. The first one provides a higher driving force for separation, and the later one enhances the mass transfer coefficient. As a result, the mass transfer rate is enhanced (Sengupta et al., 1998).

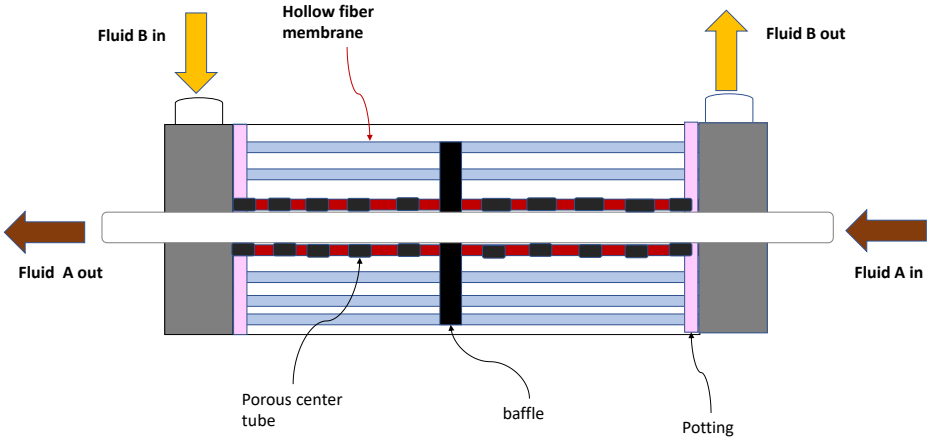

Figure 2.8: *"Liqui-Cell Extra-Flow"* membrane contactor. Adapted from Sengupta et al. (1998).

Cross-flow module

Even though parallel-flow modules are the most researched, cross-flow modules are the most efficient . Because the several baffles introduced on the shell-side of the module minimize shell side fluid bypass and channelling, and increase flow turbulence (Wickramasinghe et al., 1992). A typical example of cross-flow module is the membrane contactor

patented by Aker Kvaerner of Norway as shown in Figure 2.9. This membrane contactor has been tested on a pilot-scale. It was found that corrosion problems, and equipment size and weight were significantly reduced. Furthermore, higher packing density was achieved and the frequent problems of packed bed columns such as flooding, foaming, and channeling were not observed (Falk-Pedersen et al., 2005).

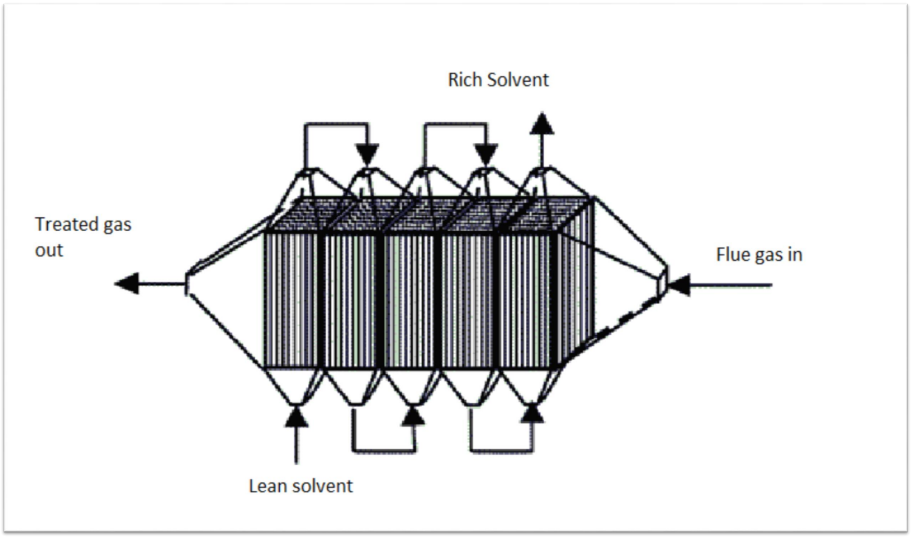

Figure 2.9: Membrane contactor with cross-flow configuration patented by Aker Kvaerner of Norway. Adapted from Hoff et al. (2004).

2.4.3 Membrane materials in membrane contactors

An ideal membrane in membrane contactors should have thermal and chemical stability, and should avoid membrane wetting (Zhao et al., 2016). Microporous membrane are usually used in membrane contactors. However, other membrane types like composite membranes, self-standing dense membrane, and membranes incorporated with nano-particles are also used for CO_2 capture. Microporous and composite membranes are discussed in the following sections.

Microporous membranes

Hydrophobic microporous membranes are the most commonly used membranes in membrane contactor. Several types of polymers such as PTFE, polypropylene (PP), polyvinylidene fluoride (PVDF), polyethylene, and polytriflouroethylene have been used for manufacturing hydrophobic microporous membranes. The surface energy (in mN m^{-1}) of these materials provided by Mulder (2012) is given below:

- PTFE : 19.1

- Polytriflouroethylene : 23.9
- PP : 30
- PVDF :30.3
- Polyethylene :33.2

The cosine of the contact angle between the membrane surface and the absorbent is lower if the surface energy of the membrane material is higher (Mulder, 2012). This condition favors membrane wetting as discussed in section 2.4.5.

Membrane mass transfer coefficient is a measure of the performance membranes. PP and PVDF are relatively inexpensive and have higher membrane mass transfer coefficient (within 10^{-3}- 10^{2} ms^{-1}) (Luis et al., 2012a), which makes them a good candidate for application in CO_2 absorption. However, these materials have a higher surface energy (as shown above), which makes them less resistant to membrane wetting. On the other hand, PTFE membranes are chemically stable, have higher resistance to membrane wetting due to their lower surface energy, and have acceptable membrane mass transfer coefficient (within 10^{-4} -10^{-3} ms^{-1}) (Chabanon et al., 2011). This makes them a potential candidate for CO_2 capture application. However, these polymers are relatively expensive.

Khaisri et al. (2009) studied absorption of CO_2 using water and MEA in HFMCs made of PP, PTFE, and PVDF. The authors indicated that PTFE had the highest performance followed by PVDF when using MEA as an absorbent. Besides, the performance of PVDF membrane was higher than that of PP membrane when using water as an absorbent. The long-term stability of the membranes was also compared and it was found that the HFMC made of PTFE maintained its performance when operated for about 60 hours while the membrane contactor made of PVDF had decreased its performance over time.

Composite membranes

As discussed in section 2.4.5, the major challenge of using hydrophobic microporous membrane is the membrane wetting by the aqueous solution. Kreulen et al. (1993b) suggested that the wetting problems of the microporous membrane could be solved by using composite membranes. Composite membranes are prepared by coating a dense, very thin polymer layer on the absorbent side of the porous membrane. This layer prevents membrane wetting, and improves the thermal and chemical stability of the membrane. However, the polymer skin should have good thermal and chemical stability, good permeability to the target component, and negligible mass transfer resistance (Zhao et al., 2016).

Poly(dimethylsiloxane) (PDMS), poly(1-trimethylsilyl-1-propyne) (PTMSP) and Teflon AF are some of the most widely utilized polymers for preparing the dense layer. Kreulen et al. (1993b) compared the mass transfer resistance of uncoated microporous membrane with a microporous coated with a thin layer of silicone rubber (0.7 micro meter). They reported that both membranes had comparable mass transfer resistance. Kneifel et al. (2006) conducted a similar study using a thin layer of silicon as a coating polymer and they found

that the CO_2 permeability of the membrane was reduced by about 20% when the coating was applied. However, they said that the reduction in membrane permeability could be compensated at the expense of applying higher pressure, which increases the driving force.

2.4.4 Choice of absorbents for membrane contactor application

Ideally, the same solvents used for chemical absorption in packed column could be applied for CO_2 absorption in membrane contactors. Several absorbents such as amines, pure water, ammonia, aqueous alkaline solutions, and amino acids have been theoretically and experimentally studied for CO_2 absorption in HFMCs. Among these, amines, especially MEA, are the most widely used and studied. An ideal absorbent for CO_2 absorption in HFMCs should have the following properties (Dindore et al., 2004; Li and Chen, 2005) together with the properties discussed in section 2.3.1:

- Higher surface tension to prevent membrane wetting. According to equation 2.15, high surface tension of a solvent leads to a high *break-through* pressure thereby reducing the membrane susceptibility to membrane wetting.
- Chemically compatible with the membrane. The solvent should not damage the membrane.
- Low viscosity to avoid high mass transfer resistance and pressure drop.

An absorbent satisfying all those criteria has not been found yet.

2.4.5 Advantages and disadvantages of membrane contactors

Membrane contactors have several advantages compared to the traditional absorption devices such as packed column, bubble column, and spray tower. These are discussed below:

- The main advantage of membrane contactors come from the combination of the principles of absorption technology, which provides selectivity, with the membrane technology, which is compact and modular (Zhao et al., 2016). Membrane contactors could enhance the surface area to volume ratio for mass transfer by 30-fold compared to the tradition gas absorption columns, which results in a higher mass transfer rate (Gabelman and Hwang, 1999). A comparison of the interfacial area (in m^2m^{-3}) of different gas-liquid contactors provided by Pozio and Tosti (2013) is given below:
  - Membrane contactor:1500-3000
  - Packed column:100-800
  - Mechanically agitated column:50-150
  - Packed/trayed column: 10-100
  - Free dispersion column:1-10

- Due to the increase in CO_2 absorption rate, the size of absorber could be significantly reduced when using membrane contactors instead of the traditional columns. According to the study conducted by Feron et al. (1992) and Klaassen et al. (2005), the volume of a membrane contactor could be reduced by a factor of 10 compared to the conventional absorber columns. Furthermore, a study conducted by Yeon et al. (2005) indicated that the energy consumption per unit of CO_2 captured in membrane contactor is lower than that of packed column.

- The specific surface area of membrane contactors depends only on the geometric characteristics of the contactor. It is independent of the operating conditions. As a result, the performance of the contactor can be easily predicted based on its geometric characteristics (Gabelman and Hwang, 1999; Li and Chen, 2005).

- The separation of the liquid-phase and gas-phase using a membrane allows control of the two phases independently. This avoids the frequent operational problems experienced in packed columns such as foaming, channeling, flooding, and entrainment (Gabelman and Hwang, 1999; Li and Chen, 2005; Cui and deMontigny, 2013).

- Membrane contactors can be easily scaled-up linearly by adding additional modules due to their modular nature(Cui and deMontigny, 2013).

- Membrane contactors can prevent emissions/losses of solvent with high volatility. The *"phase change solvents"* are typical example of solvents with high volatility as discussed in 1.1.2.

Unfortunately, membrane contactors also have some disadvantages. These are presented below (Gabelman and Hwang, 1999; Li and Chen, 2005; Cui and deMontigny, 2013; Leung et al., 2014):

- An extra mass transfer resistance is introduced by the membrane. However, this resistance is compensated by the large surface area to volume ratio offered by the membrane.

- Membrane wetting is the major challenge encountered in membrane contactors when using porous membrane. A study conducted by Rangwala (1996) indicated that at a membrane wetting of about 2%, the contribution of the membrane mass transfer resistance to the total mass transfer resistance could be greater than 60%. The principles of membrane wetting are discussed in the following section.

- Membrane fouling could occur.

- Channeling and bypass of fluid on shell side could also occur, which reduces the performance of the membrane contactor.

- Membrane degradation, and limited lifetime.

Principles of membrane wetting

As discussed previously, a hydrophobic porous membrane is the most commonly used membranes in membrane contactor. When using a hydrophobic porous membrane, the pores in the membrane can be occupied by gas components while preventing the entrance of aqueous phases. However, the operating pressure needs to be controlled to prevent mixing of the two phase. First, the pressure of the liquid-phase should be greater than or equal to the pressure of gas-phase to prevent dispersion of one phase into another phase (Drioli et al., 2011). Note that the membrane losses its hydrophobic nature if the pressure exerted on the liquid-phase surpasses a limiting pressure called *break- through* pressure. This results in wetting of the membrane pores providing additional mass transfer resistance (Li and Chen, 2005; Zhao et al., 2016). *Break-through* pressure (P_b) is defined as the minimum pressure that must be exerted on the liquid-phase if the liquid-phase is needed to enter to pores of the membrane. It is given by the Laplace-Young equation as follows (Franken et al., 1987):

$$P_b = \frac{-4B\gamma cos\theta}{d_{max}} \tag{2.15}$$

where γ, d_{max}, θ are the liquid surface tension, maximum membrane pore diameter, and the contact angle between the liquid-phase and membrane surface, respectively, and B is the coefficient of pore geometry($0 \leq B \leq 1$; B=1 for cylindrical pores).

Membrane wetting occurs when the pressure exerted on the liquid-phase is higher than the *break-through* pressure. According to equation 2.15, three approaches to prevent membrane wetting include: (i) using liquid-phase with higher surface tension, (ii) increasing the cosine of the contact angle between the membrane and the liquid-phase, and (iii) using membranes with an optimized pore dimensions, which allows to have higher *break-through* pressure while keeping higher mass transfer coefficient (Li and Chen, 2005). All these three measures maintain higher *break-through* pressure thereby preventing membrane wetting. In the case of composite membranes, the thin coating layer prevents membrane wetting by maintaining higher *break-through* pressure due to their lower d_{maz} (Zhao et al., 2016).

Membrane wetting can be partial or complete wetting. In the first case, the membrane pores are partially wetted by the liquid-phase and there is an interface between the two phases. In the complete wetting mode, the membrane pores are completely occupied by the liquid-phase and the two phases are mixed leading to loss of the membrane functionality (Cui and deMontigny, 2013).

Chapter 3

Literature Review on Modelling of Membrane Contactors for CO_2 Absorption

3.1 Introduction

Qi and Cussler (1985) introduced membrane contactors for CO_2 absorption. They investigated CO_2 absorption using NaOH solution in a HFMC made of PP. They compared HFMC with packed column, and indicated that the overall mass transfer coefficient in the HFMC was higher than that of packed column by a factor of 30. Since then, several experimental and theoretical studies on HFMCs investigate the effect of different parameters on the efficiency of CO_2 absorption. Most of the experimental investigations were performed on laboratory-scale using MEA as a solvent. For the theoretical studies of HFMCs, mathematical models of various complexities have been developed. An overview of the modelling studies of HFMCs for PCC is given in this chapter and is divided in three main sections as follows:

- Isothermal Modelling Studies of HFMCs
- Adiabatic Modelling Studies of HFMCs
- Conclusions from Literature Review

3.2 Isothermal Modelling Studies of HFMCs

Several mathematical models of CO_2 absorption in HFMCs have been developed based on the assumption of isothermal behavior thereby neglecting the heat of reaction and heat transfer between the gas and liquid-phases. These models vary from simple one-dimensional (1D) models to one dimensional-two dimensional (1D-2D) models and to

complex two-dimensional (2D) models as discussed in the sections below.

3.2.1 Isothermal 1D and 1D-2D modelling studies

Rode et al. (2012) developed an isothermal 1D model of PCC using HFMC under industrial operating conditions. They assumed axial plug flow for the gas-and liquid-phases, constant mass transfer coefficient and laminar flow. They found that a greater CO_2 capture rate can be achieved by reducing the external fiber diameter and that it should be considered a main parameter in process optimization. Furthermore, they concluded that liquid-phase flowing on the shell side and gas-phase flowing on the tube side of the HFMC gives the best separation performance.

Several authors have developed isothermal 1D-2D models of CO_2 absorption in HFMCs (Dindore et al., 2004; Wang et al., 2004; Zhang et al., 2006; Gong et al., 2006; Zhang et al., 2008; Keshavarz et al., 2008b). These models were developed based on assumptions of axial plug flow in the gas-phase while considering radial diffusion and axial convection contributions in the liquid-phase. Besides, the models considered gas-phase flowing on the shell side and liquid-phase flowing on the tube side except the study conducted by Zhang et al. (2008), which compared both flow configurations. Tables 3.1 and 3.2 presents the gas-phase and solvent conditions, and the membrane specifications used in the isothermal 1D and 1D-2D models cited in this work, respectively.

Dindore et al. (2004) performed theoretical and experimental investigations of CO_2 capture using HFMCs. The study was conducted at higher gas-phase pressures (up to 2000 kPa) using propylene carbonate (PC) as solvent. In their 1D-2D model, they assumed fully developed laminar flow and negligible axial diffusion. They found that the overall mass transfer coefficient was mainly determined by the liquid side mass transfer resistance even at elevated gas-phase pressures. Furthermore, they observed membrane wetting when the gas-phase pressure was reduced to atmospheric pressure. The authors concluded that the observed membrane wetting can be avoided by increasing the gas-phase pressure.

Wang et al. (2004) developed a 1D-2D HFMC model to study CO_2 absorption using 2-amino-2- methyl-1-propanol (AMP), MDEA and DEA as an absorbent. They used the orthogonal collocation method to solve the model, which was validated against literature data. The authors found that fiber radius and length, and flow rate and concentrations of the solvents have significant effect on CO_2 absorption using AMP and DEA. They also observed higher CO_2 flux and depletion of absorbents in the gas-liquid interface when using AMP and DEA than MDEA.

Zhang et al. (2006) developed a similar 1D-2D model to study CO_2 absorption using aqueous DEA solutions in HFMC made of PP. They assumed ideal gas, laminar flow, and negligible axial diffusion. They applied the method of lines (MOL) to solve the model equations and the model was validated against experimental data. They found that gas-phase velocity had a significant effect on chemical absorption of CO_2 while liquid-phase velocity had negligible effect. They also found that increasing the length of the membrane

beyond a certain limit did not enhance CO_2 capture. The limit increases with increase in inlet gas-phase velocity. For example, for gas-phase velocity of 0.032 ms^{-1} the limit was 112.8×10^{-3} m.

Gong et al. (2006) developed a 1D-2D mathematical model to study CO_2 absorption using aqueous solution mixtures of MEA/MDEA in HFMC. They assumed ideal gas, fully developed laminar flow and negligible axial diffusion. The model was validated against experimental data. They found that CO_2 flux increased with increasing solvent flow rate and fraction of MEA. They also observed higher depletion of MEA in the gas-liquid interface compared to MDEA.

Zhang et al. (2008) developed a 1D-2D model for CO_2 absorption in HFMCs using DEA as a solvent. In their model, they assumed fully developed laminar flow in the tube side and stagnant gas in the membrane pores. Happel's free surface model was used to characterize the flow on the shell side. The model was validated against data gained from experiments using HFMCs made of PVDF and PP. The authors observed a significant drop of CO_2 flux in both types of membranes due to membrane wetting. The wetting phenomena occurred after two days of operation for PP.

Keshavarz et al. (2008b) developed a 1D-2D model to study the effect of partial membrane wetting on CO_2 absorption in aqueous solutions of DEA in HFMC. They assumed laminar flow, ideal gas and uniform membrane pore size distribution. The model was numerically solved using finite difference scheme and validated against experimental data obtained from the literature. According to their model results, membrane wetting resulted in a significant reduction of CO_2 capture.

3.2.2 Isothermal 2D modelling studies

More rigorous isothermal 2D mathematical models for CO_2 absorption in HFMCs have also been developed by several authors (Eslami et al., 2011; Boucif et al., 2012; Chabanon et al., 2013; Saidi et al., 2014; Zaidiza et al., 2014; Farjami et al., 2015; Hosseinzadeh et al., 2017). These models consider the contributions of axial convection and radial diffusion in both the liquid and gas-phases. All studies considered gas-phase flow on the shell side and liquid-phase on the tube side. However, the study conducted by Chabanon et al. (2013) also considered the opposite configuration. Tables 3.3 and 3.4 presents the membrane specifications used in the isothermal 2D models, and the gas-phase and solvent conditions of the 2D models, respectively.

Eslami et al. (2011), Saidi et al. (2014) and Hosseinzadeh et al. (2017) proposed similar 2D mathematical models for CO_2 absorption in HFMC. COMSOL software was used to solve the mathematical models. They found that increasing solvent flow rate and concentration, and decreasing gas-phase velocity enhanced CO_2 flux. Furthermore, increasing liquid-phase temperature (Eslami et al., 2011; Saidi et al., 2014), and number of fibers (Saidi et al., 2014) had positive impact on CO_2 absorption.

Table 3.1: Liquid-phase and gas-phase conditions of 1D and 1D-2D isothermal modelling studies of CO_2 absorption in HFMCs. Unless otherwise indicated, the studies were conducted at laboratory-scale.

	(Rode et al., 2012)	(Dindore et al., 2004)	(Zhang et al., 2008)	(Zhang et al., 2006)	(Wang et al., 2004)	(Keshavarz et al., 2008)	(Gong et al., 2006)
Gas-phase							
Type	Wetted flue gas	N_2/CO_2 mixture	N_2/CO_2 mixture	N_2/CO_2 mixture	Pure CO_2	N_2/CO_2 mixture	N_2/CO_2 mixture
Velocity [ms^{-1}]	-	-	-	0.073	-	0.073	0.0035-0.023
Temperature [K]	313	293.16-298.16	-	298	-	-	298
Pressure [kPa]	105	100-2000	-	-	-	-	121.3
CO_2 mole fraction [mol/mol]	0.15	-	0.2	0.2	-	0.2	-
CO_2 concentration [mol m^{-3}]	6.051	-	8.41	-	40.9	-	-
Liquid-phase							
Type	MEA	PC	DEA	DEA	AMP, MDEA, DEA	DEA	MEA/ MDEA mixture
Absorbent concentration [mol m^{-3}]	2544	-	2	150 - 2500	1560(AMP) 1200(DEA) 1200(MDEA)	-	-
Solvent initial loading	0.242	0	0	0	0	-	-
Velocity [ms^{-1}]	-	-	-	0.15	0.1	0.12	0.022-0.055
Temperature [K]	313	293.16-298.16	-	298	-	298	298

-= Not given

Boucif et al. (2012) developed a rigorous 2D model to study chemical absorption of CO_2 in aqueous solutions of MEA in HFMCs. They assumed negligible convective mass transfer in the membrane pores, incompressible liquid, constant gas-phase and liquid-phase diffusivities, and negligible shell side pressure drop. The model was solved using COMSOL software. Their result showed that gas-phase velocity and membrane geometry had significant impact on CO_2 capture rate; and porous membranes had better performance than non-porous membranes under identical operating parameters.

Chabanon et al. (2013) compared isothermal models of various complexities. Their models were compared against lab-and pilot-scale experimental data using the membrane mass transfer coefficient as an adjustable parameter. The authors proposed the following guidelines for choice of model complexity: i) use a simple model based on constant overall mass transfer coefficient for laboratory-scale experiments when using fresh solvent, ii) use

Table 3.2: HFMC specifications used in 1D and 1D-2D isothermal modelling studies of CO_2 absorption in HFMCs. Unless otherwise indicated, the studies were conducted at laboratory-scale.

	(Rode et al., 2012)	(Dindore et al., 2004)	(Zhang et al., 2008)	(Zhang et al., 2006)	(Wang et al., 2004)	(Keshavarz et al., 2008)	(Gong et al., 2006)
Contactor							
Type	-	PP	PP PVDF	PP	PP	-	PP
Operation	Counter-current	Semi-batch	Co-current	Co-current	Counter-current	Counter-current	Counter-current
Flow configuration	Gas in shell vs in tube	Gas in shell	Gas in shell(PP) Gas in tube(PVDF)	Gas in shell	Gas in shell	Gas in shell	Gas in shell
Inner fiber diameter [mm]	0.32-0.8	0.6	0.22(PP) 0.6(PVDF)	0.22	0.3	0.220	0.305
Outer fiber diameter [mm]	0.4-2	1	0.3(PP) 1(PVDF)	0.3	0.220	0.30	0.398
Thickness [mm]	0.04-0.6	-	-	-		-	-
Module inner diameter [mm]	-	-	-	-	-	-	15
Fiber Length [m]	-	-	0.113(PP) 0.240(PVDF)	0.113		-	0.24
Module Length [m]	-	0.27	0.188(PP) 0.27(PVDF)	0.188	0.188	0.113	-
Number of fibers	-	1	1100(PP) 60(PVDF)	1100	1100	1100	210
Porosity	-	-	0.4(PP) 0.83(PVDF)	0.4	0.4	0.4	0.58
Tortuosity	-	-	-	-	-	3.5	2.38
Packing fraction	0.6	0.6	0.6(PP) 0.62(PVDF)	-	0.388	-	-

-= Not given

1D models under laboratory-scale investigations when loaded solvent is used initially, and iii) use 2D models for pilot-scale studies. Zaidiza et al. (2014) also compared isothermal 1D and 2D models of HFMCs assuming negligible water transfer and irreversible reaction. Their result indicated that both models had comparable results under the operating conditions studied.

Farjami et al. (2015) employed 2D model for absorption of CO_2 in HFMC made of PVDF. They assumed ideal gas and non-wetting mode. The model was solved using the

Table 3.3: HFMC specifications used in isothermal 2D modelling studies of CO_2 absorption in HFMCs. Unless otherwise indicated, the studies were conducted at laboratory-scale.

	(Eslami et al., 2011)	(Saidi et al., 2014)	(Hosseinzadeh et al., 2017)	(Farjami et al., 2015)	(Boucif et al., 2012)	(Zaidiza et al., 2014)	(Chabanon et al., 2013)
Contactor							
Type	PTFE	-	PP	PVDF	PDMS PP	-	PTFE PMP
Operation	Counter-current	Counter current	Counter-current	Counter-current	Co-and Counter-Current	Counter-current	Counter-current
Flow configuration	Gas in shell	Gas in shell	Gas in shell	Gas in shell	Gas in shell	Gas in shell	Gas in shell(PMP) Gas in tube(PTFE)
Inner fiber diameter [mm]	0.344	0.22	0.38	0.6	0.305 (PDMS) 0.208 (PP)	-	0.430(PTFE) 0.20(PMP)
Outer fiber diameter [mm]	0.442	0.3	0.5	0.95	0.635 (PDMS) 0.380 (PP)	0.2-0.9	0.870 (PTFE) 0.38 (PMP)
Thickness [mm]	-	-	-	-	0.165 (PDMS) 0.500 (PP)	0.04-0.54	-
Module inner diameter [mm]	80	63.50	42	14	-	-	-
Fiber Length [m]	0.15	-	0.3	0.15	-	-	0.3 (PTFE) 0.24 (PMP)
Module Length [m]	-	0.23	0.36	0.27	0.24 (PDMS) 0.24 (PP)	-	-
Number of fibers	7000	3600	3200	30	54 (PDMS) 54 (PP)	1	27 or 119 (PTFE) 210 (PMP)
Porosity	0.45	-	0.65	0.7709	0.4 (PP)	-	-
Tortuosity	2	-	2	1.6826	6.4 (PP)	-	-
Packing fraction	0.6	-	-	-	0.128 (PDMS) 0.046 (PP)	0.6	0.13 or 0.59 (PTFE) 0.18 (PMP)

-= not given. PMP= Polymethylpentene

computational fluid dynamics (CFD) technique based on finite difference method. The authors showed that increasing fiber length, membrane porosity, and liquid-phase velocity had positive impact on CO_2 capture rate while increasing gas-phase velocity had negative impact.

Table 3.4: Gas-phase and liquid-phase conditions of isothermal 2D modelling studies of HFMCs. Unless otherwise indicated, the studies were conducted at laboratory-scale.

	(Eslami et al., 2011)	(Saidi et al., 2014)	(Hosse-inzadeh et al., 2017)	(Farjami et al., 2015)	(Boucif et al., 2012)	(Zaidiza et al., 2014)	(Chabanon et al., 2013)
Gas-phase							
Type	N_2/ CO_2 mixture	CO_2 CH_4/ N_2/ H_2O mixture	CO_2/ SO_2/ CH_4 mixture	N_2/CO_2 mixture	Flue gas	Oxygen depleted air/ CO_2 mixture	N_2/ CO_2 mixture
Velocity [ms^{-1}]	0.211	-	0.2-0.4	0.01-0.02	0.014 (PDMS) 0.013(PP)	0.32-0.78	0.5-4.5
Temperature [K]	298	303	298	299	-	313	298
Pressure [kPa]	-	-	105	-	105	105	105
CO_2 mole fraction	0.14	0.172	0.1	-	-	0.15	0.05 or 0.15
Liquid-phase							
Type	PG	PHPC	MEA	DW	MEA	MEA	MEA
Absorbent concentration [mol m^{-3}]	1	-	1	-	1200	2544	-
Solvent initial loading	-	0	0	0	0	0.242	0.242
Temperature [K]	308	303	298	278-318	-	313	293-298

-= not given. PMP= Polymethylpentene. PG=Propylene glycol. PHPC=Promoted hot potassium carbonate. DW= Distilled water.

3.3 Adiabatic Modelling Studies of HFMCs

Some authors (Hoff et al., 2004; Rongwong et al., 2013; Hoff and Svendsen, 2013, 2014; Chabanon et al., 2014; Kimball et al., 2014; Zaidiza et al., 2015; Iliuta et al., 2015; Zaidiza et al., 2016) have proposed adiabatic models of CO_2 absorption using different solvents in HFMCs . These models consider the contributions of the heat of absorption, and the heat transfer between the gas and liquid-phases. Besides, these models assume negligible heat exchange between the HFMC and the surrounding environment. All studies considered gas-phase flowing on the shell side and liquid-phase flow on the tube side. But, the study conducted by Hoff and Svendsen (2013) also considered the opposite flow configuration. Tables 3.5 and 3.6 presents the membrane specifications used in the adiabatic models, and the corresponding gas-phase and solvent conditions cited in this work, respectively. For adiabatic studies at industrial-scale (Hoff and Svendsen, 2013; Kimball et al., 2014), the operating conditions and membrane specifications are given separately in Tables 3.7 and 3.8, respectively.

Hoff et al. (2004) and Hoff and Svendsen (2014) developed a 1D-2D adiabatic diffusion-reaction model for CO_2 absorption in aqueous alkanolamines. They assumed axial plug flow for the gas-phase, and considered radial diffusion and axial convection contributions in the liquid-phase. In addition, they assumed that free amine and ionic products had the same diffusivity. The model was validated against experimental data using the diffusivity of MEA and ionic products as adjustable parameters. The study indicated that the liquid side mass transfer resistance was the dominant resistance. The authors also concluded that the rate of CO_2 absorption can be significantly enhanced if short contact time is used (less than 1 s). This prevents the diffusion of reactants away from the reaction zone. Hoff and Svendsen (2014) also developed a simplified 1D model for rapid design purposes. It was mentioned that the simplified models are good for scale-up purpose if they have been validated against experimental data and more rigorous models.

Rongwong et al. (2013) developed a rate based adiabatic 1D model for simulating CO_2 absorption using MEA in PTFE and PVDF membranes. They assumed axial plug flow, no pressure drop in the tube and shell sides, constant liquid-phase velocity and equal contact area for heat- and mass -transfer. Partial membrane wetting was considered in the model of PVDF membrane. The model was solved using the shooting method and validated against experimental data from the literature. The authors indicated that the models were sensitive to Henry's constant. The variation in the gas-phase and liquid-phase temperatures were less than 3K since low solvent conversion was obtained in their model results. Hoff and Svendsen (2013) compared industrial-scale PCC using HFMC and packed column. The use of HFMC led to reduction of total absorber volume by about 75% when the liquid-phase was flowing on the shell side.

Chabanon et al. (2014) and Kimball et al. (2014) conducted laboratory-and pilot-scale studies of CO_2 capture in HFMCs. An adiabatic 2D model was developed considering the following assumptions: i) no evaporation and condensation of water and amine, ii) uniform fiber packing and shapes, iii) no membrane wetting, and iv) negligible axial diffusion in the gas and liquid-phases. The model was compared against the lab-and pilot-scale experimental data using the membrane mass transfer coefficient as an adjustable parameter. The model fitted very well with the laboratory data. However, the model prediction and the pilot-scale data did not agree well. Significant non-idealities in the pilot-scale HFMC were the main reasons for the deviation of the simulation results from the pilot-scale experimental data. The model developed by Kimball et al. (2014) was also applied for scale-up studies of CO_2 capture from a flue gas of a coal-fired power plant. The results were compared with packed column. A significant absorber volume reduction was obtained when using the HFMC modules instead of the packed column. However, the total capital investment of the HFMC modules was higher than packed column.

Zaidiza et al. (2015) compared 1D isothermal and adiabatic models under laboratory and industrial operating conditions. They assumed plug flow in the gas and liquid-phases, laminar flow, and constant liquid-phase flow rate. Isothermal and adiabatic models showed comparable results when using fresh solvent and low absorbent conversion which corresponds to laboratory operating conditions. However, significant temperature rise in the

liquid-phase, by about 30 K, were observed when using initially loaded solvent and almost complete absorbent conversion which corresponds to industrial operating conditions.

Iliuta et al. (2015) investigated the effect of wetting on CO_2 capture using a 2D adiabatic model. They showed that membrane wetting resulted in significant drop of CO_2 flux. Moreover, they indicated that the adiabatic model studied can be considered as almost isothermal. However, low absorbent conversion, and high liquid-phase velocity relative to gas-phase velocity, which corresponds to laboratory operating conditions, were applied in the model. The result also showed that the reaction zone was located near the gas-liquid interface.

Zaidiza et al. (2016) compared adiabatic 1D and 2D models of CO_2 capture in HFMCs. They assumed multi-component transfer, solvent evaporation and condensation, and reversible reactions. The 2D model was solved using COMSOL software and the 1D model was solved using collocation method. According to the simulation results, both models resulted in solvent evaporation and temperature peak, up to 348 K, near the solvent entrance, when high absorbent conversion and initially loaded solvent were considered. HFMC and packed bed were also compared. Lower solvent losses and temperature peaks were attained in the HFMC. In addition, the radial temperature gradient in HFMC was found to be negligible compared to the packed column.

3.4 Conclusions from Literature Review

Several reports on modelling of PCC in HFMC have been published. The models were developed based on a set of assumptions. Among them, the steady state assumption was applied in all studies. Moreover, either isothermal or adiabatic assumption were also applied in all studies. Isothermal modelling of CO_2 absorption in HFMCs is extensively studied. Almost all of these isothermal models considered fresh solvent, low absorbent conversion, and irreversible reactions. However, a significant temperature variation in HFMCs is expected due to the exothermic nature of the reaction of CO_2 with alkanolamines, especially when initially loaded solvent and high absorbent conversion, which corresponds to industrial operating conditions, are considered. Some authors have developed adiabatic models to consider these effects. Based on different additional assumptions, several models of various complexities (from simple 1D models to complex 2D models) has been developed. The complex 2D models incorporate reaction kinetics and transfer fluxes which make them more rigorous. However, numerically solving the model equations is costly and time consuming.

Definition of the gas-phase conditions, liquid-phase characteristics, and specifications of membrane and module were also needed for development of the models. Absorption of CO_2 from dry CO_2/N_2 mixture using aqueous solutions of MEA at laboratory-scale HFMC was most often studied. Most of the modelling studies were performed with gas-phase flowing on the shell side while the liquid-phase flows counter-currently on the tube side.

Table 3.5: HFMC specifications used in adiabatic modelling studies of HFMCs. Unless otherwise indicated, the studies were conducted at laboratory-scale.

	(Rongwong, Assabumrungrat et al. 2013)	(Albarracin Zaidiza, Belaissaoui et al. 2015)	(Hoff et al., 2004)	(Hoff and Svendsen, 2014)	(Iliuta et al., 2015)	(Chabanon et al., 2014) and (Kimball et al., 2014)	(Zaidiza et al., 2016)
Contactor							
Type	PTFE PVDF	-	PTFE	PTFE	PTFE	PTFE	PTFE
Operation	Counter-current	Counter-current	Counter- or co-current	Counter- or co-current	Counter- and co-current	Counter-current	Counter-current
Flow configuration	Gas in shell	Gas in shell	Gas in shell	Gas in shell	Gas in shell	Gas in shell	Gas in shell
Inner fiber diameter [mm]	1 (PTFE) 0.65(PVDF)	-	3	1.09 1.15 (pilot)	1	0.43	-
Outer fiber diameter [mm]	2 (PTFE) 1 (PVDF)	0.1 - 0.5	-	1.49 1.43 (pilot)	2	0.87	0.2
Thickness [mm]	-	0.02 - 0.1	0.24	-	0.5	-	0.04
Module inner diameter [mm]	-	-	-	-	-	12.4 (lab) 105 (pilot)	-
Fiber Length [m]	-	-	0.43	0.14 0.2 (pilot)	0.4	-	0.32
Module Length [m]	0.367(PTFE) 0.27 (PVDF)	-	-	-	-	0.35 1 (pilot)	-
Number of fibers	57 (PTFE) 35(PVDF)	-	28	190 4797 (pilot)	57	119 8521(pilot)	-
Porosity	0.5 (PTFE) 0.75(PVDF)	-	0.5	0.5	0.5	0.336	-
Tortuosity	3(PTFE) 4(PVDF)	-	1.3	1.5	-	-	-
Packing fraction		0.6	-	-	0.388	0.59 0.648(pilot)	0.6

-= not given. pilot=Pilot-scale

HFMC with microporous membranes made of PP and PTFE, and with dimensions of 0.2-1 $\times 10^{-3}$inner fiber diameter and 0.14-0.43 m fiber length, were most often studied. Several authors (Hoff et al., 2004; Rongwong et al., 2013; Hoff and Svendsen, 2014; Iliuta

Table 3.6: Gas-phase and liquid-phase conditions of adiabatic modelling studies of HFMCs. Unless otherwise indicated, the studies are conducted at laboratory scale.

	(Rongwong, Assabum-rungrat et al. 2013)	(Albarracin Zaidiza, Belaiss-aoui et al. 2015)	(Hoff et al., 2004)	(Hoff and Svendsen, 2014)	(Iliuta et al., 2015)	(Chabanon et al., 2014) and (Kimball et al., 2014)	(Zaidiza et al., 2016)
Gas-phase							
Type	CO_2 in air (PTFE), Pure CO_2 (PVDF)	Satur-ated air	N_2/CO_2 mixture	N_2/CO_2 mixture	N_2/CO_2 mixture	Flue gas	Satur-ated air
Velocity [ms^{-1}]	-	-	-	-	0.05	-	0.19
Temperature [K]	296 (PTFE) 303(PVDF)	313	298-343	-	298	323 (pilot)	313
Pressure [kPa]		105		-	-	105	105
CO_2 mole fraction	0.15(PTFE)	0.14	0.05-0.1		0.2	0.134 (pilot)	0.14
Liquid-phase							
Type	MEA	MEA	MEA and MDEA	MEA and MDEA-piperazine	single and blended amines	MEA	MEA
Absorbent concentration [mol m^{-3}]	3.(PTFE) 2.(PVDF)	.	-	-	1 .	.	.
Solvent initial loading	0.3(PTFE)	0.242	0-0.4	-	-	0 0.271 (pilot)	0.242
Velocity [ms^{-1}]	1.45- 7.36 (PTFE) 0.66 - 2.1 (PVDF)	-	-	-	0.01	-	0.86 $\times 10^{-3}$
Temperature [K]	296 (PTFE), 303(PVDF)	313	-	-	298	313 (pilot)	313

-= not given. pilot= Pilot-scale

et al., 2015) used membranes of relatively larger fiber diameter which might lead to lower CO_2 absorption flux. Because, CO_2 absorption flux decreases with increase in external fiber radius (Zaidiza et al., 2015).

Many studies (Hoff et al., 2004; Wang et al., 2004; Zhang et al., 2006; Gong et al., 2006; Zhang et al., 2008; Keshavarz et al., 2008a; Rongwong et al., 2013; Hoff and Svendsen, 2014) have compared their model with a set of experimental data. Membrane mass transfer coefficient was frequently used as an adjustable parameter for fitting the models against experimental data (Chabanon et al., 2013, 2014; Kimball et al., 2014; Zaidiza et al.,

Table 3.7: Gas-phase and liquid-phase conditions of adiabatic modelling studies of HFMCs at industrial-scale.

	(Kimball et al., 2014)		(Hoff and Svendsen, 2013)
	Base case	Cooled case	
Gas-phase			
Type	Flue gas of 800 MWe power plant	Flue gas of 800 MWe power plant	Flue gas
Flow rate [m^3s^{-1}]	680	586.5	364
Temperature [K]	223	203	-
Pressure [kPa]	101.325	101.325	100
CO_2 mole fraction	0.134	0.146	0.03
Liquid-phase			
Type	MEA	MEA	MEA
Solvent concentration [wt%]	0.3	0.3	0.3
Solvent initial loading	0.271	0.271	0.21
Flow rate [m^3s^{-1}]	3.48	3.48	0.33
Temperature [K]	213	213	-

2015, 2016). Most of the experimental data were obtained at laboratory-scale considering atmospheric pressure and room temperature. Very few authors have reported flue gas treatment with pilot-scale HFMC and there is a lack of published pilot-scale experiment data of CO_2 absorption in HFMCs. There is also a lack of published work on the experimental and theoretical study of CO_2 absorption in HFMCs at industrial-scale.

Table 3.8: Membrane contactor specifications used in adiabatic modelling studies of HFMCs at industrial-scale.

	(Kimball et al., 2014)		(Hoff and Svendsen, 2013)	
	Ideal case (Base case)	Worst case (Base case)	Liquid: shell side	Liquid: tube side
Contactor				
Type	PTFE	PTFE	PTFE	PTFE
Operation	Counter-current	Counter-current	Counter/cross current	Counter/cross current
Flow configuration	Gas in shell	Gas in shell	Gas in tube	Gas in shell
Inner fiber diameter [mm]	0.43	0.43	-	-
Outer fiber diameter [mm]	0.87	0.87	-	-
Module diameter [m]	4.07	4.07	-	-
Module width [m]	-	-	3.0 x 1.0 *	3.0 x 1.0 *
Fiber Length [m]	1.23	4	3	3
# modules	100	100	25×3	40×5
# fibers/module(-)	1.2×10^7	1.2×10^7	-	-
Porosity	0.336	0.336	-	-
Packing fraction	0.648	0.648	-	-

*Cross-flow modules with W=3m, H=3m, D=1m. -= not given

Chapter 4

Model Description

In the present work, a mathematical model for CO_2 absorption using an aqueous solution of MEA in HFMC is developed. This is done by means of deriving and solving governing equations based on several assumptions. The approaches employed for deriving the mass and energy transport equations in the present work are similar with the approaches given by Hoff et al. (2002, 2004) and Hoff and Svendsen (2014). This chapter presents a description of the simulated system, model assumptions, and governing equations. Complementary sub-models and correlations for estimating reaction rate, vapor-liquid equilibrium, and physicochemical properties of the system are also presented. Finally, a description of the model implementation is presented.

4.1 System Description

HFMC made of PTFE is considered in the present work. The HFMC has an outer fiber radius Ry, an inner fiber radius R and an effective fiber length L as shown in Figure 4.1. As discussed in section 2.4.3, PTFE membranes have higher resistance to membrane wetting and have an acceptable membrane mass transfer coefficient. As an important parameter, the membrane mass transfer coefficient is one of the parameters selected for sensitivity analysis (presented in section 5.1.5) to investigate its effect on CO_2 capture performance of the HFMC.

A Mathematical model of CO_2 absorption using an aqueous solution of MEA in HFMC is developed by deriving and solving governing equations for the three domains of HFMC, namely, the shell-, membrane- and tube-domains, as shown in Figure 4.1. The equations are developed based on one fiber and then applied to all fibers in the HFMC module with the assumption of uniform fiber distribution. It has been reported that counter-current flow mode provides higher driving force for separation compared to the co-current flow mode (Tontiwachwuthikul et al., 2006). As a result, a gas-phase flowing on the shell side (entrance at z = L) and an aqueous solution of MEA flowing counter-currently on the tube

side (entrance at z = 0) is considered in the present work. This configuration is very often considered in many studies (Mansourizadeh and Ismail, 2009).

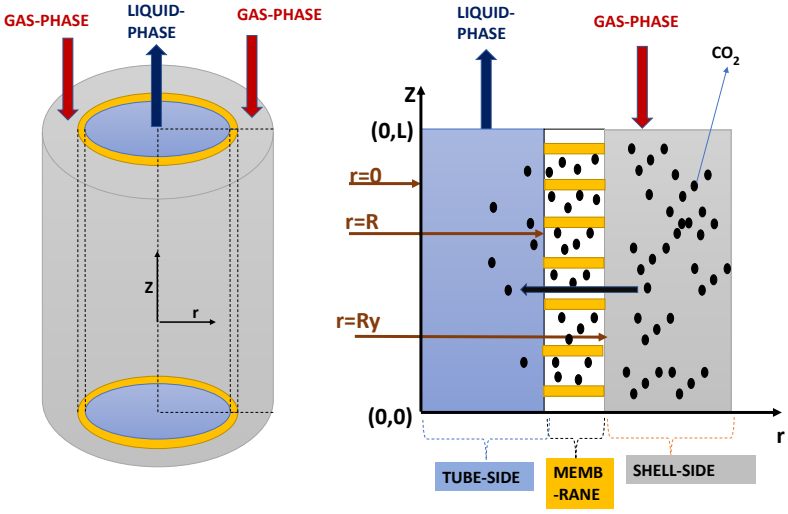

Figure 4.1: Schematic representation of the HFMC considered in the present work together with the domains used for deriving model equations.

4.2 Model Assumptions

The HFMC mathematical model is developed based on several assumptions. These assumptions are based on published works and are listed below:

1. Steady-state.
2. Ideal gas behaviour.
3. Angular symmetry.
4. Axial plug flow in the gas-phase.
5. The total pressure of the gas-phase is constant along the HFMC length.
6. Only axial convection and radial diffusion are considered in the liquid-phase.
7. Fully developed laminar flow is considered in the liquid-phase. In the present work, the liquid-phase has a density of around 1000 kgm^{-3} and a viscosity of between 1-2.6$\times 10^{-3}$ Pa.s. The inner fiber diameter is 0.43 $\times$ 10^{-3} m and the liquid-phase velocity is between 1-4 $\times$ $10^{-2} ms^{-1}$. Considering the range of these parameters, the Reynolds number is below 20, which supports the assumption of laminar flow.

8. The diffusivity of $MEACOO^-$ in the liquid-phase is set equal to the diffusivity of MEA .

9. Mass transfer in the membrane pores is by diffusion only.

10. The HFMC operates adiabatically.

11. Only CO_2 is considered as a transfer component between the gas-phase and liquid-phase.

12. The concentrations of total MEA and water in the liquid-phase are assumed constant along the HFMC length.

13. The transfer of CO_2 from the gas-phase to the liquid-phase is accompanied by increase in the density and mass flow rate of the liquid-phase. Thus, the volumetric flow rate of the liquid-phase, which is the total mass flow rate divided by the density of the liquid-phase, is assumed constant along the HFMC length.

14. Thermal conductivity of the liquid-phase is assumed constant along the radial direction.

15. Uniform distribution of fibers in the HFMC module.

16. Local temperature and local concentrations in the liquid-phase are used for calculating the reaction rate.

4.3 Liquid-phase Governing Equations

4.3.1 Liquid-phase species mole balance

The general species mole balance can be represented by the following equation (Jakobsen, 2008):

$$\frac{\partial C_i}{\partial t} + \nabla.(C_i \mathbf{v}) = -\nabla.J_i + r_i \tag{4.1}$$

where C_i, r_i, and **v** represents concentration, reaction rate, and velocity terms, respectively; J_i represents diffusive flux which is expressed by the Fick's law in the present work.

From assumptions 3 and 6, angular symmetry is considered, axial diffusion is negligible compared to axial convection; and mass transport in the radial direction is pure diffusional. Thus, the steady-state species mole balance of the liquid-phase in cylindrical coordinates can be expressed as:

$$v_z \frac{\partial C_i}{\partial z} = \frac{1}{r}\frac{\partial}{\partial r}(r D_i \frac{\partial C_i}{\partial r}) + r_i \tag{4.2}$$

where D_i represents diffusion coefficient of species i in the liquid-phase.

From assumption 7, fully developed laminar flow is considered in the liquid-phase. Thus, the radial velocity profile of the liquid-phase flow in the tube can be represented by the "*Haggen-Poiseuille law*" (simple parabolic profile) (Jakobsen, 2008):

$$v_z = 2v_{z,av}\Big[1 - \big(\frac{r}{R}\big)^2\Big] \tag{4.3}$$

where $v_{z,av}$ represents the volumetric average velocity of the liquid-phase and R is the internal radius of the tube(or fiber).

In-compressible fluid (constant density and viscosity) is among the assumptions used for deriving the "*Haggen-Poiseuille law*". However, the density and viscosity of the liquid-phase are a function of temperature and CO_2 loading as given in sections 4.8.1 and 4.8.2, respectively. CO_2 loading is expected to vary along the radial direction during the absorption of CO_2 using the aqueous solution of MEA in HFMC. As a result, the density and viscosity of the solution are also expected to vary along the radial direction (Hoff and Svendsen, 2014). This is in disagreement with the assumptions used to derive the "*Haggen-Poiseuille law*. However, the effect of radial variation of viscosity and density on simple parabolic velocity profile was investigated by Hoff et al. (2002), and the authors found a negligible effect. Therefore, the simple parabolic velocity profile, which was derived with the assumption of incompressible fluid, is kept in this work.

Substituting equation 4.3 to equation 4.2, we get:

$$2v_{z,av}\Big[1 - \big(\frac{r}{R}\big)^2\Big]\frac{\partial C_i}{\partial z} = \frac{1}{r}\frac{\partial}{\partial r}(rD_i\frac{\partial C_i}{\partial r}) + r_i \tag{4.4}$$

The diffusion coefficient term, D_i, is a function of the viscosity of the liquid-phase as discussed in section 4.8.3. During CO_2 absorption, radial variation of the diffusion coefficient is expected due to the expected radial viscosity gradient (Hoff et al., 2002). Thus, a radial gradient of the diffusion coefficient is implemented in the model as shown in equation 4.5, which is obtained after manipulation and rearrangement of equation 4.4.

$$2v_{z,av}\Big[1 - \big(\frac{r}{R}\big)^2\Big]\frac{\partial C_i}{\partial z} = D_i(\frac{1}{r}\frac{\partial C_i}{\partial r}) + D_i(\frac{\partial^2 C_i}{\partial r^2}) + \frac{\partial D_i}{\partial r}\frac{\partial C_i}{\partial r} + r_i \tag{4.5}$$

Concentrations of MEA, $MEACOO^-$ and CO_2 in the liquid-phase are estimated by implementing equation 4.5 for each component. The concentration of $MEAH^+$ is estimated from total amine balance. That is, $C_{MEAH^+} = C_{MEA_{tot}} - C_{MEA} - C_{MEACOO^-}$. Note that from assumption 12, the concentrations of total MEA ($C_{MEA_{tot}}$) and water (C_{H2O}) in the liquid-phase are assumed constant along the HFMC length. All these concentration terms are required for estimating reaction rate (equation 4.44). Moreover, C_{CO_2}, C_{MEAH^+} , C_{MEA} and C_{MEACOO^-} are required for estimating the CO_2 loading, which is used for calculating the equilibrium partial pressure of CO_2 which is then used for estimating the driving force in equation 4.40.

The complexity of equation 4.5 can be reduced by converting it into dimensionless form. Equation 4.5 is transformed into dimensionless form (equation 4.6) by introducing dimensionless independent variables $\varepsilon = \frac{z}{L}$ and $\gamma = \frac{r}{R}$, and dimensionless dependent variables $\chi_i = \frac{C_i}{C_{i0}}$ and $\beta = \frac{D_i}{D_{i0}}$.

$$\frac{\partial \chi_i}{\partial \varepsilon} = \frac{L}{2v_{z,av}C_{i0}(1-\gamma^2)}\Big[D_{i0}\frac{C_{i0}}{R^2}\Big(\beta\frac{1}{\gamma}\frac{\partial \chi_i}{\partial \gamma} + \beta\frac{\partial^2 \chi_i}{\partial \gamma^2} + \frac{\partial \beta}{\partial \gamma}\frac{\partial \chi_i}{\partial \gamma}\Big) + r_i\Big] \tag{4.6}$$

where C_{i0} represents the initial concentration of species i; and D_{i0} represents the diffusion coefficient of species i at the center of the tube.

4.3.2 Liquid-phase thermal balance

Like the liquid-phase species mole balance, the derivation of liquid-phase thermal balance can be started from the following general expression (Jakobsen, 2008):

$$\rho_L C_{P_L}\Big[\frac{\partial T_L}{\partial t} + \mathbf{v}.\nabla T_L)\Big] = \nabla.(\lambda_L \nabla T_L) + \sum_j -\Delta H_{r_j} r_j \tag{4.7}$$

where ρ_L, C_{P_L} and λ_L are density, specific heat capacity and thermal conductivity of the liquid-phase, respectively; ΔH_{r_j} represents heat of j^{th}reaction.

Like the assumptions of the liquid-phase species mole balance, angular symmetry is considered, and only axial convection and radial conduction terms are considered. In addition, the thermal conductivity of the liquid-phase is assumed constant along the radial direction as per assumption 14. Applying these assumptions and using the simple parabolic velocity profile, the steady-state thermal balance can be expressed as:

$$2v_{z,av}\Big[1-\big(\frac{r}{R}\big)^2\Big]\rho_L C_{P_L}\frac{\partial T_L}{\partial z} = \lambda_L\Big[\frac{1}{r}\frac{\partial T_L}{\partial r} + \frac{\partial^2 T_L}{\partial r^2}\Big] + \sum_j -\Delta H_{r_j} r_j \tag{4.8}$$

The heat of reaction term in equation 4.8 can be represented by a heat of CO_2 absorption as indicated by the following equation:

$$2v_{z,av}\Big[1-\big(\frac{r}{R}\big)^2\Big]\rho_L C_{P_L}\frac{\partial T_L}{\partial z} = \lambda_L\Big[\frac{1}{r}\frac{\partial T_L}{\partial r} + \frac{\partial^2 T_L}{\partial r^2}\Big] + r_{CO_2}(-\Delta H_r) \tag{4.9}$$

Where r_{CO_2} and $-\Delta H_r$ represent the rate of consumption of CO_2 and the heat of CO_2 absorption per mole of absorbed CO_2, respectively.

Using ε and γ, and introducing a dimensionless dependent variable θ_L=$\frac{T_L}{T_0}$, equation 4.9 can be expressed in dimensionless form as follows:

$$\frac{\partial \theta_L}{\partial \varepsilon} = \frac{L}{2v_{z,av}T_0\rho_L C_{P_L}(1-\gamma^2)}\Big[\lambda_L\frac{T_0}{R^2}\Big(\frac{1}{\gamma}\frac{\partial \theta_L}{\partial \gamma} + \frac{\partial^2 \theta_L}{\partial \gamma^2}\Big) + r_{CO_2}(-\Delta H_r)\Big] \tag{4.10}$$

where T_0 represents the temperature of the liquid-phase at the inlet to the HFMC (L=0).

4.3.3 Boundary conditions

The boundary conditions for the liquid-phase species mole balance and thermal balance are given below:

Initial conditions at z=0:

$$C_i = C_{i0} \tag{4.11}$$
$$T_L = T_{L0} \tag{4.12}$$

In dimensionless form, at $\varepsilon = 0$:

$$\chi_i = 1 \tag{4.13}$$
$$\theta_L = 1 \tag{4.14}$$

Axial symmetry at r=0:

$$\frac{\partial C_i}{\partial r} = 0 \tag{4.15}$$
$$\frac{\partial T_L}{\partial r} = 0 \tag{4.16}$$

In dimensionless form, at $\gamma = 0$:

$$\frac{\partial \chi_i}{\partial \gamma} = 0 \tag{4.17}$$
$$\frac{\partial \theta_L}{\partial \gamma} = 0 \tag{4.18}$$

Molar and heat flux terms at r=R:

$$D_i \frac{\partial C_i}{\partial r} = N_i \frac{R_y}{R} \tag{4.19}$$
$$D_k \frac{\partial C_k}{\partial r} = 0 \tag{4.20}$$
$$\lambda_L \frac{\partial T_L}{\partial r} = Q.\frac{R_y}{R} \tag{4.21}$$

where C_i and N_i represents concentration and flux of transfer component, which is CO_2 in the present work; C_k represents the concentration of non-transfer components, that is, $MEACOO^-$ and MEA in the present work. The molar flux (N_i) and heat flux (Q) terms are given by equation 4.40 and 4.42, respectively. The ratio ($\frac{R_y}{R}$) is used to consider the effect of curvature in the membrane fibers of the HFMC.

In dimensionless form, at $\gamma = 1$:

$$D_i \frac{\partial \chi_i}{\partial \varepsilon} = N_i \frac{R_y}{C_{i0}} \tag{4.22}$$

$$D_k \frac{\partial \chi_k}{\partial \varepsilon} = 0 \tag{4.23}$$

$$\lambda_L \frac{\partial \theta_L}{\partial \varepsilon} = Q. \frac{R_y}{T_{L0}} \tag{4.24}$$

4.3.4 Liquid-phase pressure drop

The pressure drop in the liquid-phase is estimated using the correlation proposed by Geankoplis (2003):

$$\frac{\partial P_L}{\partial z} = 4 f \rho_L \frac{v^2}{2} \frac{L}{D_h} \tag{4.25}$$

where L and D_h represent fiber length and hydraulic diameter, respectively. As per assumption 7, laminar flow is considered in the liquid-phase. Therefore, the friction factor (f) is estimated using the following equation proposed for laminar flow:

$$f = \frac{1}{Re} \tag{4.26}$$

The liquid-phase pressure drop equation is not required by any of the membrane contactor governing equations. Thus, it is estimated independently. However, in practical applications, the total pressure of the liquid-phase should be higher than the total pressure of the gas-phase to prevent bubbling (Zaidiza et al., 2015). Furthermore, the "*breakthrough*"pressure should not be exceeded to prevent membrane wetting.

4.4 Gas-phase Governing Equations

4.4.1 Gas-phase species mole balance

Like the liquid-phase species mole balance, the species mole balance in the gas-phase can also be estimated based on the general expression given by equation 4.1. From assumption 4, axial plug flow is considered in the gas-phase. Furthermore, there is no chemical reaction in the gas-phase. But, there is a transfer of CO_2 from the gas-phase to the liquid-phase. Therefore, the steady-state species mole balance in the gas-phase is given by the following equation:

$$\frac{d(v_{gs} C_{gi})}{dz} = a N_i \tag{4.27}$$

where C_{gi} represents the concentration of gas-phase components and a is membrane surface area to volume ratio. The molar flux term (N_i) is used to represent the loss of CO_2 from the gas-phase to the liquid-phase.

The superficial velocity of the gas-phase (v_{gs}) is given by:

$$v_{gs} = v_g \epsilon_g \tag{4.28}$$

where v_g is the interstitial gas-phase velocity and ϵ_g is the volume fraction occupied by the gas-phase.

Applying the ideal gas law (assumption 2) and inserting equation 4.28 into equation 4.27, the following expression is achieved::

$$\frac{d\left(\frac{p_i v_g}{R_g T_g}\right)}{dz} = N_i \frac{a}{\epsilon_g} \tag{4.29}$$

where R_g represents the gas constant and T_g is gas-phase temperature; p_i represents partial pressure of component i in the gas-phase.

Applying the chain rule on equation 4.29, and doing some re-arrangements, an expression for the partial pressure of component i is derived:

$$\frac{\partial p_i}{\partial z} = -\frac{R_g T_g}{v_g} N_i \frac{a}{\epsilon_g} - \frac{p_i}{v_g}\frac{\partial v_g}{\partial z} + \frac{p_i}{T_g}\frac{\partial T_g}{\partial z} \tag{4.30}$$

In the present work, only CO_2 is considered as a transfer component. Thus, the above equation is implemented for estimation of the partial pressure CO_2 in the gas-phase.

Equation 4.30 is converted to the following dimensionless form:

$$\frac{\partial \Delta_i}{\partial \varepsilon} = -\frac{R_g T_g L}{P_{g0} \times v_{g0} \times \mu} N_i \frac{a}{\epsilon_g} - \frac{\Delta_i}{\mu}\frac{\partial \mu}{\partial \varepsilon} + \frac{\Delta_i}{\theta_g}\frac{\partial \theta_g}{\partial \varepsilon} \tag{4.31}$$

where P_{g0} and v_{g0} are gas-phase inlet total pressure and velocity, respectively; $\Delta_i = \frac{p_i}{P_{g0}}$, $\theta_g = \frac{T_g}{T_0}$ and $\mu = \frac{v_g}{v_{g0}}$.

4.4.2 Gas-phase axial velocity profile

By applying summation to both sides of equation 4.30 and doing some rearrangements, an expression for the axial velocity profile of the gas-phase (Equation 4.32) can be found.

$$\frac{\partial v_g}{\partial z} = -\frac{R_g T_G}{P_g} \sum N_i \frac{a}{\epsilon_g} - \frac{v_g}{P_g}\frac{\partial P_g}{\partial z} + \frac{v_g}{T_g}\frac{\partial T_g}{\partial z} \tag{4.32}$$

The total pressure of the gas-phase (P_g) is assumed constant along the HFMC length as per assumption 5. Furthermore, there is only one non-zero flux term since only one species (CO_2) is considered as a transfer component. Therefore, equation 4.32 becomes:

$$\frac{\partial v_g}{\partial z} = -\frac{R_g T_g}{P_g} N_i \frac{a}{\epsilon_g} + \frac{v_g}{T_g}\frac{\partial T_g}{\partial z} \tag{4.33}$$

Equation 4.33 is transformed to the following dimensionless form:

$$\frac{\partial \mu}{\partial \varepsilon} = -\frac{R_g T_g L}{P_g v_{g0}} N_i \frac{a}{\epsilon_g} + \frac{\mu}{\theta_g}\frac{\partial \theta_g}{\partial \varepsilon} \tag{4.34}$$

4.4.3 Gas-phase thermal balance

Like the liquid-phase thermal balance, the gas-phase thermal balance can be estimated from following general energy balance:

$$\rho_g C_P\big(\frac{\partial T_g}{\partial t} + \mathbf{v}.\nabla T_g\big) = \nabla.(\lambda_g \nabla T_g) + \sum_j -\Delta H_{r_j} r_j \tag{4.35}$$

Similar to the species mole balance in the gas-phase, assuming axial plug flow and no chemical reaction in the gas-phase, equation 4.35 simplifies to the following expression for steady-state condition:

$$(v_g \epsilon_g)(\rho_g C_P)\frac{dT_g}{dz} = -Ua(T_g - T_L(R)) \tag{4.36}$$

where ρ_g and C_P are density and specific heat capacity of the gas-phase; $T_L(R)$ is the temperature of the liquid-phase at the tube wall; U represents an external heat transfer coefficient which is estimated by equation 4.43.

The density of the gas-phase can be calculated using the ideal gas law; and the specific heat capacity of the gas-phase can be converted to molar heat capacity as follows:

$$\rho_g C_P = \sum \rho_{g,i} C_{P,i} = \sum \frac{p_i}{R_g T_g} C_{p_{i,g}} \tag{4.37}$$

where $C_{p_{i,g}}$ is the molar heat capacity of component i in the gas-phase.

Substituting equation 4.37 into equation 4.36, the thermal balance of the gas-phase becomes:

$$\frac{dT_g}{dz} = -\frac{R_g T_g}{v_g \sum p_i C_{p_{i,g}}} \frac{Ua}{\varepsilon}(T_g - T_L(R)) \tag{4.38}$$

Equation 4.38 is transformed to the following dimensionless form:

$$\frac{d\theta_g}{d\varepsilon} = -\frac{L R_g T_g}{v_{g0} \mu \sum p_i C_{p_{i,g}}} \frac{Ua}{\epsilon_g}(\theta_g - \theta_L(R)) \tag{4.39}$$

where $\theta_L(R)$=$\frac{T_L(R)}{T_0}$.

4.5 Membrane-side Governing Equations

4.5.1 Molar flux

From assumption 9, the mass transfer mechanism across the membrane is only by diffusion. The molar flux of species i across the membrane is modelled using the resistance in series model according to the discussion in section 2.4.1:

$$N_i = K_{ext}(p_{gi} - p_i^*) \tag{4.40}$$

where p_{gi} is the partial pressure of transfer component i in the gas-phase; p_i^* represents the partial pressure of the transfer component i in equilibrium with the bulk liquid-phase concentration, which is estimated using an equilibrium model discussed in section 4.6. K_{ext} represents an external mass transfer coefficient based on gas-phase pressure (unit mol.s^{-1}m^{-2} kPa) and is given by the following expression:

$$\frac{1}{K_{ext}} = (\frac{1}{k_g} + \frac{1}{k_m}) R_g T_g \tag{4.41}$$

where k_g is the mass transfer coefficient for the gas-phase, which is calculated using equation 4.74; k_m is the mass transfer coefficient for the membrane, which is discussed in section 4.8.6. The effect of tube curvature is considered when deriving the boundary conditions of the liquid-phase equations. Thus, the effect of tube curvature is neglected in the above equation.

4.5.2 Heat flux

The heat flux across the membrane is calculated using equation 4.42. The equation incorporates sensible and latent heat transfer contributions. The first term considers heat transfer due to the temperature difference between the gas and liquid-phases, and the latter one considers heat transfer due to the transport of CO_2 from the gas-phase to the liquid-phase.

$$Q = U(T_g - T_L(R)) + N_i C_{p_{i,g}} (T_g - T_L(R)) \tag{4.42}$$

where U is the overall heat transfer coefficient, which is estimated based on the gas-side and membrane-side heat transfer coefficients as given below:

$$\frac{1}{U} = \frac{1}{h_g} + \frac{1}{h_m} \tag{4.43}$$

where h_g and h_m are the heat transfer coefficients of the gas-phase and the membrane, respectively.

4.6 Equilibrium Model

The following reactions are used to characterize the CO_2-MEA-H_2O system (Hessen et al., 2010):

Water ionization:

$$2H_2O <==> H_3O^+ + OH^- \tag{r1}$$

Dissociation of dissolved CO_2:

$$2H_2O + CO_2 <==> H_3O^+ + HCO_3^- \tag{r2}$$

Dissociation of bicarbonate:

$$H_2O + HCO_3^- <==> H_3O^+ + CO_3^{2-} \tag{r3}$$

Dissociation of protonated MEA:

$$H_2O + MEAH^+ <==> MEA + H_3O^+ \quad \text{(r4)}$$

Carbamate reversion to bicarbonate:

$$H_2O + MEACOO^- <==> MEA + HCO_3^- \quad \text{(r5)}$$

In this work, the electrolyte NRTL model (e-NRTL) framework, originally developed by Chen and Evans (1986), is used to correct the liquid-phase non-idealities while the Peng-Robinson equation of state (PR-EoS) takes into account the gas-phase non-idealities. This so-called "$\gamma - \phi$"- approach is used to calculate the equilibrium partial pressures and chemical speciation for the CO_2-MEA-H_2O system. The e-NRTL model parameters are taken from Putta et al. (2016) and more information can be found there and elsewhere in the literature (Hessen et al., 2010; Monteiro et al., 2013).

4.7 Reaction Mechanism and Kinetics

In the literature, the kinetics of the reaction between CO_2 and MEA have been frequently represented based on two types of reaction mechanisms: a) the zwitterion mechanism which was initially proposed by Caplow (1968), and b) the termolecular mechanism which was proposed by Crooks and Donnellan (1989). The termolecular reaction mechanism is used in the present work.

The termolecular reaction mechanism assumes that MEA reacts with CO_2 to give an intermediate loosely bound complex. This complex then reacts with a base to give a product or breaks down to the reactant in a single step. The bases considered in the MEA-CO_2-H_2O system are MEA, H_2O, OH^-, HCO_3^- and CO_3^{-2}. Among these bases, the concentrations of OH^-, HCO_3^- and CO_3^{-2} can be assumed negligible relative to the concentrations of MEA and H_2O (Putta et al., 2016). Based on these assumptions, the main reactions involved in the termolecular reaction mechanism are the following:

$$2MEA + CO_2 <==> MEACOO^- + MEAH^+ \quad \text{(r6)}$$

$$MEA + H_2O + CO_2 <==> H_3O^+ + MEACOO^- \quad \text{(r7)}$$

These reactions are obtained by adding reactions r2, r4, and r5 and reactions r2 and r5, respectively.

Based on the above reactions, the rate of consumption of CO_2 can be expressed as (Majeed et al., 2017):

$$r_{CO2} = \left[k^T_{MEA} C_{MEA} + k^T_{H_2O} C_{H_2O}\right]\left[C_{MEA} C_{CO_2} - \frac{C_{MEAH^+} C_{MEACOO^-}}{K^T_{eq}}\right] \quad (4.44)$$

The rate of consumption of MEA can be estimated similarly as follows:

$$r_{MEA} = \left[2k^T_{MEA}C_{MEA} + k^T_{H_2O}C_{H_2O}\right]\left[C_{MEA}C_{CO_2} - \frac{C_{MEAH^+}C_{MEACOO^-}}{K^T_{eq}}\right] \tag{4.45}$$

The rate of generation of $MEACOO^-$ can also be estimated from equation 4.44 as follows:

$$r_{MEACOO^-} = -r_{CO2} \tag{4.46}$$

where k^T_{MEA} and $k^T_{H_2O}$ are kinetic constants and their Arrhenius-type temperature dependency expression is given by equations 4.47 and 4.48, respectively; K^T_{eq} is an equilibrium constant, which is given by equation 4.49 as a function of activities (Majeed et al., 2017).

$$k^T_{MEA} = k_{MEA} \times exp\left(\frac{-E_{MEA}}{R_gT}\right) \tag{4.47}$$

$$k^T_{H_2O} = k_{H_2O} \times exp\left(\frac{-E_{H_2O}}{R_gT}\right) \tag{4.48}$$

$$K^T_{eq} = \frac{a_{MEACOO^-}a_{MEAH^+}}{a_{CO_2}(a_{MEA})^2} \tag{4.49}$$

The models for the kinetic and equilibrium constants used in the present work are obtained from Svendsen (2017). The equilibrium constant used in the present work was modelled at 30 wt.% MEA, 313.15 K and 0.5 mol/mol CO_2 loading. The models for the kinetic constants are given below:

$$k^T_{MEA} = 1.4122 \times 10^{10} \times exp\left(\frac{-4419.9}{T}\right) \tag{4.50}$$

$$k^T_{H_2O} = 4.3959 \times 10^{6} \times exp\left(\frac{-3118}{T}\right) \tag{4.51}$$

4.8 Model Parameters

The governing equations derived in the previous sections require several parameters such as density, viscosity, diffusivity, heat capacity, thermal conductivity, etc. Table 4.1 provides a list of the most important parameters used in the present work with their corresponding literature sources. The functional dependence of these parameters are discussed in the following sections.

4.8.1 Density of the liquid-phase

In the present work, the density of the CO_2-loaded aqueous MEA solution is calculated as a function of the amount of CO_2 added and density of the unloaded solution using the following equation obtained from Hartono et al. (2014):

$$\rho_{loaded} = \frac{\rho_{unloaded}}{1 - w_{CO_2added}.(1 - \Phi^3)} \tag{4.52}$$

Table 4.1: List of parameters used in the present work along with their literature sources.

Parameter		Source
Density		
	Pure water and Pure MEA	(Pinto et al., 2014,)
	Loaded and unloaded MEA solution	(Hartono et al., 2014)
Viscosity		
	Pure water and Pure MEA	(Hsu and Li,1997)
	Loaded and unloaded MEA solution	(Hartono et al., 2014)
	Gas-phase	(Wilke, 1950)
Diffusivity		
	MEA and CO_2 in loaded MEA solution	(Versteeg and Van Swaalj,1988)
	CO_2 in pure water	(Versteeg and Van Swaalj,1988)
	MEA in pure water	(Snijder et al., 1993)
	CO_2 in gas-phase	(Poling et al., 2001)
Liquid specific heat capacity		(Cheng et al., 1996)
Gas specific heat capacity		(Poling et al., 2001)
Gas mass transfer coefficient		(Luo et al., 2012)
Gas heat transfer coefficient		(Bird et al., 2007)
Gas thermal conductivity		(Poling et al., 2001)
Liquid thermal conductivity		(Cheng et al., 1996)

where $\rho_{unloaded}$ represents density of CO_2-free aqueous MEA solution; Φ represents volume expansion due to CO_2 addition; w_{CO_2added} is mass fraction of the CO_2 added to the solution, which is calculated by the following correlation:

$$w_{CO_2added} = \frac{\alpha_{CO_2}.y_1.M_3.}{y_1.M_1 + (1 - y_1 - \alpha_{CO_2}.y_1).M_2 + \alpha_{CO_2}.y_1.M_3} \tag{4.53}$$

where M_1,M_2 and M_3 are molecular weights of MEA, H_2O and CO_2, respectively; α_{CO_2} is CO_2 loading in the MEA solution; y_1 is mole fraction of MEA.

The volume expansion in the solution due to the addition of CO_2 (Φ) is calculated by the following correlation:

$$\Phi = \frac{a_1.y_1.\alpha_{CO_2} + a_2.y_1}{a_3 + y_1} \tag{4.54}$$

where a_1, a_2 and a_3 are model parameters.

Density of unloaded MEA solution ($\rho_{unloaded}$) is calculated by the following correla-

tion obtained from Hartono et al. (2014):

$$\rho_{unloaded} = \frac{y_1.M_1 + y_2.M_2}{V^E + \frac{y_1.M_1}{\rho_{MEA}} + \frac{y_2.M_2}{\rho_{H2O}}} \tag{4.55}$$

where ρ_{H2O} and ρ_{MEA} are density of pure water and pure MEA, respectively; y_2 is mole fraction of water; V^E is an excess molar volume, which is calculated from the correlation proposed by Hartono et al. (2013):

$$V^E = (-1.9210 + 1.6792 \times 10^{-3}T - 3.0951y_2 + 3.4412y_2^2)y_2(1 - y_2)10^{-6} \tag{4.56}$$

Densities of pure MEA and water are calculated from the following correlations given by Pinto et al. (2014b):

$$\rho_{MEA} = (-0.3544 \times 10^{-6} \times T^2 - 0.5765 \times 10^{-3}T + 1.2153) \times 10^3 \tag{4.57}$$

$$\rho_{H2O} = (-3.3461 \times 10^{-6} \times T^2 + 1.7296 \times 10^{-3}T + 0.77853) \times 10^3 \tag{4.58}$$

4.8.2 Viscosity of the liquid-phase

In the present work, the viscosity of the CO_2 loaded aqueous MEA solution is calculated using the following correlation obtained from Hartono et al. (2014):

$$ln(\eta_{loaded}) = y_3 \times ln(\eta^{**}) + (1 - y_3) \times ln(\eta_{unloaded}) \tag{4.59}$$

where y_3 is mole fraction of CO_2 in the solution; $\eta_{unloaded}$ is viscosity of unloaded aqueous MEA solution; η^{**} represents viscosity deviation, which is calculated using the following correlation:

$$ln(\eta^{**} \times 10^3) = \frac{6.98y_1 + 10.48\alpha_{CO_2}y_1}{0.049 + y_1} \tag{4.60}$$

Viscosity of the unloaded aqueous MEA solution is estimated using the following correlation (Hartono et al., 2014):

$$ln(\eta_{unloaded}) = ln(\eta_\gamma) + y_1 ln(\eta_{MEA}) + y_2 ln(\eta_{H2O}) \tag{4.61}$$

where η_{MEA} and η_{H2O} are viscosity of pure MEA and water, respectively; η_γ represents viscosity deviation, which is estimated using the following correlation:

$$ln(\eta_\gamma) = (L_1 + L_2(T - 273.15) + L_3(T - 273.15)^2 + L_4y_1)y_1y_2 \tag{4.62}$$

where L_i are model parameters.

The viscosities of pure MEA and water are estimated using the following correlations obtained from Hsu and Li (1997):

$$\eta_{MEA} = \rho_{MEA} \times exp\Big(- 3.51312 + \frac{893.173}{(T - 159.612)}\Big) \times 10^{-6} \tag{4.63}$$

$$\eta_{H2O} = \rho_{H2O} \times exp\Big(- 3.28285 + \frac{456.029}{(T - 154.576)}\Big) \times 10^{-6} \tag{4.64}$$

4.8.3 Diffusivity of species in the liquid-phase

Correlations for estimating diffusivities of CO_2, $MEACOO^-$ and MEA are required in the present work. However, there are no published correlations or data for estimating the diffusivity of $MEACOO^-$. Thus, from assumption 8, the diffusivity of $MEACOO^-$ is set equal to the diffusivity of MEA.

Diffusivity of MEA in loaded aqueous MEA solution is calculated using the "*modified Stokes-Einstein relation*" as suggested by Versteeg and Van Swaalj (1988):

$$D_{MEA}^{amine} = D_{MEA}^{H_2O} \cdot \Big[\frac{\eta_{H_2O}}{\eta_{loaded}}\Big]^{0.6} \tag{4.65}$$

where $D_{MEA}^{H_2O}$ is diffusivity of MEA in pure water, which is calculated using the following correlation obtained from Snijder et al. (1993) :

$$ln(D_{MEA}^{H_2O}) = -13.275 - \frac{2198.3}{T} - 7.8142 \times 10^{-5} \times C_{MEA} \tag{4.66}$$

In the "*modified Stokes-Einstein relation*", the effect of CO_2 loading on diffusivity is indirectly incorporated by the viscosity changes.

Diffusivity of CO_2 in loaded aqueous MEA solution is estimated in similar way (Versteeg and Van Swaalj, 1988):

$$D_{CO_2}^{amine} = D_{CO_2}^{H_2O} \cdot \Big[\frac{\eta_{H_2O}}{\eta_{loaded}}\Big]^{0.8} \tag{4.67}$$

where $D_{CO_2}^{H_2O}$ represents diffusivity of CO_2 in water, which is calculated using the following correlation suggested by Versteeg and Van Swaalj (1988):

$$D_{CO_2}^{H_2O} = 2.35 \times 10^{-6} \times exp\big(\frac{-2119}{T}\big) \tag{4.68}$$

4.8.4 Heat capacity of the liquid-phase

Heat capacity of the liquid-phase is estimated using the following equation obtained from Cheng et al. (1996):

$$C_{PL} = \Big[(1-w) \times C_{P,H2O} + w \times C_{P,MEA} + w(1-w) \times \Big(-0.9198 + 0.013969 \times (T - 273.15) + \frac{69.643w}{(T-273.15)^{1.5859}}\Big)\Big] \times 10^3 \tag{4.69}$$

where w is weight fraction of MEA; $C_{P,H2O}$ and $C_{P,MEA}$ are pure water and MEA heat capacity terms, which are estimated using the following equations (Cheng et al., 1996):

$$C_{P,H2O} = \left[4.1908 - 6.62(T - 273.15) \times 10^{-4} + 9.14 \times 10^{-6}(T - 273.15)^2\right] \times 10^3 \tag{4.70}$$

$$C_{P,MEA} = \left[2.5749 + 6.612(T - 273.15) \times 10^{-3} - 1.9 \times 10^{-5}(T - 273.15)^2\right] \times 10^3 \tag{4.71}$$

4.8.5 Heat of CO_2 absorption

Several model parameters such as density, viscosity, diffusion coefficient, and reaction rate in the liquid-phase are affected by the liquid-phase temperature. Among the parameters affecting the liquid-phase temperature, heat of absorption of CO_2 is a significant contributor. Therefore, estimating this parameter is crucial in modelling of CO_2 absorption. Heat of CO_2 absorption is a combined term representing the sum of heat of reaction between MEA and CO_2, and heat of CO_2 dissolution (Svensson et al., 2013).

In the present work, the heat of absorption of CO_2 per moles of absorbed CO_2 (ΔH_r) is estimated using the following correlation obtained from Svendsen (2017):

$$\Delta H_r = 1000 \times \left[84.68 - 0.1135(T - 273.15) + 0.0027(T - 273.15)^2\right] \tag{4.72}$$

4.8.6 Mass transfer coefficients

Gas-phase mass transfer coefficient

Mass transfer coefficient of the gas-phase is estimated using the following correlation obtained from Luo et al. (2012):

$$k_g = \frac{Sh_g D_{CO_2,g}}{D_h} \tag{4.73}$$

$$Sh_g = 0.6655 Sc_g^{1/3} Re_g^{0.5} \tag{4.74}$$

where $D_{CO_2,g}$ and D_h are the diffusivity of CO_2 in the gas-phase and hydraulic diameter, respectively; Sh_g, Sc_g, and Re_g are the Sherwood, Schmidt, and Reynolds numbers, respectively.

Membrane mass transfer coefficient

Membrane mass transfer coefficient (k_m) can be calculated using the following equation for non-wetting mode (Kreulen et al., 1993a):

$$k_m = \frac{D_{P,i}\epsilon_m}{\tau}\frac{1}{\delta_{dry}} \tag{4.75}$$

where ϵ_m and τ are porosity and tortuosity of the membrane, respectively; $D_{P,i}$ represents effective gas diffusivity; δ_{dry} represent thickness of the membrane. However, the magnitude of k_m cannot be precisely estimated with this equation due to different reasons (Chabanon et al., 2013). Some of them are discussed below:

- The magnitude of $D_{P,i}$ is affected by diameter of the membrane pores and pore size distribution. Average value of the pore size is taken by most of authors. However, the effect of pore-size distribution, which is most of the time unknown, should be considered to get a precise estimate of the parameter.
- The numerical value of τ is estimated empirically and varies from one up to ten depending on the structure of the membrane. Precise estimation of this parameter needs detailed knowledge of the membrane geometrical parameters. Several authors estimate the value of τ from ϵ_m using different relations such as $\tau = 5\epsilon_m$ (Zaidiza et al., 2014) and $\tau = (2 - \epsilon_m)^2/\epsilon_m$ (Boucif et al., 2012).

Therefore, different values of k_m can be estimated based on different assumptions for the same membrane material, which could lead to different conclusions. Due to these uncertainties in estimating the value of k_m, several authors (Chabanon et al., 2014; Kimball et al., 2014; Zaidiza et al., 2015, 2016) used an experimental value of k_m in their modeling. The same approach is followed in the present work, and a literature value of k_m is used. The numerical value k_m used in the present work is within the range of values experimentally obtained by Ansaloni (2017a). To investigate the effect of k_m on separation performance of the HFMC, a sensitivity analysis was performed (see section 5.1.5).

4.8.7 Heat transfer coefficients

Membrane heat transfer coefficient

Membrane heat transfer coefficient (h_m) is estimated using the resistance in parallel model as proposed by Hoff and Svendsen (2014):

$$h_m = \frac{\epsilon_m \lambda_g + (1 - \epsilon_m)\lambda_m}{R \times ln(\frac{R_y}{R})} \tag{4.76}$$

Where λ_g and λ_m are thermal conductivity of the gas-phase and membrane, respectively. PTFE membrane is considered in the present work and thermal conductivity of this membrane is set to 0.22 ($\frac{W}{mK}$) which is found from Rongwong et al. (2013).

Gas-phase heat transfer coefficient

The Chilton-Colburn analogy is used to estimate heat transfer coefficient of the gas-phase from the gas-phase mass transfer coefficient (Bird et al., 2007):

$$h_g = k_g \Big[\frac{\rho_g C_{Pg} \lambda_g^2}{(D_{CO_2,g})^2} \Big]^{1/3} \tag{4.77}$$

where C_{Pg}, and λ_g are specific heat capacity, and thermal conductivity of the gas-phase, respectively; $D_{CO_2,g}$ represents diffusivigy of CO_2 in the gas-phase.

4.8.8 Physical properties of the gas-phase

Density of the gas-phase

From assumption 4, the gas-phase is assumed to be ideal. Thus, density of the gas-phase is calculated using the ideal gas law:

$$\rho_g = \frac{P_g.M_g}{R_g T_g} \tag{4.78}$$

where M_g is average molecular weight of the gas-phase, which is given by:

$$M_g = \sum_{i=1}^{n} M_i.x_i \tag{4.79}$$

where M_i and x_i are molecular weight and mole fraction of pure components in the gas-phase.

Viscosity of the gas-phase

Viscosity of the gas-phase is calculated as a function of viscosity and molecular weight of the pure components in the gas-phase using the following equation proposed by Wilke (1950):

$$\eta_g = \sum_{i=1}^{n} \frac{\eta_i}{1 + \frac{1}{x_i}\sum_{j=1,j\neq i}^{j=n}(x_j.A_{ij})} \tag{4.80}$$

where η_i represents viscosity of component i in the gas-phase; n represents the total number of components in the gas-phase.

The interaction parameter for gas-phase viscosity (A_{ij}) is given by the following equation:

$$A_{ij} = \frac{\left[1 + (\eta_i/\eta_j)^{1/2}.(M_j/M_i)^{1/4}\right]^2}{2\sqrt{2}\left[1 + M_i/M_j\right]^{1/2}} \tag{4.81}$$

Viscosities of the pure components in the gas-phase are estimated using the Chapman-Enskog theory as described by Brodkey and Hershey (2003):

$$\eta_i = 2.6693.10^{-26}\frac{\sqrt{M_i.T_g}}{\sigma_i^2.\Omega_{\mu_i}} \tag{4.82}$$

where σ is collision diameter of the components, which is given in table 4.2; Ω_μ represents collision integral of the pure components of the gas-phase, which is estimated using the following correlations:

Non-polar components:

$$\Omega_\mu = \frac{1.1645}{T^{*0.14874}} + \frac{0.52487}{exp(0.77320 \times T^*)} + \frac{2.16178}{exp(2.43787 \times T^*)} \tag{4.83}$$

Table 4.2: Collision diameter and collision integral of pure gases (Brodkey and Hershey, 2003).

	N_2	H_2O	CO_2	O_2	Ar
$\sigma[\times 10^{-10}\text{m}]$	3.798	2.642	3.941	3.467	3.542
ϵ/k[K]	71.4	809.1	195.2	106.7	93.3

Polar components:

$$\Omega_\mu = \frac{1.1645}{T^{*0.14874}} + \frac{0.52487}{exp(0.77320 \times T^*)} + \frac{2.16178}{exp(2.43787 \times T^*)} + 0.2 \times \frac{\sigma^2}{T^*} \quad (4.84)$$

where T^* is a dimension-less temperature estimated using:

$$T^* = \frac{T_g}{\epsilon/k} \quad (4.85)$$

where ϵ/k is an energy ratio which given in table 4.2.

Thermal conductivity of the gas-phase

Thermal conductivities of the polyatomic gases (CO_2, N_2, H_2O, and O_2) are estimated using the Eucken correlation (equation 4.86) and modified Eucken equation (equation 4.87) as discussed by Brodkey and Hershey (2003). The thermal conductivity estimated using Eucken correlation is lower than experimental values while thermal conductivity estimated using the modified Eucken equation is higher than experimental values; for example, each being about 3% different when applied for estimating thermal conductivity of air (Brodkey and Hershey, 2003). Thus, the thermal conductivity of the polyatomic gases used in the present work is taken as the average value of the two equations.

The Eucken equation for estimating thermal conductivity (λ_i) of poly-atomic gases is given by (Brodkey and Hershey, 2003):

$$\lambda_i = \eta_i.(C_{Pi} + \frac{5R}{4.M_i}) \quad (4.86)$$

The Modified Eucken equation for estimating thermal conductivity of poly-atomic gases is given by (Brodkey and Hershey, 2003):

$$\lambda_i = \eta_i.(1.32\frac{C_{Pi}}{\Gamma_i} + \frac{1.4728 \times 10^4}{M_i}) \quad (4.87)$$

Thermal conductivity of monoatimic gases (argon) is estimated using the Champman-Enskog theory as described by Brodkey and Hershey (2003), with the constants given in table (4.2):

$$\lambda_{Ar} = 8.3224.10^{-22}\frac{(T_g/M_{Ar})^{0.5}}{(\sigma_{Ar}^2 * \Omega_{Ar})}; \quad (4.88)$$

Table 4.3: Parameters for estimating $C_{p,g,i}$ using equation 4.91 (Poling et al., 2001).

	CO_2	H_2O	N_2	O_2	Ar
$a_{(i,0)}$	3.259	4.395	3.539	[3.630	2.500
$a_{(i,1)}$	1.356^{-3}	-4.186^{-3}	-0.261^{-3}	-1.794^{-3}	0
$a_{(i,2)}$	1.502^{-5}	1.405^{-5}	0.007^{-5}	0.658^{-5}	0
$a_{(i,3)}$	-2.374^{-8}	-1.564^{-8}	0.157^{-8}	-0.601^{-8}	0
$a_{(i,4)}$	1.056^{-11}	0.632^{-11}	-0.099^{-11}	0.179^{-11}	0

Thermal conductivity of the gas-phase is calculated using the Wassiljewa equation (Poling et al., 2001):

$$\lambda_g = \sum_{i=1}^{n} \frac{\lambda_i}{1 + \frac{1}{x_i} \sum_{j=1, j\neq i}^{j=n} (x_j . A_{ij})} \tag{4.89}$$

The interaction parameter A_{ij} is approximated using equation 4.81 .

Diffusivity of CO_2 in the gas-phase

Diffusivity of CO_2 in the gas-phase is estimated using the Fuller equation (Poling et al., 2001):

$$D_{AB} = \frac{1.013 \times 10^{-2} T_g^{1.75} (1/M_A + 1/M_B)^{0.5}}{P_g \left[(\sum_A v)^{1/3} + (\sum_B v)^{1/3} \right]^2} \tag{4.90}$$

where $\sum v$ represents sum of atomic volumes of each component. During implementation of the above equation, a binary mixture of CO_2 (A) and inert gas (B), which are the remaining gas components is considered.

Heat capacity of gas-phase components

Molar heat capacities of the pure components in the gas-phase are estimated using the following equation obtained from Poling et al. (2001):

$$C_{p,g,i} = R_g \Big(a_{(0,i)} + a_{(1,i)} T_g + a_{(2,i)} T_g^2 + a_{(3,i)} T_g^3 + a_{(4,i)} T_g^4 \Big) \tag{4.91}$$

where the parameters in the equation are given in table 4.3.

4.9 Numerical Solution of Model Equations

An appropriate numerical method is required to solve the set of partial differential equations in the developed HFMC model. Hoff et al. (2002) studied numerical solution of two-dimensional membrane contactor model equations using the finite volume and the method of lines (MOL)/ finite difference (FD) methods. It was found that the speed and stability of the MOL/FD is the best. However, the MOL/FD method is not mass conservative, which could lead to loss of mass. The authors suggested that the liquid-phase diffusion coefficient should not be considered constant along the radial direction to minimize loss

of mass. Therefore, radial variations of diffusivity terms in the liquid-phase mole balance equations are considered in the present work as discussed in section 4.3.1.

In the present work, the MOL/FD method is used to solve the HFMC model equations in the programming language MATLAB. The MOL is based on converting the set of partial differential equations to a set of ordinary differential equations (ODEs), which are then integrated using appropriate ODE solver (Schiesser, 2012). This is done by discretizing all dimensions except one which is treated as a continuous variable. In the present work, dss020 and dss042 FD routines (Schiesser, 2012) are used for discretization of the first order and second order derivatives in the radial direction, respectively. Due to the relatively high rate and heat of reactions between CO_2 and MEA, the resulting set of ODEs are stiff (Zaidiza et al., 2016). Hence, ODE15s is used for integrating the resulting systems of ODEs in the z-direction. ODE15s is a popular, variable order MATLAB routine used for solving stiff problems (Shampine and Reichelt, 1997).

The reactions between MEA and CO_2 are very fast and occur near the membrane-liquid interface, which could lead to very steep gradients near the interface (Hoff et al., 2004; Hoff and Svendsen, 2014; Zaidiza et al., 2014, 2016). Thus, many discretization points near the interface are needed to get high resolution of the gradients. To achieve this, two sub-domains in the radial direction with a separate number of discretization points are considered, and the derivatives in the radial direction are discretized on each domain (Hoff et al., 2004; Hoff and Svendsen, 2014; Zaidiza et al., 2014, 2016). This approach decreases the order of the numerical method, which may affect its numerical stability (Hoff et al., 2002). Therefore, a lower value of absolute tolerance is used.

ODE15s needs initial values for integrating the resulting system of ODEs. However, since counter-current flow configuration is considered in the present work, the liquid-phase enters the HFMC at z=0 while the gas-phase enters at z=L. Thus, the inlet conditions of the liquid-phase and the outlet conditions of the gas-phase should be supplied as initial conditions to the integrator. This requires an initial guess of the outlet conditions of the gas-phase. For this purpose, an iteration loop with the Broyden method is used. Broyden's method is a quasi-Newton method which is used to solve a system of non-linear equations (Keil et al., 2012). Unlike Newton's method, which calculates the Jacobine matrix in each iteration for solving non-linear equations of the form $\mathbf{f(x) = 0}$, the Broyden's method uses an approximation of the Jacobian, which is then updated at each iteration (Kelley, 2003). This reduces the complexity and cost of computing the Jacobian matrix. Details about the Broyden's method can be found in the literature (Kelley, 2003; Keil et al., 2012).

In the present work, initial guesses of the gas-phase outlet conditions are provided to the Broyden method routine, which in turn sends them to the integrator. Then the ODE15s integrates the sets of ODEs starting from the liquid-phase inlet to the liquid-phase outlet along the HFMC length. Then the actual initial conditions of the gas-phase are compared with the inlet gas-phase conditions calculated from the numerical method. The iteration continues until the error is below the specified tolerance or until the specified maximum number of iterations are exceeded. A schematic representation of the model implementa-

tion is shown in Figure 4.2.

As mentioned earlier, the use of the MOL/FD method for solving the model equations may lead to loss of mass. To estimate the amount of mass loss, a separate total mole balance on the shell side and tube side of the HFMC is performed and compared as presented in the following section.

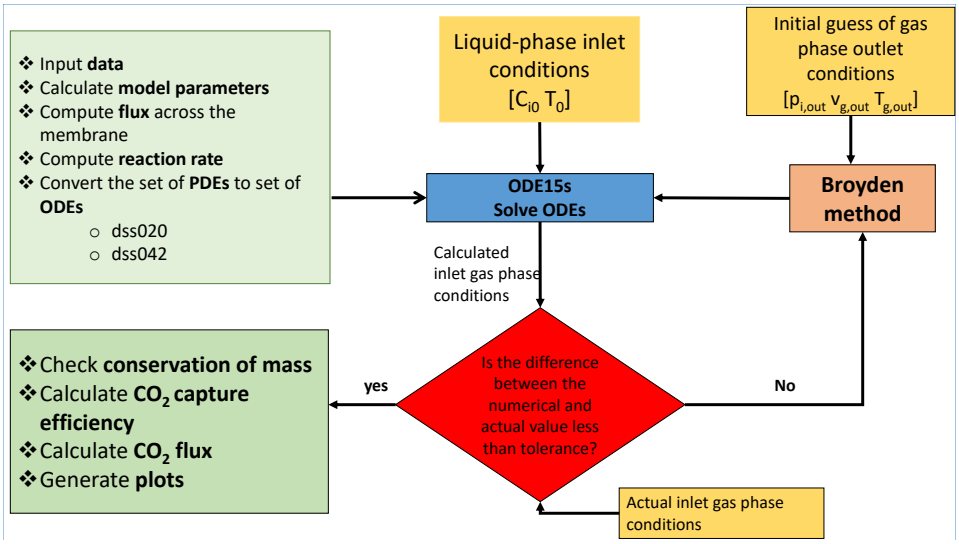

Figure 4.2: Schematic representation of model implementation.

Total CO_2 mole balance on the gas-phase:

$$\Delta n_{CO_2} = n_{CO_2,0} - n_{CO_2} \tag{4.92}$$

where Δn_{CO_2} represent the rate of CO_2 absorption based on the mole balance on the gas-phase; $n_{CO_2,0}$ and n_{CO_2} are the moles of CO_2 per second in the inlet and outlet gas-phase, respectively. They are given by the following equations:

$$n_{CO_2,0} = \frac{A_g v_{g0} p_{CO_2,0}}{R_g T_{g0}} \tag{4.93}$$

$$n_{CO_2} = \frac{A_g v_g p_{CO_2}}{R_g T_g} \tag{4.94}$$

where, $v_{g,0}$ and v_g are the inlet and outlet gas-phase velocity, respectively; $p_{CO_2,0}$ and p_{CO_2} are the inlet and outlet partial pressures of CO_2 in the gas-phase, respectively; A_g represents gas-phase flow cross section area.

Total CO_2 mole balance on the liquid-phase:

$$\Delta m_{CO_2} = m_{CO_2} - m_{CO_2,0} \tag{4.95}$$

where Δm_{CO_2} represent the rate of CO_2 absorption based on the mole balance on the liquid-phase; $m_{CO_2,0}$ and m_{CO_2} are the liquid-phase inlet and outlet total moles of CO_2 per second, which are given by the following equations:

$$m_{CO_2,0} = v_{vav} A_L (C_{CO2,0} + C_{MEACOO,0}) \tag{4.96}$$

$$m_{CO_2} = n_{tubes} \int_0^{2\pi} \int_0^R \Big[C_{CO2}(r) + C_{MEACOO}(r) \Big] v_z(r) r dr d\theta \tag{4.97}$$

$$\tag{4.98}$$

where A_L is liquid-phase flow cross section area; n_{tubes} is number of fibers in the HFMC module; $v_z(r)$ is radial velocity profile of the liquid-phase at the outlet; $C_{CO2,0}$ and $C_{MEACOO,0}$ are the inlet concentrations of free CO_2 and C_{MEACOO^-} in the liquid-phase, respectively; $C_{CO2}(r)$ and $C_{MEACOO^-}(r)$ are radial concentration profiles of free CO_2 and C_{MEACOO^-} at the liquid-phase outlet.

Δm_{CO_2} and Δn_{CO_2} are compared to check mass conservation and the error found is less than 0.2%, which is lower than the results of Hoff et al. (2004) (1%). Therefore, the loss of mass in the present work can be considered negligible and as in Hoff et al. (2004) the MOL/FD method can be used to solve the set of differential equations.

CO_2 removal efficiency and CO_2 absorption flux are used to measure the performance of the HFMC. The equations used for estimating these parameters are presented in the following section.

CO_2 removal efficiency

The following equation is used to calculate CO_2 removal efficiency:

$$CO_{2,removal}(\%) = \frac{\Delta n_{CO_2}}{n_{CO_2,0}} \times 100 \tag{4.99}$$

CO_2 absorption flux

CO_2 absorption flux is defined as the total absorbed moles of CO_2 per unit area and is estimated using the following equation:

$$CO_{2,flux} = \frac{\Delta n_{CO_2}}{A_t} \tag{4.100}$$

where A_t represents the total mass transfer area.

Chapter 5

Results and Discussion

The developed HFMC model was applied for simulation of CO_2 capture from a flue gas of an 800 MWe coal-fired power plant. First, sensitivity analysis of important model parameters was performed. Then design of industrial-scale HFMC modules for 90% CO_2 capture from the flue gas of the power plant was performed and compared with the specifications of packed column applied for the same case study. Finally, the HFMC model results were compared with pilot-scale experimental data. This chapter presents results and discussion of these points in the respective order.

5.1 Sensitivity Analysis

In this section, the influence of important parameters such as liquid-phase velocity, gas-phase velocity, solvent lean loading, membrane fiber length, and membrane mass transfer coefficient on CO_2 absorption flux and CO_2 removal efficiency is presented. Investigation of these parameters allows identification of the main variables that have a significant impact on CO_2 capture performance of the HFMC modules. Additional results on the effect of these parameters on solvent rich loading are presented in Appendix A. The specifications of the industrial-scale HFMC modules used for sensitivity analysis are given in Table 5.1. Table 5.2 lists the base case value and corresponding variation ranges of the five parameters selected for the sensitivity analysis. The operating conditions are listed in Table 5.3. The base case values were estimated based on information obtained from Kimball et al. (2014). For example, the base case value of the flue gas velocity used for the sensitivity analysis was 1.16 ms^{-1}. This was estimated based on the gas-flow rate given in Table 5.3 and the cross-sectional area available for the gas-phase flow, which was estimated based on the HFMC specifications listed in Table 5.1.

5.1.1 Effect of gas-phase velocity

Figure 5.1 shows the influence of gas-phase velocity on CO_2 removal efficiency and CO_2 absorption flux in the HFMC modules. Decreasing the gas-phase velocity decreases the

Table 5.1: Specifications of industrial-scale HFMC modules used for sensitivity analysis (Kimball et al., 2014).

	Value	Unit
Module diameter	4.07	m
Number of modules	100	-
Number of fibers per module	1.2×10^{7}	-
Specific interfacial area	1250	m^2m^{-3}
Fiber inner diameter	4.3×10^{-4}	m
Fiber outer diameter	8.7×10^{-4}	m
Material	PTFE	-

Table 5.2: Base case values and their corresponding variation ranges of five variables used for a sensitivity analysis.

Variable	Base case	Min value	Max value	Unit
Gas velocity (v_g)	1.16	0.93 (-20%)	1.39 (+20%)	ms^{-1}
Liquid velocity (v_{av})	1.99×10^{-2}	1.19×10^{-2} (-40%)	3.98×10^{-2} (+100%)	ms^{-1}
Fiber length (L)	1.23	0.98 (-20%)	1.48 (+20%)	m
Lean loading (α_{lean})	0.26	0.10 (-60%)	0.34 (+30%)	-
Membrane mass transfer coefficient (k_m)	2.58×10^{-4}	3.1×10^{-5} (-88%)	3.1×10^{-4} (+20%)	ms^{-1}

Table 5.3: Flue gas conditions of an 800 MWe coal-fired power plant and solvent conditions used in the present work (Kimball et al., 2014).

	Value	unit
Flue gas		
Flow rate	680	m^3s^{-1}
Temperature	323	K
Pressure	101.325	kPa
Compositions:		
CO_2	13.4	Vol.%
O_2	3.6	Vol.%
N_2	71.1	Vol.%
H_2O	11.9	Vol.%
Solvent		
Temperature	313	K
MEA weight fraction	30	wt%

partial pressure of CO_2 at the gas-liquid interface, which decreases the driving force for transfer of CO_2 toward the liquid-phase. In addition, decreasing the gas-phase velocity increases the thickness of the gas- film, which increases the gas-film mass transfer resistance. Thus, CO_2 absorption flux decreases with the decrease in the gas-phase velocity. Similar trends were obtained by several studies (Mavroudi et al., 2006; Atchariyawut et al., 2007; Boributh et al., 2011). Decreasing the gas-phase velocity also increases the residence time of the flue gas in the HFMC modules, which increases CO_2 removal efficiency. This behavior is also observed in Figure 5.1 and several studies (Mavroudi et al., 2006; Bottino et al., 2008; Eslami et al., 2011; Hua et al., 2013; Hassanlouei et al., 2013) have reported a similar trend.

The investigations on the effect of the gas-phase velocity indicated that the gas-phase velocity has a contrasting effect on CO_2 absorption flux and CO_2 removal efficiency. That is, increasing gas-phase velocity increases CO_2 absorption flux, and decreases CO_2 removal efficiency. Thus, the gas-phase velocity is one process parameter that can be optimized taking into account the trade-off of the CO_2 absorption flux and the fraction of CO_2 in the flue gas that permeates the membrane. In practical applications of HFMC modules, decreasing gas-phase velocity also decreases the impact of erosion but increases the chance of ash drop out (Kimball et al., 2014). Thus, the design of HFMC modules should also consider these cases during optimization of the gas-phase velocity.

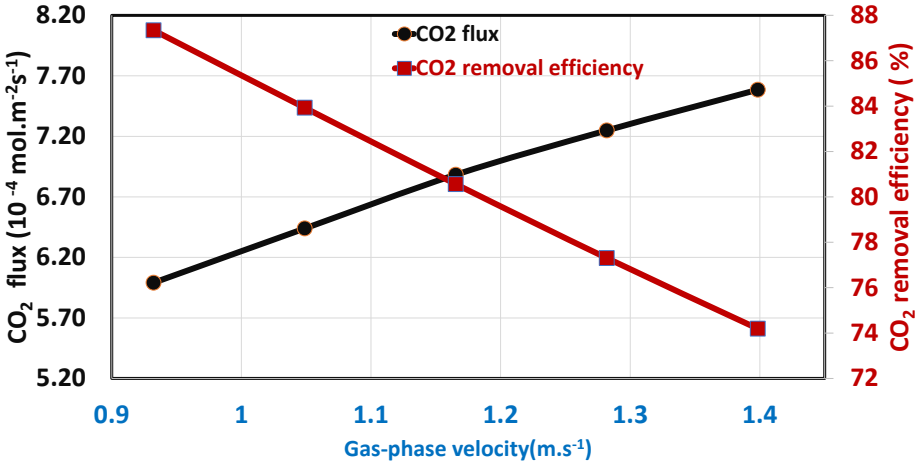

Figure 5.1: Effect of gas-phase velocity on CO_2 removal efficiency and CO_2 absorption flux.

5.1.2 Effect of liquid-phase velocity

The effect of liquid-phase velocity on CO_2 absorption flux and CO_2 removal efficiency is shown in Figure 5.2. The liquid-phase velocity was varied from 1.19×10^{-2} to 3.98×10^{-2}

ms^{-1} to cover a wide range of values around the base case value. It is obvious that increasing the liquid-phase velocity increases active MEA at the gas-liquid interface, which increases the rate of reaction between CO_2 and MEA at the interface. This increases the CO_2 concentration gradient between the gas and liquid-phases. In addition, increasing the liquid-phase velocity also decreases the thickness of the liquid-film, which decreases the liquid-side mass transfer resistance (Franco et al., 2008). Due to these two factors, CO_2 absorption flux is expected to increase with the increase in the liquid-phase velocity. However, the profile in Figure 5.2 does not show this expectation.

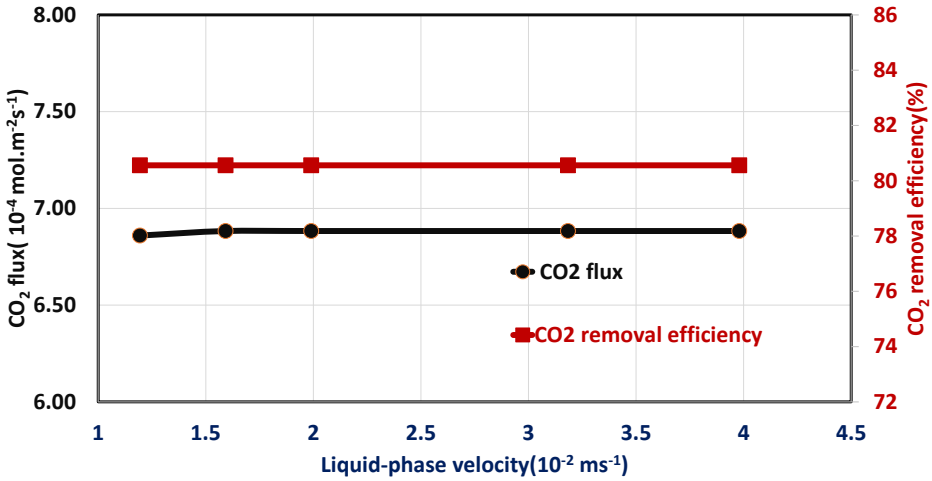

Figure 5.2: Effect of liquid-phase velocity on CO_2 removal efficiency and CO_2 absorption flux.

When the liquid-phase velocity increases from 1.2×10^{-2} to 1.6×10^{-2} ms^{-1}, CO_2 absorption flux slightly increases from 6.86×10^{-4} to 6.88×10^{-4} mol m^{-2} s^{-1}, which is negligible and most likely due to a convergence/numerical issue. For all practical purposes, they are considered the same value. Then the CO_2 absorption flux steadies out at 6.88×10^{-4} mol m^{-2} s^{-1} for any further increases in the liquid-phase velocity. To see if the liquid-phase velocity has some effect on the performance of the HFMC, a very small velocity was tried. However, the simulation failed when implementing a very small velocity (below $1.2 \times 10^{-2} ms^{-1}$). The residence time of the gas-phase was fixed constant in this case. If the CO_2 absorption flux is not changing and the residence time of the gas-phase is constant, then the CO_2 removal efficiency will be constant as shown in Figure 5.2. These observations indicate that the liquid-phase velocity has a negligible effect on the CO_2 absorption flux and CO_2 removal efficiency under the operating conditions considered. The probable reason for these observations is discussed in the following paragraphs.

Three resistances in series are involved in the transfer of CO_2 from the gas-phase to the liquid-phase. These are the gas-film, membrane, and liquid-film mass transfer resistances.

In the present work, a separate equation for the liquid-phase mass transfer coefficient was not used. Instead, a rigorous two-dimensional mass balance was considered for the liquid-phase (see equation 4.2). The liquid-phase mass transfer resistance is usually small due to the fast chemical reactions between CO_2, H_2O, and MEA involved (Hassanlouei et al., 2013). Therefore, in the present work, the diffusion of the species in the liquid-phase was considered to be not limiting the transfer of CO_2 from the gas-phase to the liquid-phase (this is discussed in section 5.4.1). The molar flux equation (equation 4.40) is based on the gas-phase mass transfer coefficient (k_g) and membrane mass transfer coefficient (k_m). The gas-phase and membrane mass transfer resistances were compared during the simulation and the mass transfer resistance due to the membrane was found to be dominant. For example, in one of the cases, the k_g was 0.1 ms^{-1}, and the k_m was 2.58$\times$ 10^{-4} ms^{-1}. Therefore, the increase in driving forces due to the increase in liquid-phase velocity is outweighed by the large membrane mass transfer resistance. Thus, the liquid-phase velocity has a negligible effect on CO_2 absorption flux and CO_2 removal efficiency. Studies conducted by Hassanlouei et al. (2013) reported similar trends. In another study conducted by Franco et al. (2008), membrane wetting resulted in a significant increase in the overall mass transfer resistance and become rate limiting. Thus, the effect of liquid-phase velocity on the overall mass transfer coefficient and thus on CO_2 absorption flux was found to be negligible. Rongwong et al. (2013) compared the effect of liquid-phase velocity on CO_2 absorption flux under non-wetted and partially-wetted modes. The authors indicated that the increases in CO_2 absorption flux with liquid-phase velocity was insignificant under partially-wetted mode than that of non-wetted mode because the mass transfer resistance was significantly increased due to membrane wetting. The value of k_m of PTFE (2.58 $\times$ 10^{-4} ms^{-1}) used in the present work is within the lower ranges of the values reported in the literature (10^{-4}-10^{-3} ms^{-1}) (Chabanon et al., 2011). The PTFE considered in the present study had been used for several months (Chabanon et al., 2014) and thus membrane wetting could be the main reason for the lower k_m value. Therefore, the main reason for the negligible effect of liquid-phase velocity on CO_2 absorption flux is due to the large membrane mass transfer resistance that was considered.

However, there are also studies that do not fully support the observations in the present work. For example, in a study conducted by Zhang et al. (2006), CO_2 absorption rate increased with increasing liquid-phase velocity when the liquid-phase velocity was low ($<$0.05 ms^{-1}). The authors said that depletion of active absorbents at the gas-liquid interface was the reason for this trend. In this case, the CO_2 absorption rate was influenced by liquid-side mass transfer resistance, which depends on liquid-phase velocity. However, the CO_2 absorption rate was independent of liquid-phase velocity at high liquid-phase velocity ($>$0.1 ms^{-1}) where there was no depletion of active absorbents at the gas-liquid interface. Thus, CO_2 absorption rate was influenced by kinetics and was independent of the liquid-phase velocity (Kumar Paramasivam Senthil, 2002). Kumar Paramasivam Senthil (2002), Dindore et al. (2005) and Rongwong et al. (2013) also reported similar trends. As mentioned before, unfortunately, cases at low liquid-phase velocities could not be simulated. Therefore, this asymptotic trend could not be verified. Besides, depletion of MEA at the gas-liquid interface was not observed in the present work. The difference in the results of the present work with the literature cited could have also stemmed from the large

membrane mass transfer resistance considered in the present work. Moreover, the operating conditions used in the present work are different from the literature works cited here. However, the cited works and the present work indicate that the effect of liquid-phase velocity on the performance of HFMC module depends, primarily, on the membrane mass transfer coefficient (membrane type and wetting status). A study conducted by Tontiwachwuthikul et al. (2006) strongly supports this conclusion. The authors reported that the performance of HFMC made of PTFE was independent of the liquid-phase flow rate. However, the same study has reported that the liquid-phase flow rate enhanced the performance of HFMC made of PP.

5.1.3 Effect of membrane fiber length

The effect of membrane fiber length on the performance of HFMC modules was also investigated. Increasing the length of membrane fiber increases the contact area and contact time between the liquid and gas-phases. This favors diffusion of CO_2 from the gas-phase to the liquid-phase and reaction of CO_2 with MEA. Thus, the CO_2 removal efficiency increases with the increase in the membrane fiber length as shown in Figure 5.3. According to the simulation results, CO_2 removal efficiency was increased by 4.5%, 3.8% and 3% when the membrane fiber length was increased from 1.11 to 1.23 m (11% length increase), 1.23 to 1.35 m (10% length increase), and 1.35 to 1.48 m (10% length increase), respectively. A similar trend was obtained by Boributh et al. (2011). They showed that CO_2 removal efficiency was, respectively, 14.5%, 23.19% and 29.77% when the membrane fiber length was 0.25, 0.5 and 0.75 m showing similar observations as in the present work.

As shown before, the CO_2 removal efficiency is not directly proportional to membrane fiber length. The CO_2 concentration gradient (driving force) between the gas and liquid-phases will decrease along the membrane fiber length. This is due to the saturation of the liquid-phase and the decrease in the partial pressure of CO_2 in the gas-phase along the membrane fiber length. This results in a decrease of CO_2 absorption flux with the increase in the membrane fiber length as shown in Figure 5.3. Similar trends were obtained by several authors (Kumar Paramasivam Senthil, 2002; Boributh et al., 2011). It should be noted that the gas-phase pressure drop was assumed negligible in the present work. However, in practical applications, the gas-phase pressure drop increases with increase in membrane fiber length. This would decrease further the partial pressure of CO_2 in the gas-phase, which, in turn, would decrease the CO_2 absorption flux more. This implies that the decrease in CO_2 absorption flux with the increase in the membrane fiber length would have been more significant if the gas-phase pressure drop had been considered. In addition, in practical applications, the use of too long membrane fibers together with the relatively higher viscosity of the liquid-phase could result in a higher pressure drop in the liquid-phase . The liquid-phase pressure drops obtained from the simulations were 6.8, 8.6 and 10.2 kPa for membrane fiber length of 1, 1.2 and 1.5 m, respectively. The *"break-through"* pressure could be exceeded due to these pressure drops. This could cause membrane wetting, which would result in a significant reduction of CO_2 capture performance of the HFMC modules. It should also be noted that commercial membrane

fibers are usually smaller than 1 m in length (Ansaloni, 2017a). Thus, a few membrane modules in series would be required when membrane fiber length larger than 1 m is considered.

In addition to the increase in CO_2 removal efficiency and the decrease in CO_2 absorption flux, the increase in membrane fiber length leads to:

i. increase in capital cost: increase in membrane fiber length means an increase in investment,

ii. increase in operating cost: increase in membrane fiber length increases the pressure drop as mentioned earlier. This increases power requirement of a blower, which increases the operating costs.

This indicates that the capital and operating costs of CO_2 capture in HFMC modules should be minimized while achieving the desired objective of CO_2 capture.

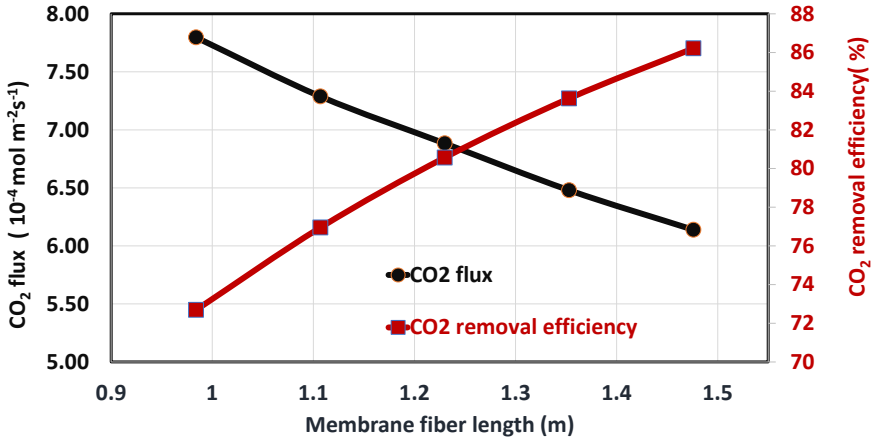

Figure 5.3: Effect of membrane fiber length on CO_2 removal efficiency and CO_2 absorption flux.

5.1.4 Effect of solvent lean loading

The effect of solvent lean loading on CO_2 removal efficiency and CO_2 absorption flux was also investigated. The solvent lean loading was varied from 0.1 to 0.34 to cover a relatively wide range of values around the base case value. It is obvious that as the solvent lean loading increases, the partial pressure of CO_2 in equilibrium with the bulk liquid-phase concentration increases and the availability of active MEA at the gas-liquid interface decreases. This decreases the driving force for transfer of CO_2 towards the liquid-phase.

Therefore, a reduction in CO_2 absorption flux with an increase in solvent lean loading is expected. However, Figure 5.4 shows that the CO_2 removal efficiency and CO_2 absorption flux are independent of the solvent lean loading. The explanation for this behavior is the same to the explanation used for the effect of liquid-phase velocity. The external mass transfer resistance, which is the sum of the gas-film ($k_g{}^{-1}$) and membrane ($k_m{}^{-1}$) resistances, outweighs the change in driving force. And the membrane mass transfer resistance is dominant. As mentioned earlier, the k_g was 0.1 ms^{-1}, and the k_m was 2.58×10^{-4} ms^{-1}. Thus, the rate of CO_2 absorption is limited by the availability of CO_2 in the gas-phase and is independent of solvent lean loading. In a study conducted by Zaidiza et al. (2015), solvent lean loading had no effect on CO_2 absorption flux when the MEA conversion, which is a function of lean and rich loading, was less than 0.6. 0.6 MEA conversion represents, for example, a rich loading of 0.43 if the solvent lean loading is 0.3. For higher absorbent conversions, CO_2 absorption flux was affected by the solvent lean loading. However, the membrane mass transfer coefficient used in that study (k_m=10^{-3} ms^{-1}) is higher than that of the present study (k_m=2.58×10^{-4} ms^{-1}). Thus, the membrane mass transfer resistance was not rate limiting in that study.

Solvent lean loading is an important parameter in CO_2 capture by chemical absorption. This parameter determines the cyclic capacity of an absorbent and has a significant effect on re-boiler energy requirement during solvent regeneration. A study conducted by Xu et al. (2016) showed that the re-boiler duty significantly decreased with an increase in solvent lean loading up to 0.27 mol/mol. The re-boiler duty then becomes independent of the solvent lean loading beyond this point. Another study conducted by Alie (2004) showed a similar trend. Therefore, even though the present study indicated that the solvent lean loading has a negligible effect on the performance of the HFMC modules, the solvent lean loading has to be taken into account during design of HFMC modules for CO_2 capture as this will affect the process energy requirement.

5.1.5 Effect of membrane mass transfer coefficient

Figure 5.5 shows the influence of membrane mass transfer coefficient (k_m) on CO_2 removal efficiency and CO_2 absorption flux. k_m was varied from 3.1×10^{-5} to 3.1×10^{-4} ms^{-1} to investigate its effect on the performance of HFMC modules if it is changed by one order of magnitude. The Figure shows that CO_2 removal efficiency and CO_2 absorption flux increase with the increase in k_m, unlike the gas-phase velocity and membrane fiber length which have contrasting effects on CO_2 removal efficiency and CO_2 absorption flux. The Figure also indicates that a reduction of k_m from 3.1×10^{-4} to 3.1×10^{-5} ms^{-1}, which is one order of magnitude, results in a reduction of CO_2 removal efficiency and CO_2 absorption flux by around 80%. In this case, it can be stated that membrane wetting significantly increased the membrane mass transfer resistance (Chabanon et al., 2011). This indicates that the value of k_m has a significant effect on the CO_2 capture performance, and design of HFMC modules. Similar trends were observed in several studies (Zaidiza et al., 2015, 2016). As discussed in section 2.4.5, membrane wetting can be prevented by maintaining high "*break-through* "pressure. Composite membranes have high "*break-through* "pressure due to the thin coating layer on the liquid-side of the membrane (Zhao

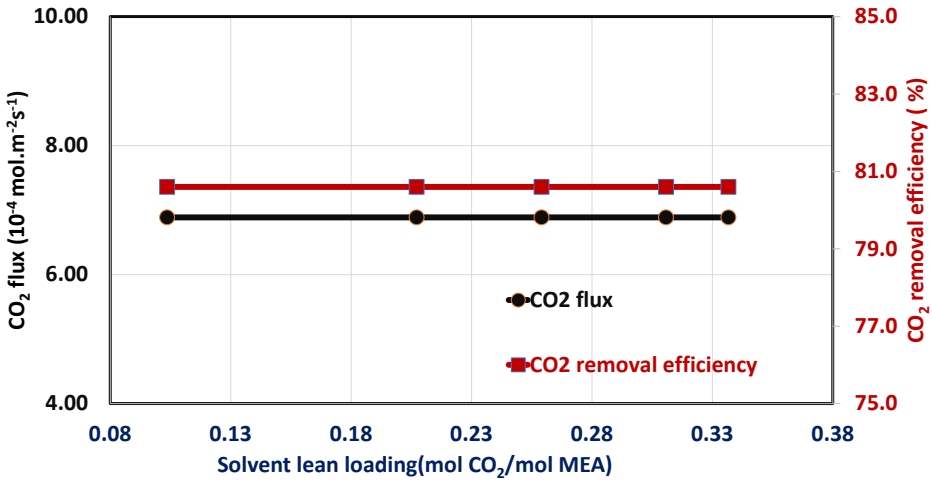

Figure 5.4: Effect of solvent lean loading on CO_2 removal efficiency and CO_2 absorption flux

et al., 2016). Therefore, composite membranes can overcome membrane wetting and thus prevent the increase in membrane mass transfer resistance due to membrane wetting.

5.2 Design of Industrial-scale HFMC Modules for 90% CO_2 Capture

After performing the sensitivity analysis, it was identified that few process parameters could influence in the capture rate. Based on the previous analysis, the membrane fiber length was optimized to capture 90% CO_2 from the flue gas of the 800 MWe coal-fired power plant. And a simulation of 90% CO_2 capture from the flue gas of the power plant was performed. The operating conditions presented in Table 5.3 were also used in this case. The value of inner and outer membrane fiber diameters and membrane specific contact area used in this study were the same as the values used for the sensitivity analysis (Table 5.1). Besides, the flue gas velocity used in this simulation was set to 1.16 ms^{-1}. The number and diameter of the HFMC modules were determined in such a way to allow this gas velocity. Since the diameter of commercial HFMC modules is less than 0.5m (Ansaloni, 2017a), this constraint was also considered when calculating the number of modules and module diameter. The number of fibers per module was then determined based on the given surface area to volume ratio and the calculated module diameter. k_m=2.58$\times 10^{-4}$ ms^{-1} was used and uniform distribution of fibers in the HFMC modules was assumed (Chabanon et al., 2014). Table 5.4 shows a summary of the results from the design of the industrial-scale HFMC modules. Comparison of the total gas-liquid contact area and the total volume of the HFMC modules with that of a structured packed column applied for the same case study is also provided in the same table. The specifications of the packed col-

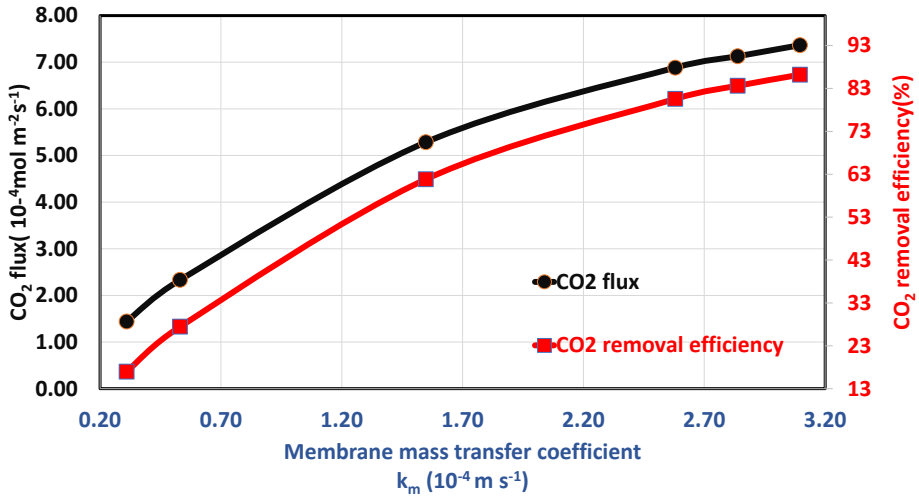

Figure 5.5: Effect of membrane mass transfer coefficient on CO_2 removal efficiency and CO_2 absorption flux

umn were developed under the EU sponsored FP7 project CESAR (Kimball et al., 2014) and are given below:

- Total surface area = 2.01 $\times$ 10^6 m^2
- Total volume = 16500 m^3

The results in Table 5.4 show that the total surface area required for 90% CO_2 capture in the HFMC modules is 1.37 times higher than that of structured packed column. As mentioned in the sensitivity analysis, the membrane mass transfer resistance is the rate limiting in the present work. Thus, the slightly higher required surface area of the HFMC modules is due to the large membrane mass transfer resistance. The results in Table 5.4 also show that there is 86% reduction in total absorber volume when HFMC modules are used instead of the structured packed column for 90% CO_2 capture. An absorber volume reduction by 75% was obtained by Hoff and Svendsen (2013) when replacing packed columns with membrane contactors for large-scale PCC. However, the authors used cross-flow modules, and the liquid-phase was flowing on the shell side and the gas-phase was flowing on the tube side. In the present work, a parallel-flow configuration was considered and the liquid-phase flows on the tube side. Using k_m=2.58$\times 10^{-4}$ ms^{-1}, and similar flow configuration and flue gas conditions with the present work, a study conducted by Kimball et al. (2014) also reported an absorber volume reduction by 90% when HFMC modules (total surface area=22 $\times$ 10^6 m^2 and total volume = 1597 m^3) were used instead of the packed column. The slight differences between the results of Kimball et al. (2014) and the results obtained in the present work might be due to differences in the governing

Table 5.4: Results from simulations of 90% CO_2 capture from a flue gas of an 800 MWe coal-fired power plant using 30wt% MEA in industrial-scale HFMC modules made of PTFE and comparison with structured packed column applied for the same purpose.

Parameter	value	unit
HFMC		
k_m	2.58×10^{-4}	ms^{-1}
# modules in parallel	1×10^4	#
Module diameter	0.407	m
# fibers per module	1.2×10^5	#
Fiber length	1.7	m
Total surface area	2.76×10^6	m^2
Total volume	2210.59	m^3
Liquid-phase pressure drop	12.5	kPa
Gas-phase velocity	1.16	ms^{-1}
Liquid-phase velocity	2.0×10^{-2}	ms^{-1}
Lean loading	0.27	mol/mol
Rich loading	0.43	mol/mol
HFMC vs Packed column		
Surface area ratio vs. Packed column	1.37	-
Volume ratio vs. Packed column	0.13	-

equations and assumptions, equilibrium model, reaction kinetics, and correlation of model parameters used in the HFMC model.

As discussed in section 2.3, the two major bottlenecks of CO_2 capture using chemical absorption in packed column are the high investment cost due to the large absorber size and the high operating cost due to the high solvent regeneration energy requirement. Among the several advantages that can be offered by HFMCs, one of the most important contribution to cost reduction is by decreasing the size of the absorber (i.e, by process intensification). Thus, the present work has shown the intensification potential of HFMCs. Nevertheless, 86% reduction in total absorber volume may or may not result in a reduction of total cost compared to that of packed column. To the best of my knowledge, there are very few studies (Kimball et al., 2014; NETL, 2005) that compared the economic analysis of HFMCs with that of packed column. In the study conducted by Kimball et al. (2014), the investment cost of the HFMC modules that resulted in 90% volume reduction was about 130% higher than the cost of the structured packed column. The rise in cost becomes even higher (above 600%) when lower value of k_m (k_m=5.31×10^{-5} ms^{-1}) was considered, which resulted in 70% volume reduction. However, a cost reduction by 34% when using HFMCs instead of random packing tower was reported by NETL (2005). These two contradictory reports suggest that a detailed economic analysis, which is beyond the scope of the present study, is required to evaluate the contribution of the intensification potential of the HFMC technology on cost reduction.

As mentioned earlier, solvent lean-loading should be considered in the design of HFMC modules because it affects the solvent cyclic capacity and the re-boiler energy requirement during solvent regeneration. Solvent rich loading also affects these parameters and thus should be considered in the design of HFMC modules. The re-boiler energy requirement is a sum of three heat requirements: heat required to reverse the reaction between CO_2 and MEA; heat required to increase temperature of the rich solvent to boiling point (sensible heat); and heat required for vaporization of water (Xu et al., 2016). A study conducted by Xu et al. (2016) indicated that re-boiler energy requirement decreases with increase in solvent rich loading. This is due to the increase in equilibrium partial pressure of water with the increase in solvent rich-loading (Xu et al., 2016). This decrease the heat required for vaporization of water. Moreover, increasing the solvent rich loading decreases the sensible heat since the mass flow rate of CO_2 increases with the increase in the solvent rich loading (Li et al., 2013). Therefore, higher solvent rich loading has an advantage as far as regeneration energy requirement is concerned. In the literature, a solvent lean loading between 0.242-0.271, and a solvent rich loading between 0.45-0.484 are recommended to minimize the re-boiler energy requirement (Steeneveldt et al., 2006; Abu-Zahra et al., 2007; Tobiesen et al., 2007; Kimball et al., 2014; Zaidiza et al., 2015). In the present work, a solvent lean loading of 0.27 and solvent rich loading of 0.43 are considered (see Table 5.4). The solvent rich loading is slightly outside the range of the recommended values. From sensitivity analysis (Appendix A.2) the solvent rich loading can be increased to 0.45 and above without affecting the CO_2 removal efficiency by decreasing the liquid-phase velocity. However, unfortunately, it was not possible to implement low liquid-phase velocity due to convergence problems as mentioned earlier. Sensitivity analysis (Appendix A.4) also indicated that increasing the solvent lean loading can increase the solvent rich loading without affecting the CO_2 removal efficiency. However, the solvent lean loading would be outside the range of the recommend values if it is increased beyond 0.27.

5.3 General Design Considerations of HFMC Modules

Even-though the results of the present study show that HFMC technology can provide a significant absorber volume reduction, there are several limitations, challenges, and factors that should be considered in the design of HFMC modules for large-scale PCC. These are discussed in the following paragraphs.

i. **Precise estimation of $\mathbf{k}_m$** :

   As discussed in section 5.1.5, the performance of HFMC modules is significantly influenced by the magnitude of k_m. The value of k_m can be traditionally estimated using equation 4.75 for a non-wetted mode. Nevertheless, the value of k_m obtained using that equation is subjected to large deviations; several authors have compared a theoretical value of k_m estimated using equation 4.75 with experimental values and they found errors of several orders of magnitude (Favre and Svendsen, 2012). The precise estimation of k_m is challenging due to the uncertainties in the parameters that affect it such as porosity, tortuosity, pore size distribution, and membrane

wetting (Favre and Svendsen, 2012; Chabanon et al., 2013) as discussed in section 4.8.6. Thus, the estimated surface area and volume of the HFMC modules in the present work can significantly increase or decrease if the value of k_m is changed. For example, the study conducted by Kimball et al. (2014) reported that the HFMC modules total volume and surface area increased by above 300% when k_m was decreased by a factor of five. Therefore, a method for precise estimation of k_m is required to estimate the specifications of the large-scale HFMC modules precisely.

ii. **Modularity and limitations in the size of HFMC modules:**

As shown in Table 5.3, the volumetric flow rate of the flue gas from the coal-fired power plant is very large. To increase the capacity of HFMC, 10000 modules in parallel are required when using HFMC modules with 0.407 m in diameter (see Table 5.4). The total number of HFMC modules can be increased if a fiber length larger than 1 m is used. In the present work, the membrane fiber length required for 90% CO_2 capture is 1.7 m (see Table 5.4). According to Ansaloni (2017a), the length of commercial membrane fibers is less than one meter. Thus, two HFMC modules with membrane fibers of 0.85 m length each can be used in series to obtain 1.7 m membrane fiber length. Therefore, the total number of HFMC modules (in series and parallel) required for 90% CO_2 capture from the flue gas of the 800 MWe power plant will be 20000. This large number of HFMC modules make the technology less practical. Because the number of HFMC modules in parallel determines the floor size of the HFMC; distribution of the inlet phases to the modules and collection of the outlet phases from the modules would be complex and difficult. Furthermore, maintenance and installation of large HFMC modules are difficult (Kimball et al., 2014).

Increasing diameter of the modules can decrease the number of modules in parallel. For example, the number of modules can be decreased to 100 (a factor of 100) by increasing the diameter of the modules to 4.07 m (a factor of 10), and the number of membrane fibers per module by a factor of 100. Simulation was performed based on these new dimensions. And the resulting total surface area and volume required for 90% CO_2 capture were the same as the results given in Table 5.4. This is due to the linear scalability of HFMC technology. A study conducted by Kimball et al. (2014) also used 100 membrane modules in parallel with 4 m in diameter. However, according to Ansaloni (2017a), diameter of a commercial HFMC module does not exceed 0.30 - 0.50 m. The HFMC module diameter used in the present work (0.407 m) was chosen based on this recommendation as mentioned earlier. Besides, the use of HFMC modules with a small diameter is recommended for improving the efficiency of chemical absorption (Kimball et al., 2014). Using a rectangular cross-flow modules of 1 m in depth and 3 by 3 m in width, a study conducted by Hoff and Svendsen (2013) decreased the number of modules in parallel to 25. The gas-phase flow rate employed in that study was half of the gas flow rate used in the present study. This rectangular cross-flow membrane module could be an interesting alternative to reduce the floor size of the HFMC modules in the present work; never-

theless, these dimensions are also not commercially available (Hoff and Svendsen, 2013). Increasing the number of modules in series can also decrease the number of modules in parallel. However, this would lead to increase in pressure drop. Therefore, the limitations in the size of HFMC modules and the large number of HFMC modules posed a challenge on the application of HFMC technology for large-scale PCC. On the other side, there is no such kind of size limitation and modularity in the conventional absorbers (Hoff and Svendsen, 2013). Thus, the numbers and dimensions of the HFMC modules in the present work are only used as a base case value for comparison; further studies on how to solve the challenges is required.

iii. **Gas-phase pressure drop:**

Negligible gas-phase pressure drop was assumed in the present work. However, a significant gas-phase pressure drop may occur due to the large number of fibers per module (1.2×10^5) and the large surface area (2.76×10^6 m^2) of the HFMC modules (see Table 5.4) (Favre and Svendsen, 2012). A small increase in gas-phase pressure drop increases the duty of a blower significantly (Li et al., 2017). For example, in a 500 MW power plant, a gas-phase pressure drop of 20 kPa resulted in an increase of power requirement by 50-60 MW (Le Moullec and Kanniche, 2011). Thus, the energy penalty of the power plant rises substantially due to the gas-phase pressure drop. In addition, if the gas-phase pressure drop exceeds 10 kPa, conventional blowers could not be utilized (Hoff and Svendsen, 2013). Therefore, the gas-phase pressure drop is another challenge that must be considered in the design HFMC modules for large-scale applications.

iv. **Liquid-phase pressure drop and membrane wetting:**

The membrane in HFMC technology brings additional mass transfer resistance to the CO_2 capture system, which becomes more significant under wetted conditions. To maintain non-wetted conditions, the *"break-through"* pressure should not be exceeded. However, a liquid-phase pressure drop of 12.5 kPa is obtained in the present work (see Table 5.4). This could cause membrane wetting by overtaking the *"break-through"* pressure. Besides, the liquid-phase pressure drop increases with increase in membrane fiber length (Mansourizadeh and Ismail, 2009). Thus, the liquid-phase pressure drop provides a constraint on the maximum length of membrane fibers that can be utilized at industrial-scale (Hoff and Svendsen, 2013, 2014). Furthermore, maintaining a higher *"break-through"* pressure using the suggestions discussed in section 2.4.5 is an important factor that should be considered in industrial applications of HFMC technology.

v. **Shell side vs tube side liquid flow**:

In HFMC modules, the liquid-phase can flow either on the tube side or shell side. These configurations determine the contact time between the gas- and liquid-phases, and liquid-phase pressure drop. Several authors have shown that higher CO_2 capture performance can be achieved by HFMC modules when the liquid-phase flows

on the tube side compared with the opposite configuration (Qi and Cussler, 1985; Tontiwachwuthikul et al., 2006). The performance of HFMC modules when the liquid-phase flows on the shell side was low due to channeling of the liquid-phase on the shell side. Besides, the liquid-phase flow on the tube side produces lower liquid-phase pressure drop compared to liquid-phase flow on the shell side. This decreases the operating costs of a power plant (Luis et al., 2011). For example, in a study conducted by Hoff and Svendsen (2013), the liquid-phase pressure drops were 5.7 kPa and 49.20 kPa when the liquid-phase was flowing on the tube side and shell side, respectively. However, at industrial-scale, pumping of the liquid-phase to the tube-side could be costly when using fibers with a small internal diameter (Keshavarz et al., 2008a). In addition, according to Hoff and Svendsen (2014), the liquid-side mass transfer resistance when the liquid-phase flows on the tube side is higher under laminar flow regime. The authors proposed that the liquid-side mass transfer resistance can be reduced by flowing the gas-phase on the tube side and the liquid-phase on the shell side, and then mix the liquid-phase laterally. This reduces the residence time of the liquid-phase at the gas-liquid interface. Therefore, the total volume of the HFMC modules in the present work could decrease more when considering liquid-phase flow on the shell side and then mix the liquid-phase. Besides, according to Ansaloni (2017b), the latter configuration (gas-phase on the tube side and liquid-phase on the shell side) is easier from a manufacturing point of view, especially, if composite membranes are used. Because coating of an inner wall of fibers is complicated and a continuous coating of hollow fiber can be obtained only on the outer side. However, the CO_2 capture performance could also decrease due to channeling and by-pass of the liquid-phase on the shell side (Mansourizadeh and Ismail, 2009). Additionally, the mass transfer theory when the liquid-phase flows on the shell side is not clearly understood (Gabelman and Hwang, 1999).

The above discussions show that the two flow configurations have their advantages and disadvantages. However, these have not been scientifically examined. A detailed comparison of these two flow modes is beyond the scope of the present study. In the present work, a liquid-phase flowing on the tube side and a gas-phase flowing counter-currently on the shell side was considered. This is the most often studied configuration. Nevertheless, a future work focusing on comparison of the two flow configurations would be a key to select the best one for large-scale application of HFMC technology as long as there are no limitations on manufacturing a membrane for use in either of the flow configurations.

vi. **Membrane lifetime**:

Membrane lifetime is another factor that should be considered when studying HFMC modules for industrial applications. The lifetime of membranes in HFMC modules could be limited due to its poor thermal stability. The temperature of flue gases coming from power plants is high (Luis et al., 2011) and the temperature of the liquid-phase rises during absorption of CO_2 in HFMCs. The maximum temperature of the liquid-phase obtained in the present work was around 333 K. Even higher

temperature peaks (up to 348 K) in the liquid-phase were obtained by several authors (Zaidiza et al., 2014, 2016). Due to these higher temperatures of the liquid and gas-phases, a membrane material with high thermal stability would be required or additional costs for periodic replacement of the membrane would be incurred. In fact, the flue gas could be cooled if found to be beneficial; but it would result in additional cost. Another challenge related to membrane lifetime is the chemical stability of membrane materials. Many solvents may react with the membrane material leading to limited lifetime (Luis et al., 2011; Favre and Svendsen, 2012; Ansaloni et al., 2016). For example, the contact between amine solvents such as MEA and membrane materials such as PP and PVDF resulted in an irreversible degradation products (Favre and Svendsen, 2012). Additionally, membrane materials such as PTFE and PP are incompatible with blend solvents based on DEEA/MAPA (Ansaloni et al., 2016). Therefore, membrane material with long term chemical stability or membrane materials with cheaper replacement cost would also be required for industrial application of HFMC technology.

The ideas discussed above and other ideas such as:

- the effect of impurities in the gas-phase on separation performance of HFMCs,
- ensuring uniform distribution of the large number of fibers in the modules,
- bending of the long membrane fibers,

should be considered in the design of HFMCs for large-scale PCC. Detailed study of these factors is beyond the scope of the present study. At this stage of the present work, an absorber volume reduction when using HFMC modules instead of packed column is shown. The flexibility of the HFMC technology due to its modularity is also shown.

5.4 Concentration, Viscosity, and Temperature Profiles

Concentration, temperature, and viscosity profiles generated from the simulation of 90% CO_2 capture from the flue gas of the 800 MWe coal-fired power plant are presented in this section. Supplementary concentration and density profiles are also given in Appendix B.

5.4.1 Free CO_2, bound CO_2, and free MEA concentration profiles

Three-dimensional concentration profiles of free CO_2, $MEACOO^-$ and free MEA in the liquid-phase are shown in Figures 5.6, 5.7 and 5.8, respectively. At the inlet of the HFMC (z/L=0), a partially loaded solvent was used. And the species in the liquid-phase were initially assumed to be at equilibrium and their composition was considered uniform along the radial direction. This is clearly shown by the flat radial concentration profiles at the liquid-phase inlet (z/L=0) in the Figures 5.6, 5.7 and 5.8.

The axial and radial concentration profiles of CO_2 are rather flat, except in the locations close to the gas-liquid interface (r/R=1) as shown in Figure 5.6. This shows that the

chemical reactions involved in CO_2 absorption are quick. Thus, CO_2 is immediately consumed and most of the reaction products are produced near the gas-liquid interface. The Figure also shows an initial sudden increase in the concentration of the absorbed CO_2 at the tube wall (at r/R=1 and z/L=0) due to the higher driving force when the solvent lean loading was initially contacted with the gas-phase. The concentration of CO_2 at the tube wall then slightly increases along the axial direction (z/L $>$ 0 and r/R=1). This reveals that the reverse reactions must be considered at higher CO_2 removal efficiency, and MEA conversion. Besides, the accumulation of free CO_2 at the tube wall (at r/R=1) demonstrates the reason why two sub-domains in the radial direction with a separate number of discretization points were considered during the model implementation as discussed in section 4.9.

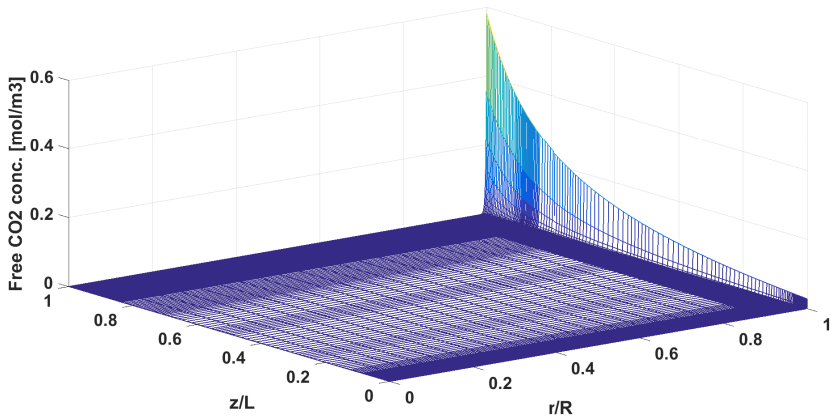

Figure 5.6: Liquid-phase concentrations of free CO_2 as a function of the dimensionless fiber radius and length. (13.4 % v/v CO_2 in flue gas, gas-phase velocity is 1.16 m s^{-1}, liquid-phase velocity is 2×10^{-2}ms^{-1}, initial loading is 0.27 and k_m=2.58×10^{-4} m s^{-1}).

Axial profiles of the concentrations of the chemical species in the liquid-phase at the tube wall and tube center are also given in Figures 5.9 A and B, respectively. The Figures show that the concentration of free CO_2 in the liquid-phase is negligible relative to the concentrations of other chemical species in the liquid-phase. In addition, a drop in the concentration of MEA and rise in the concentrations of the reaction products ($MEAH^-$ and $MEACOO^-$) at the tube wall along the axial direction is observed (see Figure 5.9 A). This is due to the chemical reactions between CO_2, MEA, and H_2O. Along the axial direction, the concentrations of the species at the tube center also slightly increase for the reaction products and slightly decreases for MEA (see Figure 5.9 B). This indicates diffusion, to some extent, of the reaction products from the tube wall towards the tube center and diffusion of MEA from the tube center towards the tube wall.

However, radial concentration gradients of $MEACOO^-$ and MEA are observed along the axial direction as shown in Figures 5.7 and 5.8, respectively. The radial concentration

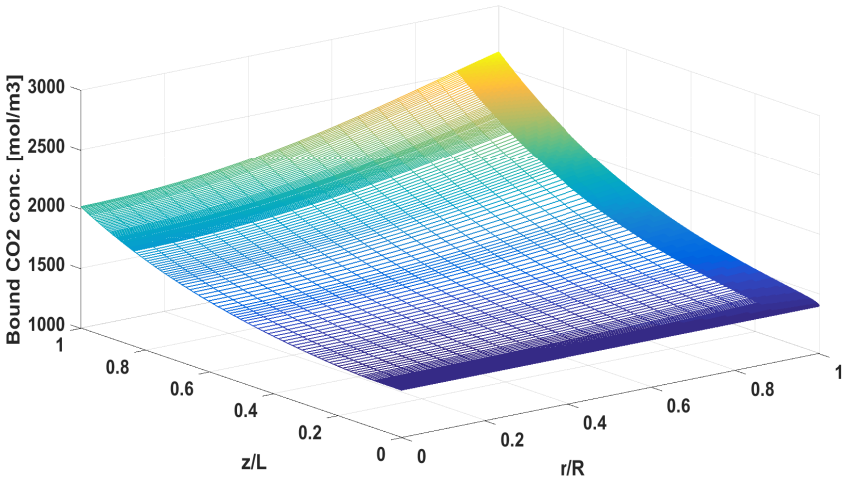

Figure 5.7: Liquid-phase concentrations of $MEACOO^{-}$ as a function of the dimensionless fiber radius and length. (13.4 % v/v CO_2 in flue gas, gas-phase velocity is 1.16 m s^{-1}, liquid-phase velocity is 2×10^{-2} ms^{-1}, initial loading is 0.27 and k_m=2.58×10^{-4} m s^{-1}).

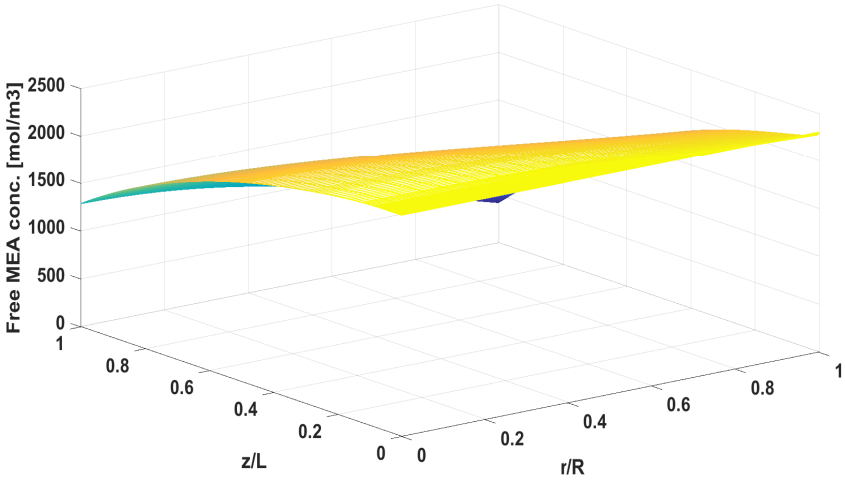

Figure 5.8: Liquid-phase concentrations of free MEA as a function of the dimensionless fiber radius and length. (13.4 % v/v CO_2 in flue gas, gas-phase velocity is 1.16 m s^{-1}, liquid-phase velocity is $2\times 10^{-2}ms^{-1}$, initial loading is 0.27 and k_m=2.58×10^{-4} m s^{-1}).

gradient of MEA and $MEACOO^{-}$ is zero at the HFMC inlet (z/L=0) due to the assumption of uniformity at the inlet as mentioned earlier. The radial concentration gradient

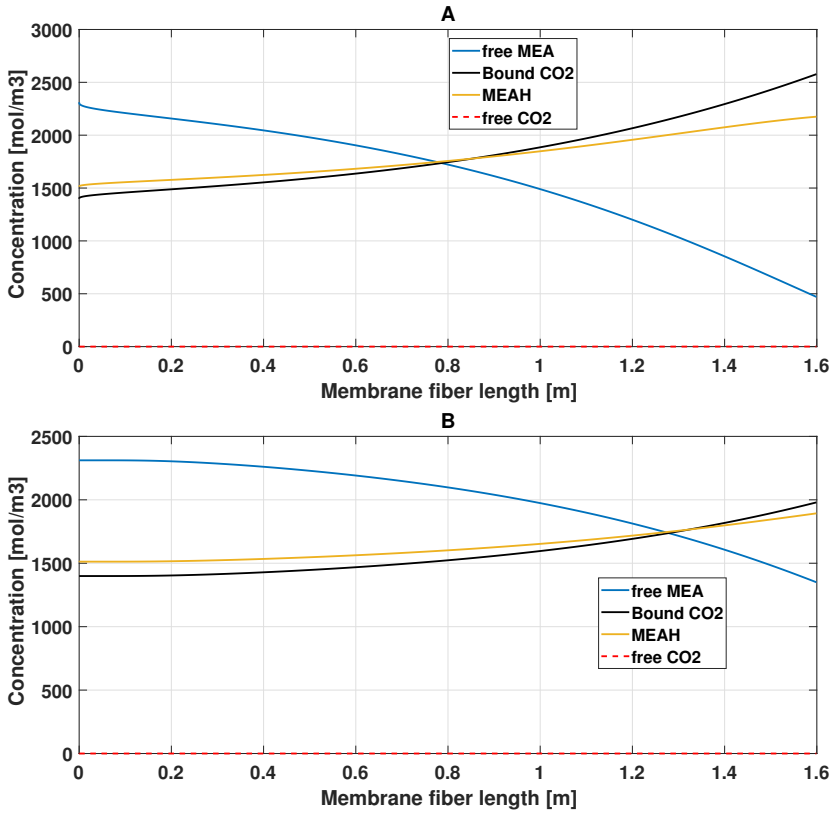

Figure 5.9: Liquid-phase concentrations of free MEA, $MEACOO^-$, $MEAH^+$ and free CO_2 as a function of membrane fiber length at the: **A**) tube wall, and **B**) tube center. (13.4 % v/v CO_2 in flue gas, gas-phase velocity is 1.16m s^{-1}, liquid-phase velocity is 2×10^{-2}ms^{-1}, initial loading is 0.27 and k_m=2.58$\times10^{-4}$ m s^{-1}).

gradually develops along the HFMC length and becomes relatively higher at the exit of the HFMC. For example, the radial concentration gradient for $MEACOO^-$ at the HFMC exit (z/L=1) is above 500 mol.m^{-3}. In a study conducted by Zaidiza et al. (2016), there was no radial concentration gradient of MEA and $MEACOO^-$ along the HFMC length. They concluded that diffusion of the chemical species in the liquid-phase was not limiting the rate of CO_2 absorption. However, the authors used much slower liquid-phase velocity (8.6×10^{-4} ms^{-1}) in their study, which gives sufficient time for the species to diffuse along the radial direction towards the center of the tube (r/R=0). The liquid-phase velocity used in the present work is around 2×10^{-2} ms^{-1}. This relatively higher velocity results in a relatively lower contact time, which limits homogeneous distribution of MEA, $MEACOO^-$ and $MEAH^+$ along the radial direction. However, in the present work, the main mass transfer resistance resides in the membrane. Thus, it can also be concluded that diffusion of the chemical species in the liquid-phase was not limiting the rate of CO_2 absorption under the operating conditions considered even though radial concentration gradient of the

chemical species in the liquid-phase is observed.

5.4.2 Radial profile of viscosity, and total CO_2

The viscosity of the liquid-phase increases with increase in the amount of CO_2 (sum of free CO_2 and bound CO_2) absorbed according to equation 4.59. The concentration of total CO_2 in the liquid-phase increases towards the tube wall as shown in Figure 5.10. Thus, the viscosity of the liquid-phase also follows the same profile (see Figure 5.10). This result supports the reason why radial variation of diffusion coefficient, which is a function of viscosity, was implemented in the model as discussed in section 4.3.1. The radial viscosity profile of the liquid-phase is also affected by the radial temperature profile of the liquid-phase. However, the radial temperature profile of the liquid-phase is almost flat in this case (see Figure 5.11). Thus, the radial viscosity gradient is mainly affected by the radial concentration gradient of total CO_2 in the liquid-phase. It should be noted that the radial concentration gradient of total CO_2 increases with increase in liquid-phase velocity. Because this results in low contact time preventing diffusion of the species towards the tube center. Thus, the radial gradient of viscosity and diffusivity would also increase with the increase in the liquid-phase velocity. This indicates that the implementation of the radial variation of the diffusivity in the HFMC model would become more important if a liquid-phase velocity higher than the velocity used in the present work has been used.

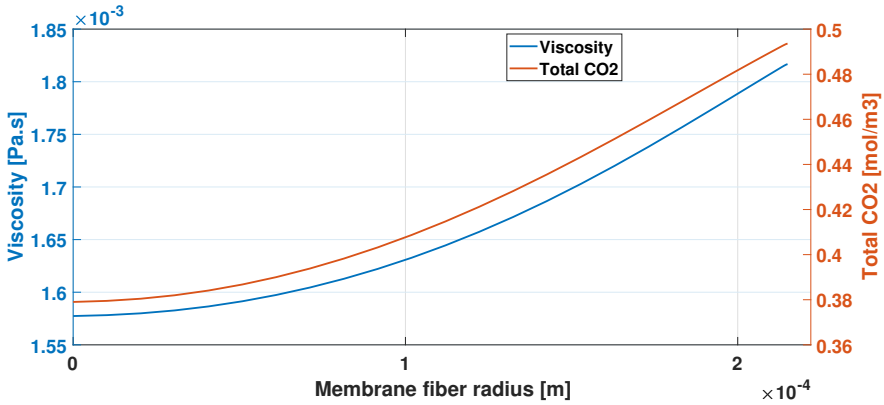

Figure 5.10: Radial profiles of liquid-phase viscosity, and concentration of total CO_2 (sum of free CO_2 and bound CO_2) in the liquid-phase at the exit of the HFMC. (13.4 % v/v CO_2 in flue gas, gas-phase velocity is 1.16m s^{-1}, liquid-phase velocity is $2\times10^{-2}ms^{-1}$, initial loading is 0.27 and k_m=2.58$\times$ 10^{-4} m s^{-1}).

5.4.3 Temperature profile

Figure 5.11 shows three-dimensional temperature profile of the liquid-phase predicted by the HFMC model. The Figure shows a negligible radial variation of the liquid-phase temperature. This is due to an excellent heat transfer along the radial direction in the liquid-phase (Zaidiza et al., 2015, 2016). Similar trends were obtained by several authors (Zaidiza

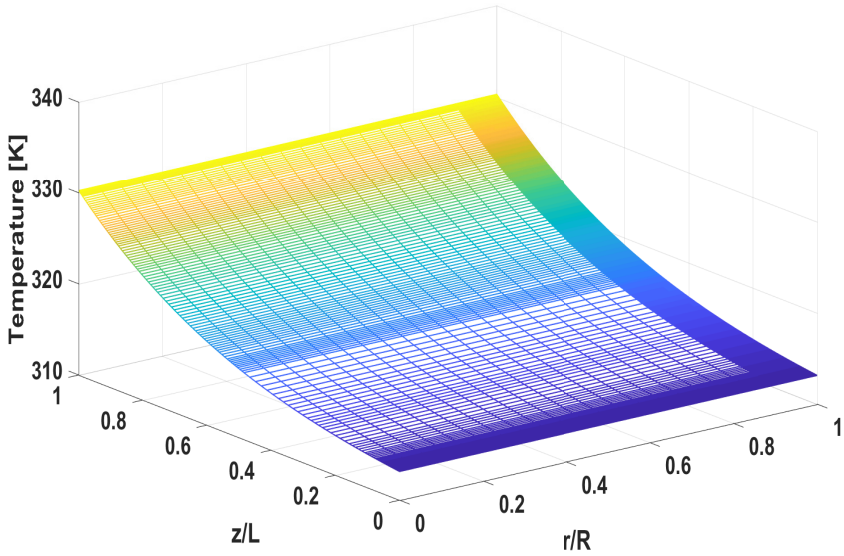

Figure 5.11: Liquid-phase temperature profile as a function of the dimensionless membrane fiber radius and length.(13.4 % v/v CO_2 in flue gas, gas-phase velocity is 1.16m s^{-1}, liquid-phase velocity is 2×10^{-2}ms^{-1}, initial loading is 0.27 and k_m=2.58 $\times$ 10^{-4} m s^{-1}).

et al., 2015, 2016). Figure 5.11 also shows that temperature of the liquid-phase increases along the HFMC length. The resulting temperature difference between the inlet and outlet liquid-phase temperature along the axial direction is around 20 K.

The heat of CO_2 absorption is the main contributor to the temperature increase. Latent heat transfer term accounting the heat added due the transfer of CO_2 from the gas-phase to the liquid-phase is also contributing. However, the sensible heat transfer due to the temperature difference between the liquid and gas-phases is not considered in this case due to numerical stability problems. At lower CO_2 removal efficiency (up to 66 %), the numerical method was stable when the sensible heat transfer was considered. But, when the CO_2 removal efficiency was increased further by increasing the membrane fiber length, the model became unstable and the simulation failed. The use of two sub-domains with a separate number of discretization points during the model implementation decreases the order of the numerical method, which could cause stability problems (Hoff et al., 2002). This is the probable reason for the failure of the simulation at higher CO_2 removal efficiency when sensible heat transfer was considered. The effect of sensible heat transfer on CO_2 removal efficiency (up to 66 %) was analyzed separately and it was found to be negligible under the operating conditions considered. Based on this result, the effect of sensible heat transfer on the prediction of the model at higher CO_2 removal efficiency (above 66 %) was assumed to be negligible in the present work. This was done by setting the overall heat transfer coefficient (U) equal to zero, which makes the gas-phase temperature constant.

Table 5.5: Specifications of pilot-scale HFMC module (Kimball et al., 2014).

	Value	Unit
Module diameter	0.105	m
Effective fiber length	0.88	m
Number of fibers	8521	-
Specific interfacial area	1329	m^2/m^3
Fiber inner diameter	4.3×10^{-4}	m
Fiber outer diameter	8.7×10^{-4}	m
Material	PTFE	-

This will be one of the important issues that should be considered when the model is to be further improved in the future.

5.5 Comparison with Pilot-scale Experimental Data

There is a lack of experimental data on large-scale PCC in HFMCs. Therefore, the model results were compared with pilot-scale experimental data obtained from Kimball et al. (2014) and Chabanon et al. (2014). To best of my knowledge, this is the only pilot-scale experimental data available open in the literature. The pilot-scale experiments were performed using partially loaded, 30 wt% MEA solution and a N_2/CO_2 dry gas mixture with inlet CO_2 volume fraction of about 15%. The geometrical characteristics of the pilot-scale HFMC module used for generating the experimental data are shown in Table 5.5.

The membrane fiber length, the diameter of membrane fiber and module, and the gas and liquid-phase conditions are known. The only parameter which is difficult to estimate precisely is k_m as discussed in section 4.8.6. As a result, the simulation results were fitted to the experimental data using this parameter as the only adjustable parameter. The volume fraction of CO_2 in the gas-phase outlet was the variable compared. Average absolute relative deviation (AARD) (equation 5.1) was used to quantify the deviation of the numerical results from the experimental results.

$$AARD = \frac{100}{N}\sum_{i}^{N}\frac{|y_{exp} - y_{model}|}{y_{exp}} \tag{5.1}$$

where N represents the number of experiments; y_{exp} and y_{model} are the experimental and model volume fraction of CO_2 in the gas-phase outlet, respectively.

Figures 5.12 A, B and C show comparison between experimental and simulation results as a function of liquid-phase flow rate for three cases of gas-phase flow rate (F_g): A) F_g= 8.33×10^{-3} m^3s^{-1}, B) F_g= 2.77×10^{-3} m^3s^{-1} and C) F_g= 1.53×10^{-3} m^3s^{-1}. It

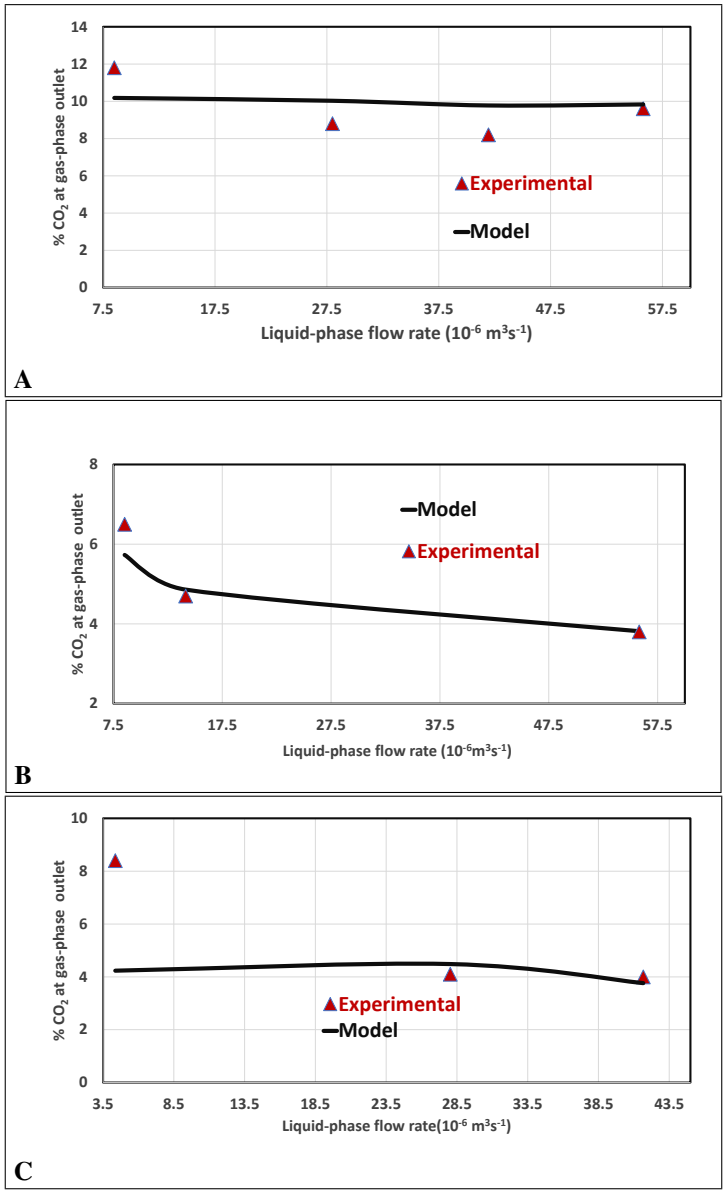

Figure 5.12: Comparison of pilot-scale experimental data and simulation results for a liquid-phase flow rates of 4.17 to 55 $\times 10^{-3}$ m^3s^{-1} and three different gas-phase flow rates. Volume fraction of CO_2 at the gas-phase outlet when the gas-phase flow rate is: (A) 8.33×10^{-3} m^3s^{-1}, (B) 2.77×10^{-3} m^3s^{-1} and (C) 1.53×10^{-3} m^3s^{-1}. Data taken from Kimball et al. (2014) and Chabanon et al. (2014).

should be noted that the values of solvent lean loading and initial volume fraction of CO_2

used in each pilot-scale experiment were slightly different. Details about the experimental data and simulation results from the pilot-scale HFMC module are given in Appendix C.

Considering the number of fixed parameters included in the simulation, Figures 5.12 A, B, and C show that the numerical and experimental results have shown satisfactory agreement. The AARD obtained was about 12.3%, 4.3%, and 21.7% for cases A, B, and C, respectively. The only big deviation observed is at low liquid-phase flow rate for case C (Figure 5.12 C). The model over-predicted CO_2 removal efficiency at low gas-phase and liquid-phase flow rates. Possible reasons for these deviations can be attributed to the following cases:

- Uniform distribution of fibers in the HFMC module and thus uniform gas-phase and liquid-phase flows were assumed when developing the HFMC model. However, commercial HFMC modules have a random distribution of fibers, variation in membrane fiber diameters, bending of fibers, dead-zones, and transverse flow (Keshavarz et al., 2008a; Kimball et al., 2014). These affect the performance of the HFMC, for example, by fluid channeling and bypass on the shell side. This results in a lower CO_2 capture performance of the pilot-scale HFMC than theoretically predicted. Accounting these factors in the model is very challenging.

- The total gas-phase pressure was also assumed constant along the HFMC length. However, a significant pressure drop could result at low gas-phase and liquid-phase velocities when using long membrane fibers, which could reduce the partial pressure of CO_2 in the gas-phase. This results in a reduction of driving force for separation, which reduces the amount of CO_2 transferred to the liquid-phase. This will also result in a lower CO_2 removal efficiency of the pilot-scale HFMC than the efficiency predicted by the model.

- In the present work, only CO_2 was considered as a transfer component. However, the vapor pressure of water and MEA increases with increase in liquid-phase temperature. A temperature rise by about 9 K along the length of the pilot-scale HFMC module was observed from the simulation. The temperature rise increases with increase in solvent conversion. Depending on the water partial pressure difference between the gas and liquid-phases, water transfer from gas-phase to liquid-phase (condensation) or from liquid-phase to gas-phase (evaporation) can take place. Evaporation of water decreases temperature of the liquid-phase, and partial pressure of CO_2 in the gas-phase. The first affects different parameters such as viscosity, density and reaction kinetics. The latter decreases the driving force for transport of CO_2 towards the liquid-phase by decreasing the partial pressure of CO_2 in the gas-phase. Condensation has the opposite effect. Like the water, evaporation of MEA could also happen depending on the driving force. Since a dry gas-phase was considered in the pilot-scale experimental data, the effect of evaporation of water could be significant. But, during the simulation of CO_2 capture from the flue gas of the 800 MWe coal-fired power plant, the water vapor content of the flue gas was 13.4 vol%. Thus, the driving force for transfer of water between the gas and liquid-phases could be low. As a result, the effect of evaporation and/or condensation of water between the two phases would be less significant compared to the pilot-scale case where a dry

gas mixture was considered. Nevertheless, implementation of the evaporation and condensation of water and MEA is recommended to see the effects.

- Errors in the equations used for estimating reaction kinetics, CO_2 absorption flux and model parameters. For example, the equilibrium constant used in the present work was modeled at 313.15 K, 0.5 mol/mol, and 30 wt% MEA. The CO_2 absorption process is exothermic and the equilibrium constant is expected to decrease with increase in temperature. Thus, the equilibrium of the reactions would shift to the left depending on the extent of temperature rise. This could be also one of the reasons for over-prediction of the model at low gas-and-liquid phase velocities. Therefore, simulating the effect of temperature, loading, and non-idealities in the system on the equilibrium constant could have given a different result.

- Errors in measurement.

Table 5.6 presents the value of the k_m obtained through fitting the model results with the experimental data for the three cases. The fitting was obtained by trial and error and no optimization routine was used. The magnitudes of the fitted k_m obtained for PTFE are comparable to the magnitudes of k_m of PTFE reported in the literature (Matsumoto et al., 1995; Chabanon et al., 2011). It lies within the lower range of reported k_m values and could indicate membrane wetting. Chabanon et al. (2014) indicated that the membrane material used for generating the pilot-scale experimental data have been used for several months. Therefore, the lower values of the fitted k_m obtained could be due to aging and/or wetting of the membrane.

Table 5.6: Values of k_m obtained by fitting model results with pilot-scale experimental data for three different gas-phase flow rates (HFMC made of PTFE).

F_g ($m^3 s^{-1}$)	8.33×10^{-3}	2.77×10^{-3}	1.53×10^{-3}
k_m ($m\ s^{-1}$)	1.81×10^{-4}	1.38×10^{-4}	0.96×10^{-4}

The value of fitted k_m slightly increases with increasing gas-phase flow rate (but in the same order of magnitude). This indicates that the simulation results could not fit all experimental data using a single value of the adjustable parameter. This is probably due to the random distribution of fibers, variations in diameter of membrane fibers, dead-zones, wall effects, bend in fibers, and transverse flow in the pilot-scale HFMC, which are not accounted in the model as mentioned earlier. These cause uneven distribution of flows and deviations from the assumption of uniform shell side and tube side fluid flows (Keshavarz et al., 2008a; Favre and Svendsen, 2012; Kimball et al., 2014). These are the main challenges that make the simulation of large-scale HFMC modules difficult. All the other reasons listed above also apply here. Several modelling works (Chabanon et al., 2013; Kimball et al., 2014; Chabanon et al., 2014; Zaidiza et al., 2015, 2016) also found that their model results could not fit all pilot-scale experimental data with one value of k_m as an adjustable parameter. Kimball et al. (2014) and Chabanon et al. (2014) concluded that there were a significant non-idealities in the pilot-scale HFMC module and a more rigorous mass transfer model is needed to account for these non-idealities. Chabanon et al.

(2013) used k_m as an adjustable parameter for fitting four models of different complexity against experimental data. The value of fitted k_m was different from model to model for the same PTFE membrane material. The value of k_m also slightly increased with increase in liquid-phase velocity, packing fraction and mass fraction of MEA. They proposed two hypotheses based on this observation: i) k_m depends on operating conditions; or ii) the use of one adjustable parameter in fitting models against experimental data is good for modelling approaches. The parameter would help for lumping different non-idealites in the system.

Validating the model against a wide range of operating conditions would be of interest; but, it is beyond the scope of the present study. Besides, there is a lack of experimental data on PCC using large-scale HFMC modules. The main target of the comparison was to make sure that the model prediction does not deviate much from the actual performance of HFMC modules. Thus, the comparison is satisfactory at this stage of present study. However, the comparison of the simulation results with the pilot-scale experimental data show that simulation of the performance of large-scale HFMC modules is demanding and more robust models are needed.

Chapter 6

Conclusions

6.1 Conclusions of this Work

The aim of the present work was to develop a comprehensive 2D mathematical model capable of predicting the behavior of CO_2 absorption by aqueous MEA solution in HFMC. This was done in collaboration with the 3GMC project at NTNU. A set of partial differential equations in the HFMC model was solved using the MOL/FD method in the programming language MATLAB. The operating conditions selected were representative of a flue gas of an 800 MWe coal-fired power plant. This was intended to provide useful insights into modelling and design of industrial-scale HFMC modules for PCC.

Sensitivity analysis was performed to evaluate the effect of parameters such as liquid-phase velocity, gas-phase velocity, solvent lean loading, membrane fiber length, and k_m on CO_2 capture performance of the HFMC modules. Results reveal that CO_2 absorption flux and CO_2 removal efficiency increase with the increase in the value of k_m. In addition, increasing the gas-phase velocity and decreasing the membrane fiber length increases the CO_2 absorption flux, and decreases the CO_2 removal efficiency. Finally, the solvent lean loading and the liquid-phase velocity have a negligible effect on CO_2 absorption flux, and CO_2 removal efficiency. Because, in the present work, the main mass transfer resistance resides in the membrane; therefore, the transport of CO_2 is limited by the availability of CO_2 in the gas-phase and is independent of the solvent-lean loading and liquid-phase velocity.

The HFMC model was then applied to design of industrial-scale HFMC modules for 90% CO_2 capture from the flue gas of the 800 MWe coal-fired power plant. Based on the sensitivity analysis, the membrane fiber length was adjusted to get the 90% CO_2 capture. The resulting design of the HFMC modules was compared with that of a structured packed column applied for the same case study from the literature. Results show that a significant absorber volume reduction (by 86%) can be obtained when replacing the structured packed column with the HFMC modules. The HFMC technology also offers flexibility due to its

linear scalability. However, the capacity of the model to predict the performance of the HFMC modules is sensitive to the value of the k_m. And k_m is challenging to precisely estimate due to the uncertainties in estimating the parameters that affect it. Therefore, the method employed for estimating the value of the k_m is a key to get a precise approximation of the length of the membrane fibers in the industrial-scale HFMC modules.

The limitations in the size of commercial HFMC modules and the large number of modules required to handle the large volume of flue gases coming from power plants make the application of the HFMC technology for industrial-scale PCC less feasible even though it offers reduced absorber volume and flexibility. There is no such kind of limitations in the conventional absorbers. In addition, the gas-phase and liquid-phase pressure drops provide a limitation on the maximum length of the membrane fibers that can be used. The present study also suggest that several factors such as long-term stability of membranes, the non-idealities in the large-scale HFMC modules, the effect of gas-phase impurities on the performance of HFMC modules, and a choice of shell-side vs tube-side liquid-phase flow should be considered and examined in the design of large-scale HFMC modules.

The HFMC model predicts three-dimensional concentration, temperature, and viscosity profiles in the liquid-phase. During the 90% CO_2 capture, an excellent radial heat transfer and an axial temperature rise by 20 K in the liquid-phase were observed. Besides, the radial profile of the liquid-phase viscosity, which affect the diffusivity, follows the radial profile of the total CO_2 concentrations in the liquid phase. In the present work, as mentioned earlier, the main mass transfer resistance resides in the membrane; thus, it was considered that the diffusion of the ionic reaction products ($MEAH^+$ and $MEACOO^-$) was not limiting the mass transfer even though their radial concentration profile was not flat.

The model results were compared with pilot-scale experimental data using the k_m as an adjustable parameter for three different gas-phase flow rates. Satisfactory results with AARD of about 4.3%, 12.3%, and 21.7% were obtained for the three cases. However, the model over-predicted CO_2 capture efficiency at low gas-phase and liquid-phase flow rates. Additionally, the values of the fitted k_m obtained for the three cases were not exactly equal; but, in the same order of magnitude with each other and are in the range of values reported in the literature. These indicate that predicting the performance of large-scale HFMC modules is demanding due to the significant non-idealities in the system. Thus, further improvements of the model are required to develop a more robust model capable of predicting the performance of large-scale HFMC modules with high precision. These areas of improvement are presented in the following section.

6.2 Recommendations for Future Work

As mentioned above, the model need further improvements to obtain a more robust model. The most important areas that need improvement are present below:

- The model in the present work has been developed based on the assumption of uniform fluid flows on the shell, and tube sides of the HFMC module. However, in large-scale HFMC modules, there are several factors such as an irregular distribution of membrane fibers, variations in membrane fiber diameters, and bending of membrane fibers that can cause deviations from the assumption of uniform flow. These are the main factors that make the prediction of the performance of large-scale HFMC modules difficult. Therefore, developing a model that considers some of these factors would be vital to predicting the performance of large-scale HFMC modules with a good precision. However, this is expected to be demanding since it is a new area of study and there is a lack of published work on this area.

- Evaporation and/or condensation of water was assumed negligible in the present work. However, evaporation or condensation of water may take place depending on the concentration gradient (driving force) between the gas- and liquid-phases. Evaporation of water reduces the temperature of the liquid-phase and the partial pressure of CO_2 in the gas-phase also decreases which reduces the driving force for CO_2 transport from the gas-phase to the liquid-phase. Condensation of water has the reverse effect. Therefore, water should be included as a transfer component to investigate its effect. Considering MEA as a transfer component would also be important to estimate MEA loss during CO_2 capture.

- Although the gas-phase pressure drop has been considered negligible in the present work, it should be implemented in the HFMC model. This would be particularly important when considering long membrane fibers. Due to the large volume of flue gases of power plants together with long membrane fibers, a significant gas-phase pressure drop might be resulted. This could significantly affect the transfer of CO_2 towards the liquid phase by decreasing the partial pressure of CO_2 in the gas-phase.

- The sensible heat transfer due to the temperature difference between the gas- and liquid-phases should be implemented in the model. In the present study, this has not been considered due to convergence problems.

- An equilibrium constant modeled at 313.15 K, 0.5 mol/mol loading and 30 wt% MEA was used in the present work. It was not possible to implement the effect of the change in liquid-phase temperature, and loading on the equilibrium constant. Therefore, implementation of a rigorous model that considers the effect of the liquid-phase temperature, non-idealities, and loading on the equilibrium constant is recommended. However, this could require a solution method with high accuracy and speed.

Finally, it should be noted that the present study is one of the very few studies focusing on modelling and design of HFMC modules for industrial-scale PCC; most of the modelling studies of PCC in HFMC modules were conducted at laboratory-scale. Furthermore, the application of HFMC technology for PCC is a new and un-mature technology unlike the PCC in packed columns, which is very mature and commercialized. The present study has shown the absorber volume reduction and flexibility offered by the HFMC technology, and the demanding nature of predicting the performance of large-scale HFMC modules.

Thus, more studies on large-scale PCC in HFMC modules should be performed. Furthermore, an economic analysis that compares the HFMC technology with the conventional absorbers should be studied since there is a lack of publish work on this area.

Bibliography

Aaron, D., Tsouris, C., 2005. Separation of co2 from flue gas: a review. Separation Science and Technology 40 (1-3), 321–348.

Abu-Zahra, M. R., Schneiders, L. H., Niederer, J. P., Feron, P. H., Versteeg, G. F., 2007. Co 2 capture from power plants: Part i. a parametric study of the technical performance based on monoethanolamine. International Journal of Greenhouse gas control 1 (1), 37–46.

Al-Fattah, S. M., Barghouty, M. F., Dabbousi, B. O., 2011. Carbon Capture and Storage: Technologies, Policies, Economics, and Implementation Strategies. CRC Press.

Alie, C., 2004. Co 2 capture with mea: Integrating the absorption process and steam cycle of an existing coal-fired power plant.

Ansaloni, L., 2017a. Personal communication, April 25, email.

Ansaloni, L., 2017b. Personal communication, May 23, email.

Ansaloni, L., Arif, A., Ciftja, A. F., Knuutila, H. K., Deng, L., 2016. Development of membrane contactors using phase change solvents for co2 capture: Material compatibility study. Industrial & Engineering Chemistry Research.

Ansaloni, L., Rennemo, R., Knuutila, H. K., Deng, L., 2017. Development of membrane contactors using volatile amine-based absorbents for co 2 capture: amine permeation through the membrane. Journal of Membrane Science.

Arshad, M. W., Fosbøl, P. L., von Solms, N., Svendsen, H. F., Thomsen, K., 2013. Heat of absorption of co2 in phase change solvents: 2-(diethylamino) ethanol and 3-(methylamino) propylamine. Journal of Chemical & Engineering Data 58 (7), 1974–1988.

Atchariyawut, S., Jiraratananon, R., Wang, R., 2007. Separation of co 2 from ch 4 by using gas–liquid membrane contacting process. Journal of membrane science 304 (1), 163–172.

Bird, R. B., Stewart, W. E., Lightfoot, E. N., 2007. Transport phenomena. John Wiley & Sons.

Blomen, E., Hendriks, C., Neele, F., 2009. Capture technologies: improvements and promising developments. Energy Procedia 1 (1), 1505–1512.

Boributh, S., Assabumrungrat, S., Laosiripojana, N., Jiraratananon, R., 2011. A modeling study on the effects of membrane characteristics and operating parameters on physical absorption of co 2 by hollow fiber membrane contactor. Journal of membrane science 380 (1), 21–33.

Bottino, A., Capannelli, G., Comite, A., Di Felice, R., Firpo, R., 2008. Co 2 removal from a gas stream by membrane contactor. Separation and Purification Technology 59 (1), 85–90.

Boucif, N., Corriou, J. P., Roizard, D., Favre, E., 2012. Carbon dioxide absorption by monoethanolamine in hollow fiber membrane contactors: a parametric investigation. AIChE Journal 58 (9), 2843–2855.

Bounaceur, R., Castel, C., Rode, S., Roizard, D., Favre, E., 2012. Membrane contactors for intensified post combustion carbon dioxide capture by gas–liquid absorption in mea: a parametric study. Chemical Engineering Research and Design 90 (12), 2325–2337.

Brodkey, R. S., Hershey, H. C., 2003. Transport phenomena: a unified approach. Brodkey publishing.

Bruder, P., Grimstvedt, A., Mejdell, T., Svendsen, H. F., 2011. {CO2} capture into aqueous solutions of piperazine activated 2-amino-2-methyl-1-propanol. Chemical Engineering Science 66 (23), 6193 – 6198.
URL http://www.sciencedirect.com/science/article/pii/S0009250911006208

Brunetti, A., Scura, F., Barbieri, G., Drioli, E., 2010. Membrane technologies for co 2 separation. Journal of Membrane Science 359 (1), 115–125.

Caillol, S., et al., 2011. Fighting global warming: the potential of photocatalysis against co 2, ch 4, n 2 o, cfcs, tropospheric o 3, bc and other major contributors to climate change. Journal of Photochemistry and Photobiology C: Photochemistry Reviews 12 (1), 1–19.

Caplow, M., 1968. Kinetics of carbamate formation and breakdown. Journal of the American Chemical Society 90 (24), 6795–6803.

Chabanon, E., Kimball, E., Favre, E., Lorain, O., Goetheer, E., Ferre, D., Gomez, A., Broutin, P., 2014. Hollow fiber membrane contactors for post-combustion co2 capture: A scale-up study from laboratory to pilot plant. Oil & Gas Science and Technology–Revue dIFP Energies nouvelles 69 (6), 1035–1045.

Chabanon, E., Roizard, D., Favre, E., 2011. Membrane contactors for postcombustion carbon dioxide capture: a comparative study of wetting resistance on long time scales. Industrial & Engineering Chemistry Research 50 (13), 8237–8244.

Chabanon, E., Roizard, D., Favre, E., 2013. Modeling strategies of membrane contactors for post-combustion carbon capture: A critical comparative study. Chemical engineering science 87, 393–407.

Change, C., 2001. The scientific basis, intergovernmental panel on climate change. by JT Houghton, Y. Ding, DJ Griggs, et al.

Chen, C.-C., Evans, L. B., 1986. A local composition model for the excess gibbs energy of aqueous electrolyte systems. AIChE Journal 32 (3), 444–454.

Cheng, S., Meisen, A., Chakma, A., 1996. Predict amine solution properties accurately. Hydrocarbon processing 75 (2).

Crooks, J. E., Donnellan, J. P., 1989. Kinetics and mechanism of the reaction between carbon dioxide and amines in aqueous solution. Journal of the Chemical Society, Perkin Transactions 2 (4), 331–333.

Cui, Z., deMontigny, D., 2013. Part 7: A review of co2 capture using hollow fiber membrane contactors. Carbon Management 4 (1), 69–89.

Davidson, R. M., 2007. Post-combustion carbon capture from coal fired plants: solvent scrubbing. IEA Clean Coal Centre London.

deMontigny, D., Tontiwachwuthikul, P., Chakma, A., 2005. Comparing the absorption performance of packed columns and membrane contactors. Industrial & engineering chemistry research 44 (15), 5726–5732.

Dindore, V., Brilman, D., Feron, P., Versteeg, G., 2004. Co 2 absorption at elevated pressures using a hollow fiber membrane contactor. Journal of Membrane Science 235 (1), 99–109.

Dindore, V., Brilman, D., Versteeg, G., 2005. Hollow fiber membrane contactor as a gas–liquid model contactor. Chemical Engineering Science 60 (2), 467–479.

Drioli, E., Criscuoli, A., Curcio, E., 2011. Membrane contactors: fundamentals, applications and potentialities. Vol. 11. Elsevier.

Eslami, S., Mousavi, S. M., Danesh, S., Banazadeh, H., 2011. Modeling and simulation of co 2 removal from power plant flue gas by pg solution in a hollow fiber membrane contactor. Advances in Engineering Software 42 (8), 612–620.

Falk-Pedersen, O., Dannström, H., 1997. Separation of carbon dioxide from offshore gas turbine exhaust. Energy Conversion and Management 38, S81–S86.

Falk-Pedersen, O., Grønvold, M. S., Nøkleby, P., Bjerve, F., Svendsen, H. F., 2005. Co2 capture with membrane contactors. International journal of green energy 2 (2), 157–165.

Farjami, M., Moghadassi, A., Vatanpour, V., 2015. Modeling and simulation of co 2 removal in a polyvinylidene fluoride hollow fiber membrane contactor with computational fluid dynamics. Chemical Engineering and Processing: Process Intensification 98, 41–51.

Favre, E., Svendsen, H., 2012. Membrane contactors for intensified post-combustion carbon dioxide capture by gas–liquid absorption processes. Journal of membrane science 407, 1–7.

Feron, P., Jansen, A., Klaassen, R., 1992. Membrane technology in carbon dioxide removal. Energy Conversion and Management 33 (5), 421–428.

Feron, P. H., 2010. Exploring the potential for improvement of the energy performance of coal fired power plants with post-combustion capture of carbon dioxide. International Journal of Greenhouse Gas Control 4 (2), 152–160.

Franco, J., Demontigny, D., Kentish, S., Perera, J., Stevens, G., 2008. A study of the mass transfer of co2 through different membrane materials in the membrane gas absorption process. Separation Science and Technology 43 (2), 225–244.

Franken, A., Nolten, J., Mulder, M., Bargeman, D., Smolders, C., 1987. Wetting criteria for the applicability of membrane distillation. Journal of Membrane Science 33 (3), 315–328.

Freund, P., 2003. Making deep reductions in co2 emissions from coal-fired power plant using capture and storage of co2. Proceedings of the Institution of Mechanical Engineers, Part A: Journal of Power and Energy 217 (1), 1–7.

Gabelman, A., Hwang, S.-T., 1999. Hollow fiber membrane contactors. Journal of Membrane Science 159 (1), 61–106.

Geankoplis, C. J., 2003. Transport processes and separation process principles:(includes unit operations). Prentice Hall Professional Technical Reference.

Gong, Y., Wang, Z., Wang, S., 2006. Experiments and simulation of co 2 removal by mixed amines in a hollow fiber membrane module. Chemical Engineering and Processing: Process Intensification 45 (8), 652–660.

Hartono, A., Mba, E. O., Svendsen, H. F., 2013. Prediction of n 2 o solubility in alkanolamine solutions from the excess volume property. Energy procedia 37, 1744–1750.

Hartono, A., Mba, E. O., Svendsen, H. F., 2014. Physical properties of partially co2 loaded aqueous monoethanolamine (mea). Journal of Chemical & Engineering Data 59 (6), 1808–1816.

Hassanlouei, R. N., Pelalak, R., Daraei, A., 2013. Wettability study in co 2 capture from flue gas using nano porous membrane contactors. International Journal of Greenhouse Gas Control 16, 233–240.

Hessen, E. T., Haug-Warberg, T., Svendsen, H. F., 2010. The refined e-nrtl model applied to co 2–h 2 o–alkanolamine systems. Chemical Engineering Science 65 (11), 3638–3648.

Hoff, K. A., Juliussen, O., Falk-Pedersen, O., Svendsen, H. F., 2004. Modeling and experimental study of carbon dioxide absorption in aqueous alkanolamine solutions using a membrane contactor. Industrial & engineering chemistry research 43 (16), 4908–4921.

Hoff, K. A., Poplsteinova, J., Jakobsen, H. A., Falk-Pedersen, O., Juliussen, O., Svendsen, H. F., 2002. Modeling of membrane reactor. International Journal of Chemical Reactor Engineering 1 (1), 1011.

Hoff, K. A., Svendsen, H. F., 2013. Co 2 absorption with membrane contactors vs. packed absorbers-challenges and opportunities in post combustion capture and natural gas sweetening. Energy Procedia 37, 952–960.

Hoff, K. A., Svendsen, H. F., 2014. Membrane contactors for co 2 absorption–application, modeling and mass transfer effects. Chemical Engineering Science 116, 331–341.

Hosseinzadeh, A., Hosseinzadeh, M., Vatani, A., Mohammadi, T., 2017. Mathematical modeling for the simultaneous absorption of co 2 and so 2 using mea in hollow fiber membrane contactors. Chemical Engineering and Processing: Process Intensification 111, 35–45.

Hsu, C.-H., Li, M.-H., 1997. Viscosities of aqueous blended amines. Journal of Chemical & Engineering Data 42 (4), 714–720.

Hua, C.-G., Kang, G.-D., Jia, J.-X., Li, M., Cao, Y.-M., Yuan, Q., 2013. Physical absorption of co2 using polyvinylidene fluoride membrane contactor at high pressure and mathematical simulation. Chemical Journal of Chinese Universities 34 (4), 906–912.

Iliuta, I., Bougie, F., Iliuta, M. C., 2015. Co2 removal by single and mixed amines in a hollow-fiber membrane moduleinvestigation of contactor performance. AIChE Journal 61 (3), 955–971.

Jakobsen, H. A., 2008. Chemical reactor modeling. Multiphase Reactive Flows, Berlin, Germany: Springer-Verlag.

Keil, F., Mackens, W., Voß, H., Werther, J., 2012. Scientific Computing in Chemical Engineering II: Computational Fluid Dynamics, Reaction Engineering, and Molecular Properties. Springer Science & Business Media.

Kelley, C. T., 2003. Solving nonlinear equations with Newton's method. SIAM.

Keshavarz, P., Ayatollahi, S., Fathikalajahi, J., 2008a. Mathematical modeling of gas–liquid membrane contactors using random distribution of fibers. Journal of Membrane Science 325 (1), 98–108.

Keshavarz, P., Fathikalajahi, J., Ayatollahi, S., 2008b. Analysis of co 2 separation and simulation of a partially wetted hollow fiber membrane contactor. Journal of Hazardous Materials 152 (3), 1237–1247.

Khaisri, S., Tontiwachwuthikul, P., Jiraratananon, R., et al., 2009. Comparing membrane resistance and absorption performance of three different membranes in a gas absorption membrane contactor. Separation and Purification Technology 65 (3), 290–297.

Kimball, E., Al-Azki, A., Gomez, A., Goetheer, E., Booth, N., Adams, D., Ferre, D., 2014. Hollow fiber membrane contactors for co2 capture: modeling and up-scaling to co2 capture for an 800 mwe coal power station. Oil & Gas Science and Technology–Revue dIFP Energies nouvelles 69 (6), 1047–1058.

Klaassen, R., Feron, P., Jansen, A., 2005. Membrane contactors in industrial applications. Chemical Engineering Research and Design 83 (3), 234–246.

Klaassen, R., Feron, P., Jansen, A., 2008. Membrane contactor applications. Desalination 224 (1), 81 – 87.
URL http://www.sciencedirect.com/science/article/pii/S0011916408000350

Kneifel, K., Nowak, S., Albrecht, W., Hilke, R., Just, R., Peinemann, K.-V., 2006. Hollow fiber membrane contactor for air humidity control: modules and membranes. Journal of membrane science 276 (1), 241–251.

Kreulen, H., Smolders, C., Versteeg, G., Van Swaaij, W., 1993a. Determination of mass transfer rates in wetted and non-wetted microporous membranes. Chemical Engineering Science 48 (11), 2093–2102.

Kreulen, H., Smolders, C., Versteeg, G., Van Swaaij, W., 1993b. Microporous hollow fibre membrane modules as gas-liquid contactors part 2. mass transfer with chemical reaction. Journal of Membrane Science 78 (3), 217–238.

Kumar Paramasivam Senthil, P., 2002. Development and design of membrane gas absorption processes. Ph.D. thesis, Universiteit Twente.

Le Moullec, Y., Kanniche, M., 2011. Screening of flowsheet modifications for an efficient monoethanolamine (mea) based post-combustion co 2 capture. International journal of greenhouse gas control 5 (4), 727–740.

Leung, D. Y., Caramanna, G., Maroto-Valer, M. M., 2014. An overview of current status of carbon dioxide capture and storage technologies. Renewable and Sustainable Energy Reviews 39, 426–443.

Li, J.-L., Chen, B.-H., 2005. Review of co 2 absorption using chemical solvents in hollow fiber membrane contactors. Separation and Purification Technology 41 (2), 109–122.

Li, S., Pyrzynski, T. J., Klinghoffer, N. B., Tamale, T., Zhong, Y., Aderhold, J. L., Zhou, S. J., Meyer, H. S., Ding, Y., Bikson, B., 2017. Scale-up of peek hollow fiber membrane contactor for post-combustion co 2 capture. Journal of Membrane Science.

Li, X., Wang, S., Chen, C., 2013. Experimental study of energy requirement of co2 desorption from rich solvent. Energy Procedia 37, 1836–1843.

Liebenthal, U., Pinto, D. D. D., Monteiro, J. G.-S., Svendsen, H. F., Kather, A., 2013. Overall process analysis and optimisation for co2 capture from coal fired power plants based on phase change solvents forming two liquid phases. Energy Procedia 37, 1844–1854.

Luis, P., Gerven, T. V., der Bruggen, B. V., 2012a. Recent developments in membrane-based technologies for {CO2} capture. Progress in Energy and Combustion Science 38 (3), 419 – 448.
URL //www.sciencedirect.com/science/article/pii/S0360128512000056

Luis, P., Van der Bruggen, B., Van Gerven, T., 2011. Non-dispersive absorption for co2 capture: from the laboratory to industry. Journal of Chemical Technology and Biotechnology 86 (6), 769–775.

Luis, P., Van Gerven, T., Van der Bruggen, B., 2012b. Recent developments in membrane-based technologies for co 2 capture. Progress in Energy and Combustion Science 38 (3), 419–448.

Luo, X., Hartono, A., Svendsen, H. F., 2012. Comparative kinetics of carbon dioxide absorption in unloaded aqueous monoethanolamine solutions using wetted wall and string of discs columns. Chemical engineering science 82, 31–43.

Majeed, H., Knuutila, H. K., Hillestad, M., Svendsen, H. F., 2017. Characterization and modelling of aerosol droplet in absorption columns. International Journal of Greenhouse Gas Control 58, 114–126.

Mansourizadeh, A., Ismail, A. F., 2009. Hollow fiber gas–liquid membrane contactors for acid gas capture: a review. Journal of hazardous materials 171 (1), 38–53.

Matsumoto, H., Kitamura, H., Kamata, T., Ishibashi, M., Ota, H., Akutsu, N., 1995. Effect of membrane properties of microporous hollow-fiber gas-liquid contactor on co2 removoval from thermal power plant flue gas. Journal of chemical engineering of Japan 28 (1), 125–128.

Mavroudi, M., Kaldis, S., Sakellaropoulos, G., 2006. A study of mass transfer resistance in membrane gas–liquid contacting processes. Journal of Membrane Science 272 (1), 103–115.

Metz, B., Davidson, O., De Coninck, H., Loos, M., Meyer, L., 2005. Ipcc special report on carbon dioxide capture and storage. Tech. rep., Intergovernmental Panel on Climate Change, Geneva (Switzerland). Working Group III.

Monteiro, J. G.-S., Majeed, H., Knuutila, H., Svendsen, H. F., 2015. Kinetics of co 2 absorption in aqueous blends of n, n-diethylethanolamine (deea) and n-methyl-1, 3-propane-diamine (mapa). Chemical Engineering Science 129, 145–155.

Monteiro, J. G.-S., Pinto, D. D., Zaidy, S. A., Hartono, A., Svendsen, H. F., 2013. {VLE} data and modelling of aqueous n,n-diethylethanolamine (deea) solutions. International Journal of Greenhouse Gas Control 19, 432 – 440.
URL http://www.sciencedirect.com/science/article/pii/S175058361300354X

Mulder, J., 2012. Basic principles of membrane technology. Springer Science & Business Media.

Neftel, A., Moor, E., Oeschger, H., Stauffer, B., 1985. Evidence from polar ice cores for the increase in atmospheric co2 in the past two centuries.

NETL, 2005. CARBON DIOXIDE CAPTURE FROM LARGE POINT SOURCES. [online] Available at: https://www.netl.doe.gov/research/coal/carbon-capture/post-combustion/large-point [Accessed 1 Jul. 2017].

Olajire, A. A., 2010. Co 2 capture and separation technologies for end-of-pipe applications–a review. Energy 35 (6), 2610–2628.

Parry, M. L., 2007. Climate change 2007-impacts, adaptation and vulnerability: Working group II contribution to the fourth assessment report of the IPCC. Vol. 4. Cambridge University Press.

Pinto, D. D., Knuutila, H., Fytianos, G., Haugen, G., Mejdell, T., Svendsen, H. F., 2014a. Co 2 post combustion capture with a phase change solvent. pilot plant campaign. International Journal of Greenhouse Gas Control 31, 153–164.

Pinto, D. D., Monteiro, J. G.-S., Johnsen, B., Svendsen, H. F., Knuutila, H., 2014b. Density measurements and modelling of loaded and unloaded aqueous solutions of {MDEA} (n-methyldiethanolamine), {DMEA} (n,n-dimethylethanolamine), {DEEA} (diethylethanolamine) and {MAPA} (n-methyl-1,3-diaminopropane). International Journal of Greenhouse Gas Control 25, 173 – 185.
URL http://www.sciencedirect.com/science/article/pii/S1750583614001005

Poling, B. E., Prausnitz, J. M., O'connell, J. P., et al., 2001. The properties of gases and liquids. Vol. 5. Mcgraw-hill New York.

Pozio, A., Tosti, S., 2013. Handbook of membrane reactors: Reactor types and industrial applications. Woodhead Publishing Ltd., Cambridge 16, 607.

Putta, K. R., Pinto, D. D., Svendsen, H. F., Knuutila, H. K., 2016. Co 2 absorption into loaded aqueous mea solutions: Kinetics assessment using penetration theory. International Journal of Greenhouse Gas Control 53, 338–353.

Qi, Z., Cussler, E., 1985. Microporous hollow fibers for gas absorption: I. mass transfer in the liquid. Journal of membrane science 23 (3), 321–332.

Rangwala, H. A., 1996. Absorption of carbon dioxide into aqueous solutions using hollow fiber membrane contactors. Journal of Membrane Science 112 (2), 229–240.

Rao, A. B., Rubin, E. S., 2002. A technical, economic, and environmental assessment of amine-based co2 capture technology for power plant greenhouse gas control. Environmental science & technology 36 (20), 4467–4475.

Rode, S., Nguyen, P. T., Roizard, D., Bounaceur, R., Castel, C., Favre, E., 2012. Evaluating the intensification potential of membrane contactors for gas absorption in a chemical solvent: a generic one-dimensional methodology and its application to co 2 absorption in monoethanolamine. Journal of membrane science 389, 1–16.

Rongwong, W., Assabumrungrat, S., Jiraratananon, R., 2013. Rate based modeling for co 2 absorption using monoethanolamine solution in a hollow fiber membrane contactor. Journal of membrane science 429, 396–408.

Rui, Z., Anderson, M., Lin, Y., Li, Y., 2009. Modeling and analysis of carbon dioxide permeation through ceramic-carbonate dual-phase membranes. Journal of Membrane Science 345 (1), 110–118.

Rui, Z., Ji, H., Lin, Y., 2011. Modeling and analysis of ceramic–carbonate dual-phase membrane reactor for carbon dioxide reforming with methane. International journal of hydrogen energy 36 (14), 8292–8300.

Saidi, M., Heidarinejad, S., Rahimpour, H. R., Talaghat, M. R., Rahimpour, M. R., 2014. Mathematical modeling of carbon dioxide removal using amine-promoted hot potassium carbonate in a hollow fiber membrane contactor. Journal of Natural Gas Science and Engineering 18, 274–285.

Schiesser, W. E., 2012. The numerical method of lines: integration of partial differential equations. Elsevier.

Sengupta, A., Peterson, P., Miller, B., Schneider, J., Jr., C. F., 1998. Large-scale application of membrane contactors for gas transfer from or to ultrapure water. Separation and Purification Technology 14 (13), 189 – 200.
URL http://www.sciencedirect.com/science/article/pii/S1383586698000744

Shampine, L. F., Reichelt, M. W., 1997. The matlab ode suite. SIAM journal on scientific computing 18 (1), 1–22.

Snijder, E. D., Te Riele, M. J., Versteeg, G. F., Van Swaaij, W., 1993. Diffusion coefficients of several aqueous alkanolamine solutions. Journal of Chemical and Engineering data 38, 475–475.

Songolzadeh, M., Soleimani, M., Takht Ravanchi, M., Songolzadeh, R., 2014. Carbon dioxide separation from flue gases: a technological review emphasizing reduction in greenhouse gas emissions. The Scientific World Journal 2014.

Steeneveldt, R., Berger, B., Torp, T., 2006. Co2 capture and storage: closing the knowing–doing gap. Chemical Engineering Research and Design 84 (9), 739–763.

Svendsen, H. F., 2017. Personal communication, February 21, email.

Svensson, H., Hulteberg, C., Karlsson, H. T., 2013. Heat of absorption of co 2 in aqueous solutions of n-methyldiethanolamine and piperazine. International Journal of Greenhouse Gas Control 17, 89–98.

Tans, P., 2017. Earth system research laboratory, global monitoring division. NOAA/ESRL: Boulder, CO (www. esrl. noaa. gov/gmd/ccgg/trends/). Keeling, R. Scripps CO2 Program.

Thiruvenkatachari, R., Su, S., An, H., Yu, X. X., 2009. Post combustion co 2 capture by carbon fibre monolithic adsorbents. Progress in Energy and Combustion Science 35 (5), 438–455.

Tobiesen, F. A., Svendsen, H. F., Juliussen, O., 2007. Experimental validation of a rigorous absorber model for co2 postcombustion capture. AIChE Journal 53 (4), 846–865.

Tontiwachwuthikul, P., Chakma, A., et al., 2006. Using polypropylene and polytetrafluoroethylene membranes in a membrane contactor for co 2 absorption. Journal of Membrane Science 277 (1), 99–107.

Valdés, H., Romero, J., Sanchez, J., Bocquet, S., Rios, G., Valenzuela, F., 2009. Characterization of chemical kinetics in membrane-based liquid–liquid extraction of molybdenum (vi) from aqueous solutions. Chemical Engineering Journal 151 (1), 333–341.

Versteeg, G. F., Van Swaalj, W., 1988. Solubility and diffusivity of acid gases (carbon dioxide, nitrous oxide) in aqueous alkanolamine solutions. Journal of Chemical and Engineering Data 33 (1), 29–34.

Wang, M., Lawal, A., Stephenson, P., Sidders, J., Ramshaw, C., 2011. Post-combustion co 2 capture with chemical absorption: a state-of-the-art review. Chemical Engineering Research and Design 89 (9), 1609–1624.

Wang, R., Li, D., Liang, D., 2004. Modeling of co 2 capture by three typical amine solutions in hollow fiber membrane contactors. Chemical Engineering and Processing: Process Intensification 43 (7), 849–856.

Wickramasinghe, S., Semmens, M. J., Cussler, E., 1992. Mass transfer in various hollow fiber geometries. Journal of Membrane Science 69 (3), 235–250.

Wiesler, F., 1996. Membrane contactors: an introduction to the technology. Ultrapure water 13 (4), 27–33.

Wilke, C., 1950. A viscosity equation for gas mixtures. The journal of chemical physics 18 (4), 517–519.

Xu, B., Gao, H., Chen, M., Liang, Z., Idem, R., 2016. Experimental study of regeneration performance of aqueous n, n-diethylethanolamine solution in a column packed with dixon ring random packing. Industrial & Engineering Chemistry Research 55 (31), 8519–8526.

Yeon, S.-H., Lee, K.-S., Sea, B., Park, Y.-I., Lee, K.-H., 2005. Application of pilot-scale membrane contactor hybrid system for removal of carbon dioxide from flue gas. Journal of Membrane Science 257 (1), 156–160.

Yu, K. M. K., Curcic, I., Gabriel, J., Tsang, S. C. E., 2008. Recent advances in co2 capture and utilization. ChemSusChem 1 (11), 893–899.

Zaidiza, D. A., Belaissaoui, B., Rode, S., Neveux, T., Makhloufi, C., Castel, C., Roizard, D., Favre, E., 2015. Adiabatic modelling of co 2 capture by amine solvents using membrane contactors. Journal of Membrane Science 493, 106–119.

Zaidiza, D. A., Billaud, J., Belaissaoui, B., Rode, S., Roizard, D., Favre, E., 2014. Modeling of co 2 post-combustion capture using membrane contactors, comparison between one-and two-dimensional approaches. Journal of Membrane Science 455, 64–74.

Zaidiza, D. A., Wilson, S. G., Belaissaoui, B., Rode, S., Castel, C., Roizard, D., Favre, E., 2016. Rigorous modelling of adiabatic multicomponent co 2 post-combustion capture using hollow fibre membrane contactors. Chemical Engineering Science 145, 45–58.

Zhang, H.-Y., Wang, R., Liang, D. T., Tay, J. H., 2006. Modeling and experimental study of co 2 absorption in a hollow fiber membrane contactor. Journal of membrane science 279 (1), 301–310.

Zhang, H.-Y., Wang, R., Liang, D. T., Tay, J. H., 2008. Theoretical and experimental studies of membrane wetting in the membrane gas–liquid contacting process for co 2 absorption. Journal of Membrane Science 308 (1), 162–170.

Zhao, S., Feron, P. H., Deng, L., Favre, E., Chabanon, E., Yan, S., Hou, J., Chen, V., Qi, H., 2016. Status and progress of membrane contactors in post-combustion carbon capture: A state-of-the-art review of new developments. Journal of Membrane Science 511, 180–206.

Appendix A: Sensitivity Analysis-Additional Results

This appendix gives additional results on the effect of the five parameters listed in table 5.2 on solvent rich loading. Solvent rich loading is an important parameter that affects solvent regeneration energy requirement and solvent cyclic capacity.

A.1-Effect of gas-phase velocity on solvent rich loading

The effect of gas-phase velocity on solvent rich loading is shown in Figure A.1. Solvent rich loading is defined as moles of CO_2 divided by total moles of MEA in liquid-phase at the HFMC outlet. The total moles of MEA is constant in this case, since the liquid-phase flow rate is fixed constant. Thus, solvent rich loading depends only on the moles of CO_2 absorbed. As discussed in section 5.1.1, an increase in gas-phase velocity increases the CO_2 absorption flux. This increases the amount of CO_2 in the outlet liquid-phase, since the residence time of the liquid-phase is fixed constant. As a result, solvent rich loading increases with increase in gas-phase velocity as shown in Figure A.1.

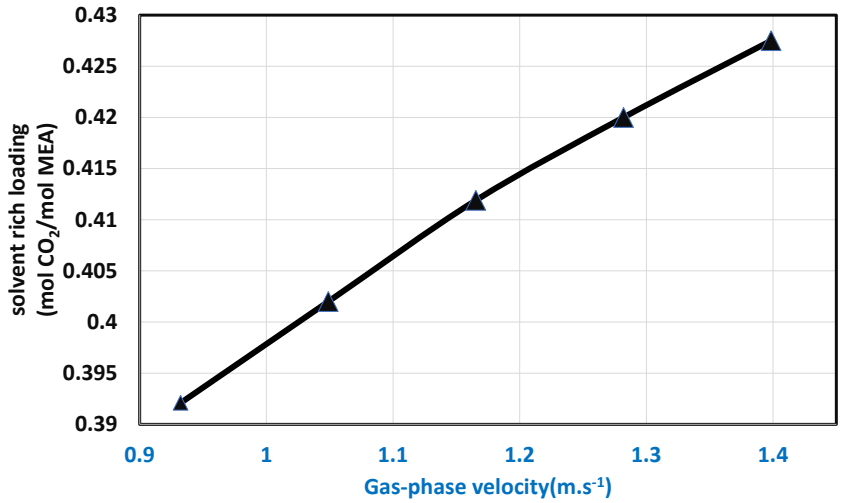

Figure A.1: Effect of gas-phase velocity on solvent rich loading.

A.2-Effect of liquid-phase velocity on solvent rich loading

As mentioned in section 5.1.2, CO_2 absorption flux and CO_2 removal efficiency are not affected by liquid-phase velocity under the operating conditions considered in this study. Therefore, the total moles of CO_2 in the liquid-phase is not affected by the liquid-phase

velocity. Furthermore, it is obvious that increasing the liquid-phase velocity increases the total moles of MEA in the solution, which is inversely proportional to solvent rich CO_2 loading. As a result, the solvent rich loading decreases with increase in liquid-phase velocity as show in Figure A.2.

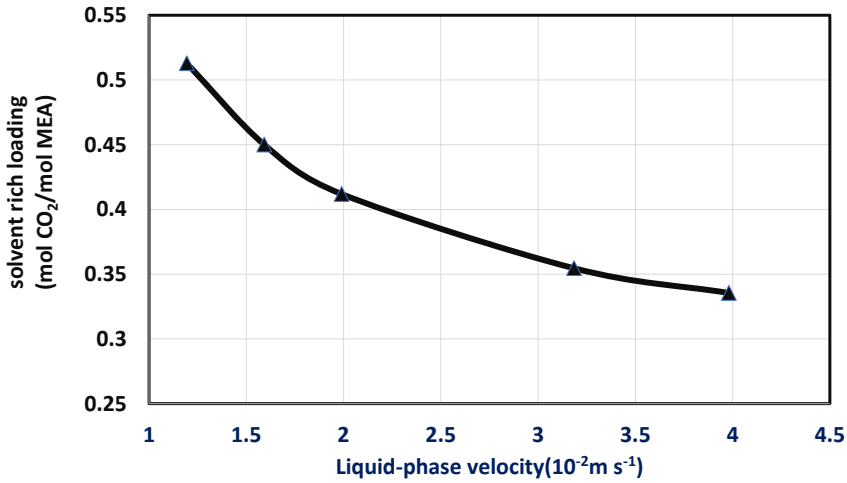

Figure A.2: Effect of liquid-phase velocity on solvent rich loading.

A.3-Effect of membrane fiber length on solvent rich loading

The CO_2 removal efficiency increases with increase in membrane fiber length (see Figure 5.3). Solvent rich loading has a direct relationship with the total moles of CO_2 in the liquid-phase. The total moles of MEA in the solution is kept constant. Therefore, solvent rich loading increases with increase in membrane fiber length due to the increase in CO_2 removal efficiency, and residence time of the solvent (Figure A.3).

A.4-Effect of lean loading on solvent rich loading

It is obvious that solvent rich loading increases with increase in solvent lean loading as shown in Figure A.4. This can be clearly demonstrated using the following equation that relates the cyclic capacity, CO_2 capture efficiency, gas-phase and liquid-phase flow rates (Hoff and Svendsen, 2013):

$$F_L = \frac{E_f F_g \frac{P_{CO_2}}{R_g T_g}}{C_S(\alpha_{rich} - \alpha_{lean})} \tag{A.1}$$

where F_L and F_g are liquid-phase and gas-phase flow rate, respectively; E_f is CO_2 capture efficiency; α_{rich} and α_{lean} are solvent rich and lean loading, respectively; P_{CO_2} is partial pressure of CO_2 in the gas-phase; T_g and R_g are gas-phase temperature and gas constant,

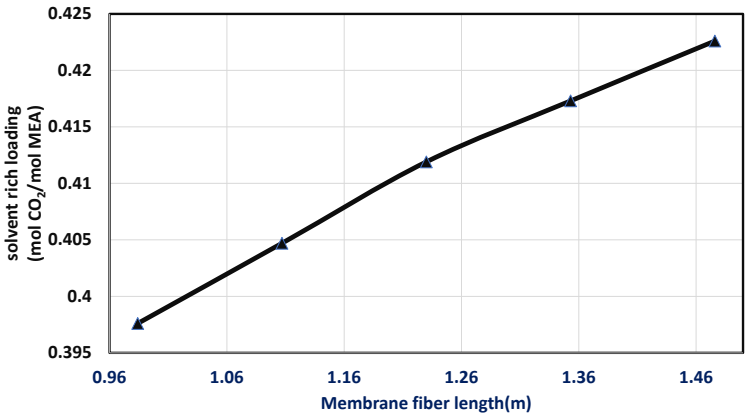

Figure A.3: Effect of membrane fiber length on solvent rich loading.

respectively; C_S is solvent concentration.

The absorption loading capacity of MEA solution is around 0.5 moles of CO_2 per moles of MEA. When MEA reaches this point, there will be no chemical absorption of CO_2 because MEA becomes fully loaded.

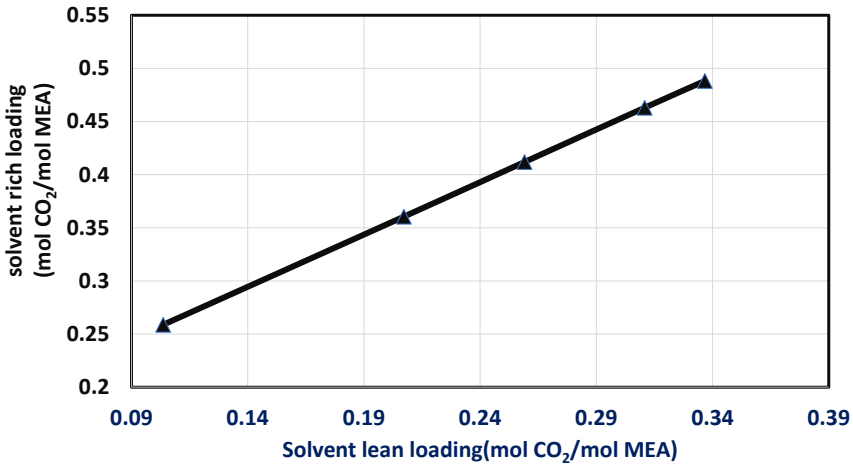

Figure A.4: Effect of solvent lean loading on solvent rich loading.

A.5-Effect of membrane mass transfer coefficient on solvent rich loading

Solvent rich loading increases with increase in membrane mass transfer coefficient as shown in Figure A.5. This is due to the increase in CO_2 removal efficiently and CO_2 absorption flux with increases in membrane mass transfer coefficient (see Figure 5.5).

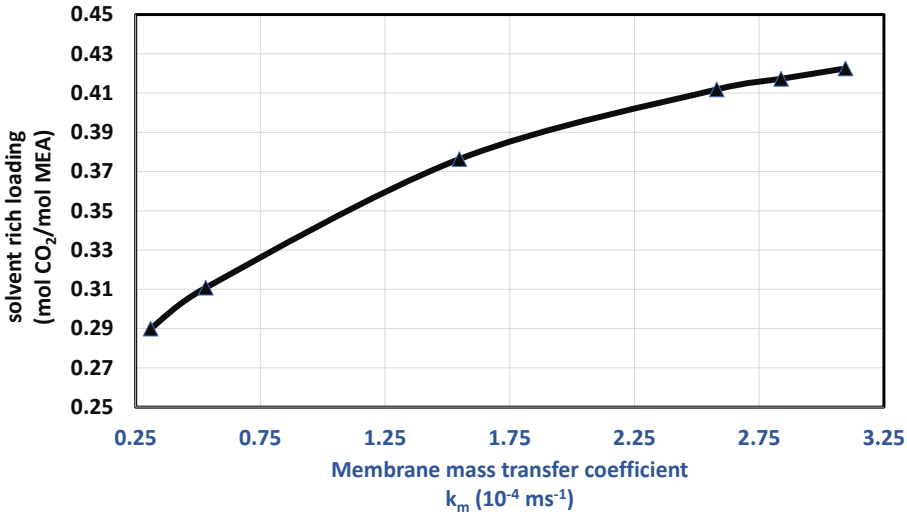

Figure A.5: Effect of membrane mass transfer coefficient on solvent rich loading.

Appendix B:Supplementary Concentration and Density Profiles

This appendix provides supplementary simulation profiles. Figure B.1 shows the profile of density of the liquid-phase along the axial and radial directions. From equation 4.52, it is expected that the density of the liquid-phase increases with increase in the amount of CO_2 absorbed (B.1). The effect of CO_2 loading on the density is clearly shown in the figure. Three-dimensional profiles of $MEAH^+$ and total CO_2 in the liquid-phase are shown in Figures B.2 and B.3, respectively.

Appendix C:Comparison with Pilot-scale Data- Supplementary Data

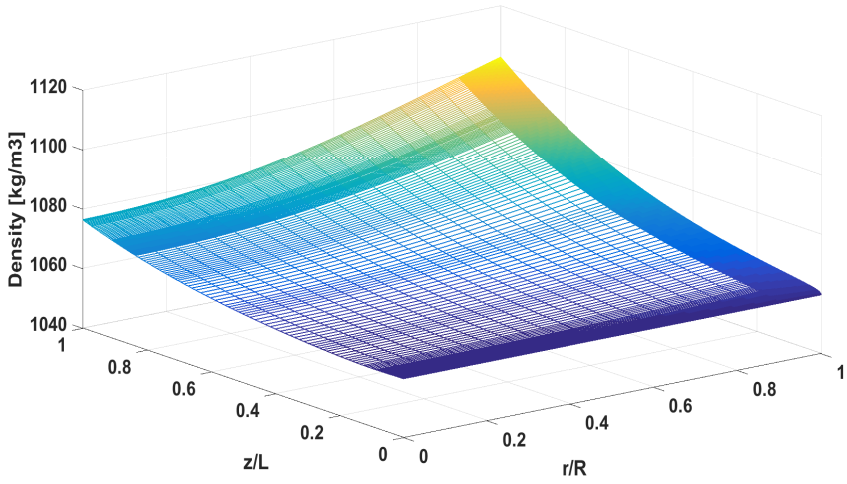

Figure B.1: Liquid-phase density as a function of the dimensionless fiber radius and length. (13.4 % v/v CO_2 in flue gas, gas-phase velocity is 1.16 m s^{-1}, liquid-phase velocity is 2×10^{-2} ms^{-1}, initial loading is 0.27 and k_m=2.58 $\times$ 10^{-4} m s^{-1}).

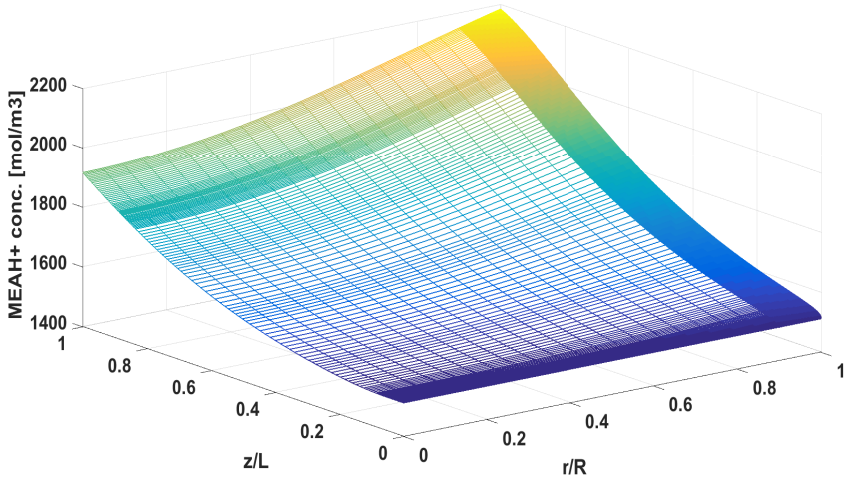

Figure B.2: Liquid-phase concentrations of $MEAH^+$ as a function of the dimensionless fiber radius and length. (13.4 % v/v CO_2 in flue gas, gas-phase velocity is 1.16 m s^{-1}, liquid-phase velocity is 2×10^{-2} ms^{-1}, initial loading is 0.27 and k_m=2.58 $\times$ 10^{-4} m s^{-1}).

This appendix gives supplementary data used for comparison of the simulation and experimental results. The percent deviation and percent average absolute relative deviation

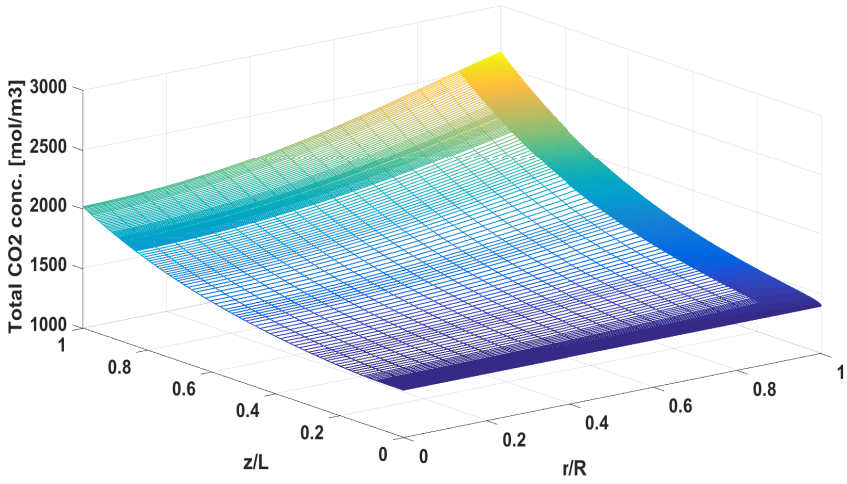

Figure B.3: Liquid-phase concentrations of total CO_2 as a function of the dimensionless fiber radius and length. (13.4 % v/v CO_2 in flue gas, gas-phase velocity is 1.16 m s^{-1}, liquid-phase velocity is 2×10^{-2} m s^{-1}, initial loading is 0.27 and k_m=2.58 $\times$ 10^{-4} m s^{-1}).

(AARD) between the simulation results and pilot scale experimental data is given in table C.1.

Table C.1: Comparison of model results and with pilot-scale experimental data for three cases of gas-phase flow rate (F_g): Case A) F_g= 8.33 $\times 10^{-3}$ $m^3 s^{-1}$, Case B) F_g= 2.77 $\times 10^{-3}$ $m^3 s^{-1}$, and Case C) F_g= 1.53 $\times 10^{-3}$ $m^3 s^{-1}$. Experimental data taken from Kimball et al. (2014).

	Liquid flow rate ($10^{-6}\frac{m^3}{s}$)	Lean loading (mol/mol)	CO_2 conc. at gas inlet (%)	CO_2 conc. at gas outlet,(%)		** Deviation (%)	*** AARD (%)
				Experimental results (y_{exp})	Model results (y_{model})		
CASE A							
	8.50	0.084	15.0	11.8	10.18	13.7	12.34
	28.00	0.088	14.8	8.8	10.0	13.96	
	41.94	0.107	14.4	8.2	9.7	19.24	
	55.78	0.183	14.5	9.6	9.8	2.44	
CASE B							
	8.53	0.046	14.9	6.5	5.73	11.8	4.25
	14.14	0.133	12.8	4.7	4.86	3.4	
	55.80	0.157	13.8	3.8	3.82	0.44	
CASE C							
	4.36	0.179	14.6	8.4	4.2	49.61	21.65
	28.03	0.195	14.6	4.1	4.4	9.36	
	41.67	0.15	15	4 *	3.7	5.98	

* data extracted from figure 9 in Chabanon et al. (2014).

** Deviation (%)= $100(\frac{y_{exp}-y_{model}}{y_{exp}})$ ***AARD (%)= $\frac{100}{N}\sum_i^N \frac{|y_{exp}-y_{model}|}{y_{exp}}$